AN ENTROPY-BASED LOW ALTITUDE AIR TRAFFIC SAFETY ASSESSMENT FRAMEWORK

by

Hsun Chao

A Dissertation

Submitted to the Faculty of Purdue University

In Partial Fulfillment of the Requirements for the degree of

Doctor of Philosophy

School of Aeronautics and Astronautics

West Lafayette, Indiana

December 2021

THE PURDUE UNIVERSITY GRADUATE SCHOOL
STATEMENT OF COMMITTEE APPROVAL

Dr. Daniel A. DeLaurentis, Chair

School of Aeronautics and Astronautics

Dr. Dengfeng Sun

School of Aeronautics and Astronautics

Dr. Jitesh H. Panchal

School of Mechanical Engineering

Dr. Mario Ventresca

School of Industrial Engineering

Approved by:

Dr. Gregory Blaisdell

TABLE OF CONTENTS

LIST OF TABLES

LIST OF FIGURES

ABSTRACT

The National Aeronautics and Space Administration (NASA) has a vision for Advanced Air Mobility (AAM) based on safely introducing aviation services to missions that were previously not served or under-served. Many potential AAM missions lie in metropolitan areas that are beset by various types of uncertainty and potential constraints. Radio interference from other electronic devices can render unreliable communication between flying vehicles to ground operators. Buildings have irregular surfaces that degrade GPS localization performance. Skyscrapers can induce spontaneous turbulence that degrades vehicles' navigational accuracy. However, the potential market demands for aerial passenger-carrying and package delivery services have attracted investments. For example, Google WingX, Amazon Prime Air, and Joby Aviation are well-known companies developing AAM systems and services. If the market visions are realized, how will safety be assessed and maintained with high-density AAM operations?

While there are multiple technology candidates for realizing high-density AAM operations in urban environments, the means to accomplish the requisite first step of assessing the airspace safety of an integrated AAM eco-system from the candidate technologies is crucial but as yet unclear. This dissertation proposes an entropy-based framework for assessing the airspace safety level for low-altitude airspace in an AAM setting. The framework includes a conceptual model for depicting the information flows between air vehicles and an air traffic authority (ATA) and the use of a probability distribution to represent the traffic state. Subsequently, the framework embeds three airspace-level metrics for assessing airspace safety and uncertainty levels. The traffic safety severity metric quantifies the traffic safety level. The traffic entropy quantifies the uncertainty level of the traffic state distribution. Finally, the temperature is the ratio of the traffic safety severity to the traffic entropy. The temperature is similar to the traffic safety severity but gives a higher weight to the instance with a safe traffic state.

Simulation studies show that the combined use of the three metrics can evaluate relative airspace safety levels even if the unsafe conditions do not occur. The use cases include using the metrics for real-time airspace safety level monitoring and comparing the design

of airspace systems and operational strategies. Additionally, this study demonstrates using a heat map to visualize vehicle-level metrics and assess designs of UAM airspace structures. The contribution of this study includes two parts. First, the temperature metric can heuristically assess a probability function. Based on the definition of the cost function, the temperature metric gives a higher weighting to the instance of the probability function with a lower cost value. This study constructs several triggers for predicting if a near-miss event would happen in the airspace. The temperature-based trigger has a better prediction accuracy than the cost-function-based trigger. Secondly, the temperature can visualize the safety level of an airspace structure with the considerations of the environmental and vehicle state measurement uncertainty. The locations with high-temperature values indicate that the regions are more likely to have endangered vehicles. Although this framework does not provide any means of resolving the unsafe conditions, it can be powerful in the comparison of different airspace design concepts and identify the weaknesses of either airspace design or operational strategies.

1. INTRODUCTION

1.1 Motivation

Advanced Air Mobility (AAM) is an emerging aviation industry which focuses on developing ecosystems for Urban Air Mobility (UAM) and Unmanned Aircraft Systems (UAS) [1]. Research reports [2], [3] estimate that UAS and UAM vehicles will create significant air traffic in urban areas when the market matures. These UAM and UAS vehicles will be fully autonomous to enable high-density urban operations, ensure airspace safety, and generate various UAM/UAS related services, like parcel delivery [1], [4], [5]. Until the autonomous technologies mature and become ubiquitous, the heterogeneous air traffic will be a mix of human-piloted, remote-piloted, and autonomous vehicles based on diverse flight mission requirements. Additionally, metropolitan areas have unpredictable micro-weather phenomena and radio interference due to buildings and civil activities [1]. These factors increase the difficulties associated with having a safe and secure AAM ecosystem and with properly assessing airspace safety level.

To integrate the new types of air vehicles to the National Airspace System (NAS), the Federal Aviation Administration (FAA) illustrates the concept of segregated airspace for UAS, UAM, and commercial aviation in the UAS Traffic Management (UTM) Concept of Operations [6]–[8] and the UAM Concept of Operations [9], [10]. In these operational concepts, the UAS Service Suppliers (USS) and the Providers of Services to UAM (PSU) receive the broadcasted flight statuses from the air vehicles. They can dynamically close and open airspace for responding to airspace complexity. However, the broadcasted vehicle flight statuses may be unreliable because of degraded vehicle navigational performances in urban environments [11]. Urban micro-weather phenomena also increase the uncertainty of assessing air vehicle status [12], [13]. Additionally, heterogeneous types of air vehicles pose the challenges of mid-air separation and real-time vehicle tracking [14]. To manage resources of the USS and PSU for monitoring and resolving any potential issues, one or several metrics are needed to quantify airspace complexity under various uncertainty sources for ensuring airspace safety [11].

It is challenging to assess the airspace-related policies due to the novel operational concepts and lack of understandings of the rapidly growing industry. Although the UAM Concept of Operation [9], [10] and the UTM Concept of Operation [6]–[8] draw a big picture about how different actors interact with each other, they are lacking detailed definitions and detailed regulations of some identified concepts. For example, the UAM Concept of Operation [9], [10] mentions that the UAM vehicles will fly in corridors between the origins and destinations. The detailed corridor descriptions are missing from the documents. Several studies [15]–[17] already show that the detailed designs of UAM corridors or conflict resolution algorithms can influence air traffic throughput and airspace safety. However, these studies do not account for vehicle navigational uncertainty. Additionally, their airspace safety metric is the number of loss of separation (LOS) [16]. If the relative distance between two vehicles are slightly higher than the LOS criterion, the number of LOS cannot be used to evaluate the effectiveness of airspace-related policies or collision resolution algorithms. If the rate of LOS is low, copious simulation data are also required for statistical analysis. Hence, the metrics should also be associated with the airspace-related policies for continuously assessing the airspace-related policies and reducing the number of required simulation runs.

The stakeholders in the AAM industry, like the PSU, the USS, remote pilots, or UAM operators, etc., are interested in different factors which are related to airspace complexity. Prof. DeLaurentis et al. [18] have justified that researchers can analyze the air transportation system (ATS) with a system-of-systems (SoS) perspective. Since the AAM is the subsystem of a whole ATS and has SoS characteristics [18]–[20], researchers need to be aware of a common phrase, "[a] whole is greater than the sum of its parts." The metrics should consider different factors, which are the focuses of different stakeholders, to represent the airspace complexity. For example, different air traffic patterns influence the number of path conflict points. Micro-weather phenomena have various impact levels on the different sizes of air vehicles. Compositions of types of vehicles in air traffic can increase air traffic heterogeneousness, which indicates the diversity of vehicle autonomous capabilities, sizes, and flight dynamics, etc. Air traffic heterogeneousness also makes airspace complexity increase.

Then, the SoS analysis methodologies provide a framework to organize the stakeholders' expectations to help this study generate metrics associated with airspace complexity.

The current NAS comprises air traffic control sectors with different capacity limits [21]. And, the airspace complexity is associated with the air traffic control sector capacity [21]. To estimate an air traffic control sector capacity limit, the current approaches rely on the number of air traffic controllers, airspace sector complexity, and airspace sector uncertainty [21], [22]. However, autonomy capability of air vehicles is not accounted for in the workload assessment models [22]. If one merely implements the same airspace capacity assessment models [22] on the AAM traffic management system, it might underestimate AAM air traffic throughput because it ignores that autonomous systems can agilely resolve some contingent events. Hence, there is a need to include autonomy capability of air vehicles to estimate AAM traffic throughput and ensure airspace safety. This study intends to use the entropy-based metrics for assessing airspace complexity to estimate AAM traffic capacity and provide suggested actions for any air traffic authorities.

1.2 System-of-Systems Perspectives to Frame Research Scope

The AAM system is part of the ATS and contains the follow six traits. Maier stated that an SoS should have the first first trait, which is the Operational & Managerial independence [19]. Hence, the AAM system is an SoS. Moreover, the AAM system also inherits the other five traits from the ATS. DeLaurentis discussed the six traits of the ATS SoS and their implications to the simulations and design methodologies [18]. In conclusion, the design and analysis of the AAM system should consider its SoS properties.

- Operational & Managerial Independence: subsystems are independently operated and managed. For example, operators of UAM/UAS vehicles and the UAM/UTM service providers are operationally and managerially independent.

- Geographic Distribution: subsystems are geographically distributed. For example, operators of air vehicles and UAM/UTM service providers are at different locations.

- Evolutionary Behavior: subsystems are never complete. For example, as technology evolves, new types of UAM/UTM infrastructures and air vehicles will emerge in the UTM system, and old subsystems may be retired.

- Emergent Behavior: properties of the AAM SoS are not apparent from the constituted subsystems. For example, the air traffic congestion can happen either en-route or at the landing ports; however, the design goals of both en-route routs or landing ports are to ensure efficient UAM/UTM operations.

- Networks: subsystems are connected via physical or abstract network connections. For example, Unmanned Aerial Vehicle (UAV) package delivery system are connected through one or more links of logistic systems. Vehicle operators connect to each other via internet for exchanging flight plans.

- Heterogeneity: subsystems of the AAM differ significantly from each other.

- Trans-domain: operations of AAM subsystems need to consider economic sustainability, community acceptance, and environmental influences.

Prof. DeLaurentis [20] proposes an SoS lexicon to categorizing subsystems of an SoS and drawing an SoS hierarchy. There are four perspectives of an SoS: Resources, Operations, Policies, and Economics. Resources represent physical components of an SoS, while Operations show activities of physical or non-physical entities. Policies include regulations which influence operations of physical or non-physical entities in an SoS, while Economics show incentives or costs for physical or non-physical entities to execute operations in an SoS. Table 1.1 shows the SoS Lexicon for the AAM Transportation System.

An SoS comprises several levels. An upper level contains collections of lower level systems. Taking the AAM SoS as an example, the α level is the component level, which includes air vehicles for airline operations and traffic surveillance radars for air traffic monitoring. The β level includes the collections of α level systems. Airlines or air service providers belong to this level. The γ level represents the collections of β level systems. For example, airlines in one nation or regional air traffic control sectors are in this level. Finally, the δ level systems

Table 1.1. System-of-Systems Lexicon for Advanced Air Mobility Transportation System

Level	**Resources**	**Operations**	**Policies**	**Economics**
δ	Global AAM industry, Global AAM infrastructures	Global AAM operations, International AAM services	International AAM standards	Values/Costs of providing international AAM services
γ	AAM service industry, National AAM infrastructure	National AAM operation, National AAM service	National AAM standards	Values/Costs of providing national AAM services
β	Regional AAM service providers	AAM fleets operation	AAM infrastructure operation standard	Values/Costs of providing AAM services
α	AAM vehicle operators, AAM vehicles, AAM infrastructure components	AAM vehicle operations, AAM infrastructure operations	Operational procedure for AAM vehicles and infrastructure	Values/Costs of operating AAM components

are the collections of γ level systems. Global ATS or international air traffic service systems are in this level.

This study intends to develop entropy-based metrics to assess airspace complexity with the considerations of various vehicle autonomy levels, environmental perturbations, and airspace-related policies. This research focuses on levels of α and β and on both Resources and Operations perspectives of the AAM Transportation System in Table 1.1.

1.3 Research Questions

Section 1.1 described why it is necessary to have metrics to assess the AAM airspace complexity with considerations of vehicle autonomous levels, localization or wind uncertainty, and airspace-related regulations. Because the AAM system is part of ATS, it is important to ensure the existence of stable-intermediate forms during ATS evolutions [18], [19]. The future AAM system should inherit features from ATS for reducing integration difficulties and ensuring a stable ATS evolution. Hence, the study proposes a novel AAM traffic framework (for both low altitude airspace and controlled airspace) with the following rules:

- The airspace is split into several airspace control sectors.
- There is at least one authority (humans or automation algorithms) in each airspace control sector monitoring air traffic.
- The authority (humans or automation algorithms) can decide whether an air vehicle can enter the airspace or not.
- Autonomous air vehicles or remote pilots have ways to communicate with the authority by sending requests or listening to commands.
- There are standard communication protocols between air vehicles and authorities.

With these assumptions in mind, the research question of this research is: *How can an air traffic control authority dynamically assess mixed air traffic conditions including vehicles with various autonomy levels and flying capabilities?* In a hypothetical scenario, even if every vehicle is autonomous with proper navigation and collision avoidance systems, collisions can still occur due to environmental uncertainty, like wind perturbations, etc. Environmental uncertainty will increase the uncertainty of a vehicle's estimated state. Hence, the air traffic authority should use metrics related to the vehicle state uncertainty to identify actions to manage the airspace complexity.

The study intends to answer the research question with a bottom-up approach. The following list shows the working tasks and the sub-questions of this study.

1. *Which metrics can quantify the uncertainty of a vehicle's estimated state with considerations of vehicle autonomy levels, vehicle flying capabilities, environmental uncertainty, and operational regulations?*

2. *How does an air traffic authority use the metrics to estimate airspace safety in real-time with at least 0.5 vehicles per square kilometers?*

3. *How does an airspace designer use the metrics for designing/enhancing air traffic management systems with at least 0.5 vehicles per square kilometers?*

1.4 Research Contribution

The contribution of this research is providing a new approach of using information theory and control theory to derive the metrics, which represent the system status of a multi-agent system under uncertainty in the air traffic management research. In the real world, knowing exact vehicle locations is impossible due to various sources of uncertainty, like radar measurement errors, wind perturbations, etc. For commercial aviation traffic, a popular approach for considering the impacts of uncertainty is introducing a safety bubble around vehicles. Vehicle manufacturers must ensure that their navigation devices can estimate vehicle status with errors within the safety bubble criterion. So, air traffic controllers only give commands to separate vehicles by ensuring no overlapping between the vehicle safety bubbles. However, the AAM industry will introduce the high density of air vehicles with different autonomous flying capabilities in metropolitan areas. Additionally, cities have various uncertainty sources, which influences AAM operations. For example, radio interference can unpredictably influence vehicle localization capabilities. Buildings can also induce spontaneous wind turbulence. These uncertainty sources may impose a large safety bubble around the vehicles with the safety bubble approach. With the conservative safety bubble criterion, the airspace may not provide enough volume to accommodate high-density urban air traffic.

Multiple control theories can estimate probability distributions of estimated vehicle statuses and are possible to replace the safety bubble criterion. Instead of estimating the exact positions of vehicles, air traffic authorities can estimate the probability distributions of vehicles and identify a minimum separation criterion. The Kalman Filter is one of the algorithms estimating the probability distribution of a vehicle status by fusing a vehicle dynamics model and different sources of vehicle status measurements together. From the air traffic authority perspective, it can estimate the vehicle status probability distributions of all vehicles in airspace. However, with the collections of the probability distributions of estimated vehicle statuses, it is unclear which metrics can help air traffic authorities assess the airspace complexity and manage air traffic. This study proposes a traffic entropy metric, a traffic temperature metric, and a traffic safety severity metric for quantifying air traffic conditions.

These metrics are independent of the vehicle's flying capabilities and autonomous levels. Several algorithms, like the Kalman filter algorithm, can estimate vehicle states with the vehicle dynamic model in the form of the vehicle probability density function. A collection of vehicle probability density functions is the traffic probability density function. The proposed metrics can quantify the traffic safety levels according to the traffic probability density function.

There are two potential use cases for these metrics. First, if the vehicle status probability distribution is associated with the real-time vehicle state, these metrics can help monitor the air traffic conditions. If the vehicle status probability distribution is associated with the average behaviors of the air vehicles in the airspace, these metrics can help decision-makers compare different airspace structure designs.

1.4.1 Real-Time Airspace Monitoring

The traffic entropy summarizes the uncertainty level of estimations of air traffic conditions and helps air traffic authorities identify when extra communication channels can reduce the vehicle state estimation uncertainty. Firstly, The traffic entropy metric can quantify the uncertainty level of an air traffic condition. By introducing information theory, the traffic entropy is associated with the information entropy and the communication channels between air vehicles and air traffic authorities. During radio interference conditions, the traffic entropy can identify if extra communication channels can improve traffic condition estimations. However, the traffic entropy only relies on probability distributions of estimated traffic statuses. The traffic entropy cannot assess how accurately air traffic follows airspace regulations, like the minimum mid-air separation requirement.

With given airspace regulations, the traffic temperature heuristically quantifies traffic status probability distributions. The traffic temperature is a ratio of a traffic safety severity to the traffic entropy. The traffic safety severity is the expected cost value based on traffic status probability distributions and the given airspace regulations. If vehicles in air traffic violate the airspace regulations, the traffic safety severity should increase based on the severity of the violations. Therefore, the traffic temperature indicates the traffic safety severity per unit of traffic status uncertainty. A higher traffic temperature implies that there is a higher confidence in the possibility of severe airspace regulation violation by the vehicles.

Finally, the definition of the traffic temperature makes the traffic temperature independent from the number of vehicles in air traffic. This property makes the traffic temperature a good metric for assessing different designs of airspace or monitoring airspace statuses.

1.4.2 Airspace Structure Design Assessment

Since the AAM is an emerging and rapidly growing industry, technologies and regulations related to airspace management are still evolving. The AAM airspace is a dynamic environment with spontaneous on-demand air traffic, unpredictable wind perturbations, or random radio interference. Hence, it is hard to compare different technologies and regulations under a dynamic environment. Researchers use the number of LOS for evaluating airspace safety [16]; however, this metric can fluctuate violently if there are strong environmental perturbations. Hence, the traffic temperature can assess the safety level of the airspace and identify potential hot spots.

The decision-makers of the airspace structure can conduct simulations to identify the vehicle status probability distributions with some airspace management technologies and regulations. Then, the decision-makers can use the temperature metric to assess airspace safety and compare airspace management technologies and regulations. The traffic temperature metric can be either at the airspace level or the vehicle level. The traffic temperature metric in the airspace level can help decision-makers compare different designs of airspace structures by comparing either the average temperature or the maximum temperature through simulations. A higher temperature value indicates a higher confidence level that the airspace is in unfavorable conditions. Additionally, the traffic temperature metric at the vehicle level can show the hot spots in the airspace. The decision-maker can create a heat map according to the locations and temperature of each air vehicle. The heat map shows hot spots and hot routes, which require extra attention from the decision-makers for resolving any unfavorable event. These hot spots can be due to high environmental perturbations, strong radio interference, or a high density of path conflict points.

2. LITERATURE REVIEW

NASA's vision of the AAM includes the new air transportation systems providing services to areas that are not served or under-served by aviation. The air transportation systems contain the existing and evolving UTM for managing air traffic and ensuring airspace safety for small UAS. The UAM is part of the AAM and encompasses freight delivery and passenger-carrying services in urban environments. The UAM also includes manual or autonomous vehicles with either conventional or vertical take-off and landing capabilities. However, these new aerial operations should not endanger the existing and busy National Airspace System (NAS). The *National Academies of Sciences, Engineering, and Medicine* also published a report [1] and listed its AAM vision and the gaps preventing the vision from being realized. They mentioned how to ensure airspace safety with introductions of new concepts of operations, technologies, and business models will be one of the technical obstacles. Moreover, Chao et al. and Reiche et al. identified that the weather issue is one of the obstacles preventing a reliable UAM service [23], [24]. Chao et al. further identified that wind perturbations are the most influential weather condition [23]. Isik et al. also identified the safety risk with the degraded accuracy of Global Navigation Satellite Systems (GNSS) based navigation [25]. The following sections will illustrate the concepts of UTM, UAM, and the NAS to create a foundation for identifying the integration challenges. Finally, the last section will show the literature review related to the identified gaps.

2.1 UAS Traffic Management

The FAA published the UTM Concept of Operations (Conops) for identifying the participants of the UTM, defining the UTM system architecture, and illustrating UTM operations under various operational conditions and environments [6]–[8]. Figure 2.1 shows the notional UTM architecture from the FAA [8]. The UTM participants and their responsibilities are as follows.

- **UAS**: The aerial vehicles fly in the air and provide aerial services.

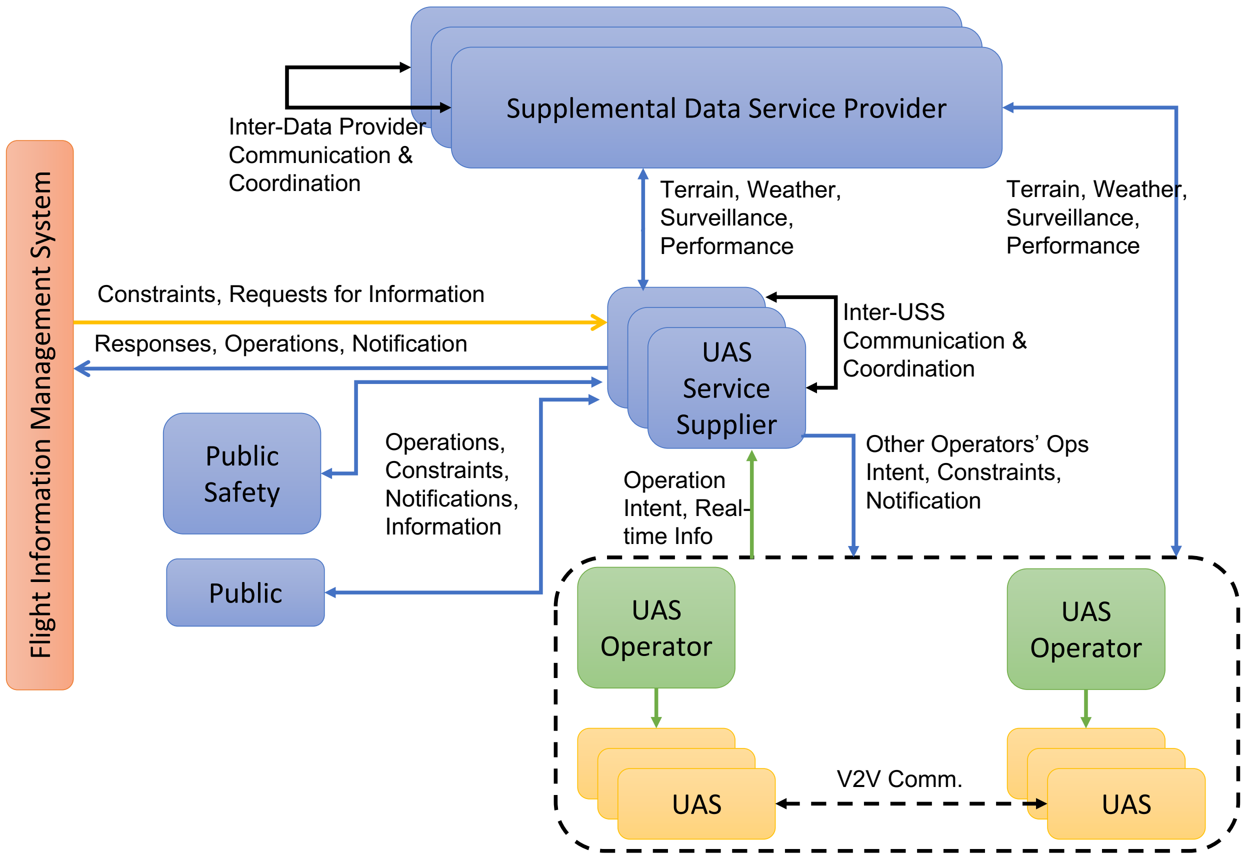

Figure 2.1. UTM Notional Architecture [8]

- **UAS Operator**: The operators of the aerial vehicles. They can be either with visual line of sight (VLOS) or beyond visual line of sight (BVLOS) from the aerial vehicles. They can be either human operators or autonomous systems monitoring vehicle operations.

- **Public Safety/Public**: The involved ground communities or entities. They can access the UTM data to ensure safety and privacy.

- **Supplemental Data Service Provider (SDSP)**: The service providers provide extra information to help operators or USS ensure airspace safety. The example data include terrain information, weather information, and constraint information.

- **UAS Service Suppliers (USS)**: The service suppliers help the UAM operators review and ensure compliance with any regulatory or operational requirements. They also provide real-time information to UAM operators to ensure airspace safety. Finally, they archive all flight data for analysis, regulatory, and Operator accountability purposes.

- **Flight Information Management System (FIMS)**: The FIMS is the gateway between the UTM and FAA systems. It can exchange airspace information, operational constraints, or other regulatory information to ensure airspace safety.

After several revisions and amendments, the 14 Code of Federal Regulation (CFR) Part 107 provides guidelines and rules for regulating small UAS operations by operators with various flight intents and skills [8], [26]. The CFR Part 107 categorizes pilots into two types, a certified remote pilot and a recreational pilot [27]. There are fewer restrictions on recreational UAS or responsibility on recreational remote operators. But, recreational operators can only operate their UAS in designated areas, which segregate the traffic of recreational UAS from others [8], [27]. For example, recreational pilots can only fly their vehicles in uncontrolled airspace and less than 400 foot. The certified remote pilots can fly VLOS, BVLOS, and in controlled airspace with Airspace Authorizations if their UAS also satisfy certification regulations [8], [27]. For example, UAS have to equip with the Remote ID system to broadcast (1) the vehicle's identification number, (2) the locations of the ground station and the vehicle, (3) a time mark, and (4) an indication of the emergency status [28].

Before the flight, the certified remote operators should file a flight intent with the flight path and the time through each waypoint. If there are conflicts between flight intents, the certified remote pilots have to negotiate and generate tactically deconflicted flight intents with the help of the USS. During the flight, the vehicles report locations and statuses back to the certified remote pilots and the USS. The USS is responsible for monitoring the airspace and ensuring the conformance of the flight intents. If there is any contingent event affecting several UAS operations in the far enough future, the USS negotiates with the impacted remote pilots for generating new conflict-free flight intents. After the vehicles land, the USS should archive the flight intent and the flight data for future analysis and study purposes [8].

The USSs have to monitor the air traffic based on the reported telemetry data from the UAS operators or UAS according to the UTM Conops [8]. Hence, the GPS signal interference directly influences the errors of telemetry data and impacts the capabilities of USS airspace monitoring. Additionally, the USS relies on the real-time air traffic information and stakeholders' requirements to generate new flight intents for tactical or strategical deconfliction when new vehicles enter the airspace or any contingent events happen [8]. The USSs have some leverages to control the air traffic operations.

2.2 Urban Air Mobility

The UAM includes various types of aerial operations in metropolitan areas. For regulating novel air operations in populated areas, the FAA and NASA published the UAM Concept of Operations [9], [10] to depict how the UAM operations will happen under different UAM Maturity Levels (UML). The FAA's Conops constructs a UAM notional architecture (Fig. 2.2) based on the UML-1 scenario, which focuses on the late-stage certification testings and operational demonstrations in a limited environment [9]. NASA's UAM Coonops focuses on the UML-4 scenario, which focuses on the medium density and complexity operations with collaborative and responsible automated systems [10]. The notional architecture identifies several stakeholders and their responsibilities as follows.

- **UAM Aircraft**: Aircraft that provide aerial services, like passenger transportation and freight delivery. Additionally, the aerial vehicles might have diverse mission profiles and flight characteristics. For example, the Joby S2 vehicle is a two-seat electric vertical take-off and landing (eVTOL) [29] with a cruise speed of 200 mph and a design range of 200 miles. The NASA X-57 Maxwell demonstrator is a fully electric conventional take-off and landing (CTOL) vehicle [30]–[32]. Both configurations could be suitable for UAM-related missions, but they have different design concepts and mission profiles.

- **UAM Operator**: The UAM operators operate the UAM vehicles for providing aerial services. They are responsible for communicating with other stakeholders and ensuring airspace safety.

- **USS**: The UTM Service Suppliers need to communicate with the UAM transportation systems to share critical information for ensuring airspace safety and efficiency.

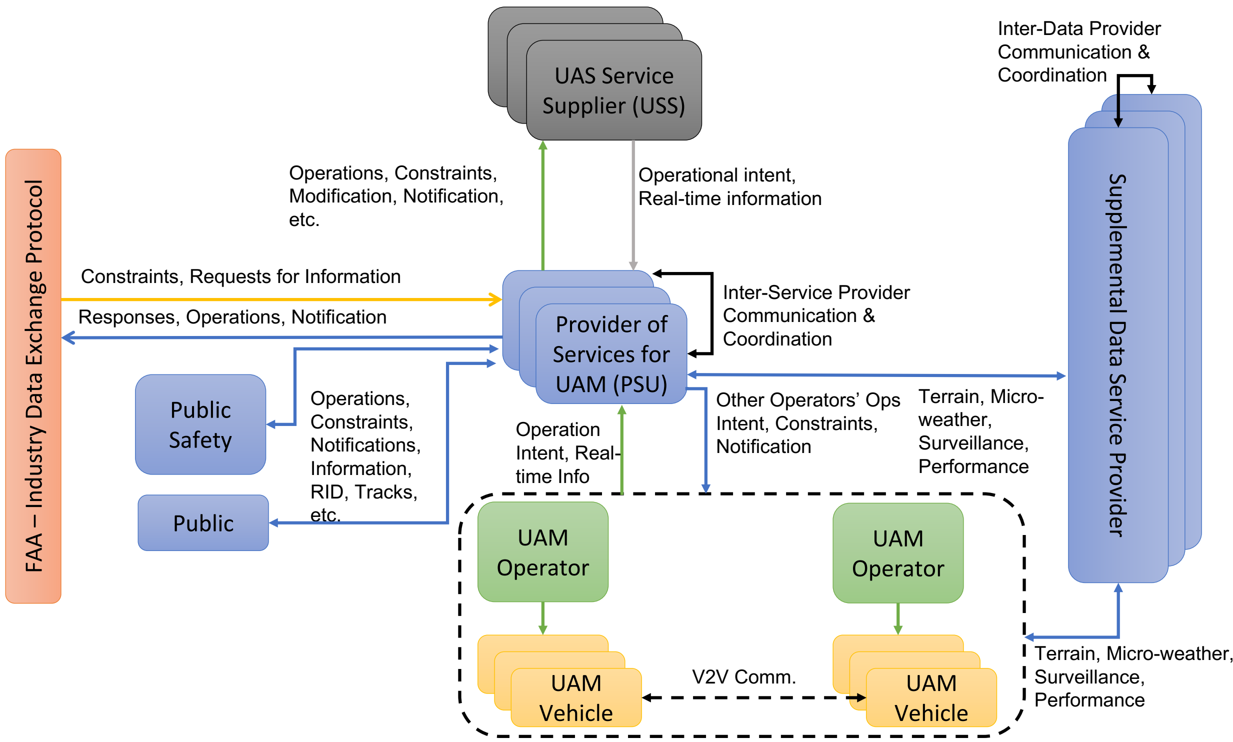

Figure 2.2. UAM Notional Architecture [9]

- **SDSP**: The SDSP from the UTM notional architecture can provide their services to the UAM stakeholders. For example, the micro-weather and terrain information is critical for both UAS and UAM aircraft to ensure safety.

- **Public Safety/Public**: The general public or law enforcement agents should have the right to be aware of the UTM and UAM operations. Additionally, due to the higher maximum take-off weights of the UAM aircraft than the small UAS, the UAM aircraft might generate more noise and create higher safety risks to local communities. Hence, it would be critical to ensure a smooth integration of UAM operations in local communities.

- **Provider of Services for UAM (PSU)**: The PSU has a similar role and responsibility as the USS from the UTM notional architecture. The PSU are responsible for helping airspace users communicate and share flight intents. The PSU aid the UAM operator in creating a conflict-free flight intent. They also monitor the UAM operation to ensure conformance with the submitted flight intent. They are responsible for helping the UAM operators to generate emergent flight intents for resolving any contingent events.

- **FAA — Industry Data Exchange Protocol**: The data gateway ensures a smooth and secured data exchanging between the systems of the UAM and FAA.

For realizing NASA's UAM vision, NASA holds the AAM National Campaign for building up discussion platforms between public and private sectors [33], [34]. According to the published documentation and the FAA's Conops, the PSU plays roles during the pre-flight, the in-flight, and the post-flight phases. Additionally, the UAM aircraft should only fly in the designated UAM corridors.

During the pre-flight phase, the PSU help the UAM operators generate a conflict-free flight intent through a series of corridors [9]. If any parts of the flight path enter controlled airspace, the PSU help the UAM operators file the flight intent to the FAA for receiving the authentication of entering the controlled airspace [9]. During the in-flight phase, the UAM operator is responsible for sending the flight telemetry information back to the PSU for ensuring the flight conformance to the submitted flight intent [9]. The PSU monitor the airspace and listen to the requests from the FAA, the UAM operators, and the general public [9]. If there is any significant change to the airspace statuses, the PSU shall collaborate with the UAM operators to generate emergent flight intents for resolving contingent events [9]. After the flight, the PSU archives the flight intents and the flight data for future analysis and study purposes [9].

The PSU from NASA's UAM Conops has a similar role as the USS from the FAA's UAM Conops. NASA's UAM Conops focuses on a scenario with more matured UAM technologies. The PSU need to help UAM operators generate flight intents, ensure flight conformance to the flight intents, and archive the flight data even if some UAM aircraft are fully autonomous or remote-pilot [10].

The PSU from both UML-1 and UML-4 scenarios have to (1) help the UAM operators generate the flight intent, (2) monitor the airspace condition, ensure the conformance to the flight intent, (3) listen to emergent requests from the UAM stakeholders, and (4) archive the flight data [9], [10]. Additionally, the PSU should (1) identify if a contingent situation arises and (2) help the UAM operators generate emergent flight intents for resolving the contingent events. The PSU have the responsibility for ensuring airspace safety and some leverages for regulating the UAM traffic.

2.3 National Airspace System

The National Airspace System (NAS) is a complicated and critical system for ensuring airspace efficiency and safety. It embraces controlled airspace and uncontrolled airspace with proper regulations and equipment for air traffic regulations. Figure 2.3 illustrates the airspace classes [35], [36], in which every airspace class except Class G is the controlled airspace. Most of the UTM traffic is in the Class G airspace. And, the UTM traffic can enter the controlled airspace around airports with Airspace Authorizations. Additionally, the UAM traffic should not enter the Class A airspace. However, the UAM traffic can enter other controlled airspace depending on mission requirements and with authorizations.

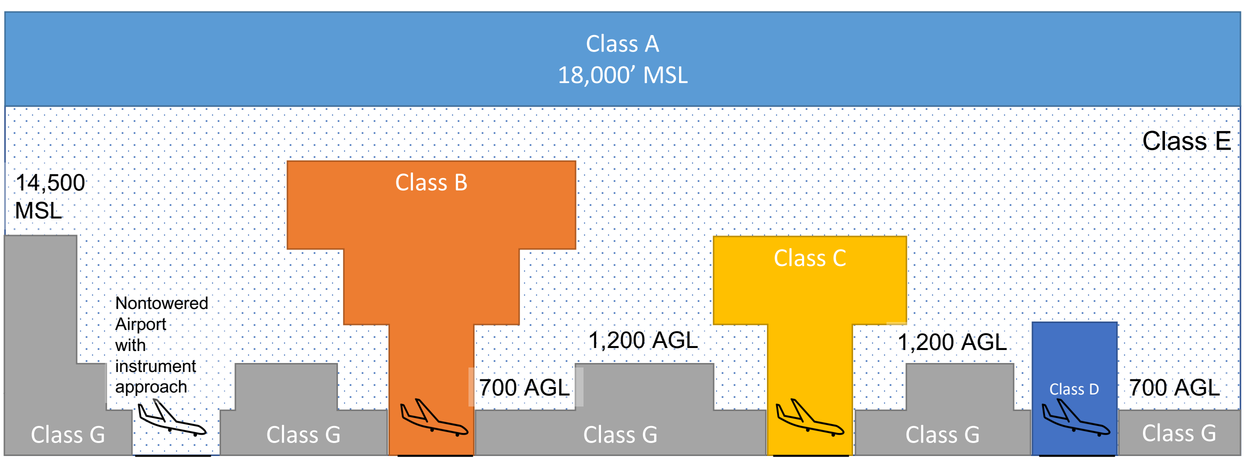

Figure 2.3. Airspace Classes Illustration

In the controlled airspace, the Air Traffic Control system oversees and regulates air vehicle operations. John Hansman et al. summarized how the Air Traffic Control (ATC) systems operate [21, Ch. 13]. The ATC system includes levels of control authorities for long-term, near-term, short-term, and real-time traffic prediction, traffic condition assessments, and traffic management. For real-time traffic management, there are three sectors regulating air traffic and ensuring airspace safety.

- **Air Traffic Control Tower (ATCT)**: The ATCT regulates the air traffic around airport areas and includes departure and arrival operations.
- **Terminal Radar Approach Control (TRACON)**: When the air traffic is too far away from airport areas, the TRACON takes over the traffic and provides guidelines and comments for ensuring airspace safety. The TRACON usually includes active surveillance radar for air traffic monitoring. Additionally, TRACON provides services to low-altitude aircraft with VFR or IFR flight plans.
- **Air Route Traffic Control Center (ARTCC)**: When the aircraft leaves from lower altitudes, the ARTCC takes over the air traffic and provides navigational services. The ARTCC has similar responsibilities as the TRACON. But, the ARTCC is responsible for high-altitude airspace.

The U.S. airspace consists of multiple airspace sectors. And the airspace sectors have one or more control authorities managing air traffic. Figure 2.4 shows the map of ARTCC sector distributions. The shapes and sizes of the ARTCC sectors depend on the amount of traffic flow and the traffic pattern. Similarly, TRACON consists of multiple airspace sectors for providing navigational services to air traffic. Regardless of the ARTCC sectors or the TRACON sectors, they collaborate and communicate for ensuring airspace efficiency and airspace safety.

The performance of air traffic controllers in ARTCC or TRACON decreases with an increasing number of aircraft in the sectors. Hence, there is a need to have the airspace sector capacity for traffic planning and managing. The ARTCC and TRACON sectors can collaborate and avoid accumulating air traffic in one airspace sector and endangering airspace safety. Because the human factor is the main bottleneck for airspace sector operations, the stream of research focuses on predicting and assessing how air traffic patterns create workloads of air traffic controllers. Majumdar et al. [22], [38] used simulation models for predicting the air traffic controller workloads and conducted surveys for adjusting model

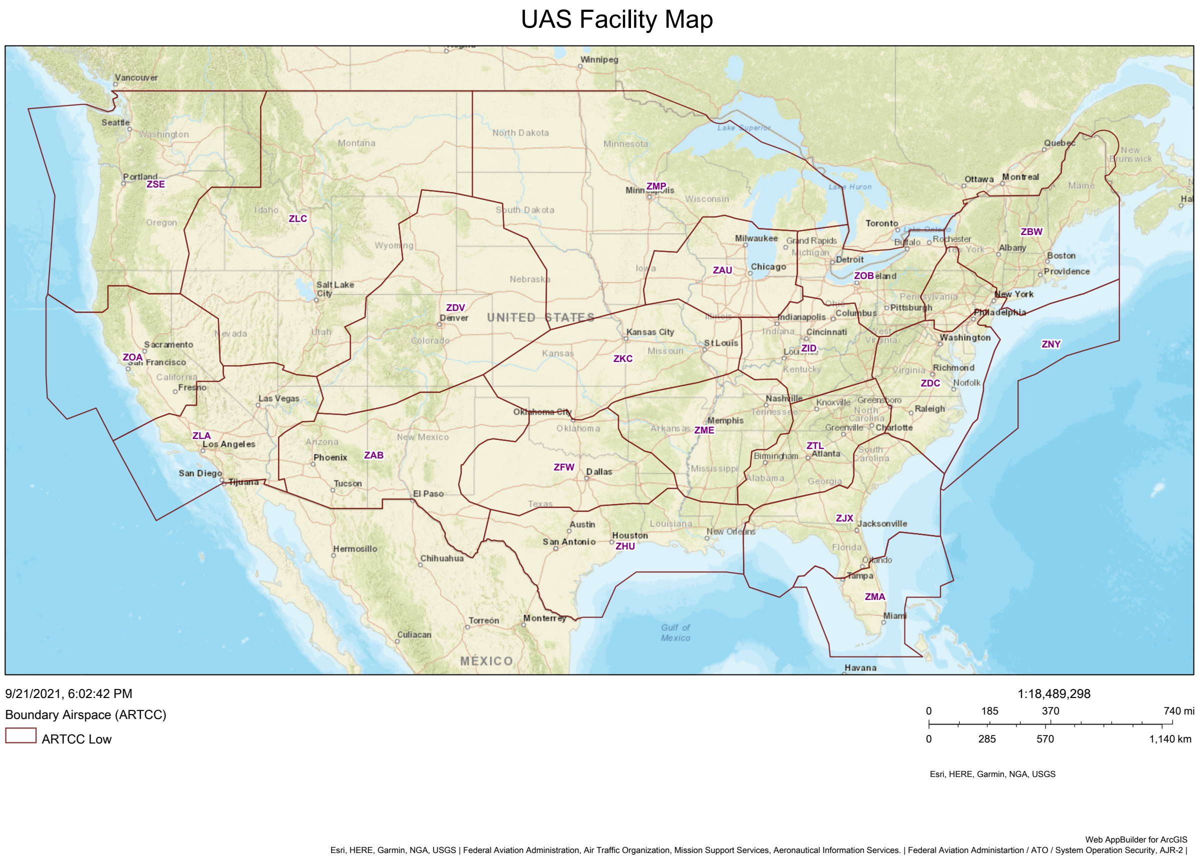

Figure 2.4. The U.S. ARTCC Sector Geographical Distribution [37]

parameters. However, their methodology may not apply to the AAM traffic management system. The new types of air vehicles, novel concepts of operations, and increasing levels of air vehicle autonomy can create different types of workloads for air traffic controllers. Additionally, air traffic controllers may longer be the bottleneck for airspace sector operations due to the introduction of autonomous functions in traffic management systems.

The future AAM traffic management system should include an actor having similar responsibilities as the ATC system. Based on the released Conops, the USS and PSU manage and monitor UAS or UAM traffic. Considering various AAM vehicles and diverse mission profiles, there is a need for having metrics assessing airspace safety for the AAM traffic management systems. The following section will review the recently developed methodologies for traffic safety assessment.

2.4 Airspace Traffic Safety Assessment

Prior works from various research fields have tried to quantify traffic complexity and safety by using physics-related quantities. For example, in traffic flow theory, Miura et al. discretized a 1-D highway, calculate the correlations among the relative distance between vehicles and their speeds, and derived the traffic entropy and temperature [39]. Kerner et al. considered the ground traffic on a highway as a compressible continuous steady flow [40] and obtained the traffic temperature and the traffic entropy. Reiss et al. discussed why the maximum entropy principle is preferable for inferencing the probability distribution of vehicle states in a traffic flow [41]. They subsequently derived the traffic temperature and the traffic pressure with the Lagrangian multiplier technique [41]. However, these research efforts are not directly applicable to real-world air traffic systems. They either rely on continuous and equilibrium flow assumptions or require the system to be 1-D, which the 3-D air traffic system cannot satisfy either assumption.

Instead of applying thermodynamics to air traffic systems, several researchers attempt to adopt thermodynamic concepts to derive entropy value to quantify the air traffic system complexity. Michael Lowry proposed how the entropy metric can be applied to the air traffic control problem [42]. Daniel et al. used a different approach by creating a hypothetical velocity field to match the known vehicle statuses of all aerial vehicles in airspace [43]. They formulated an optimization problem to minimize the difference between the actual velocity vectors reported by the aircraft and a hypothetical velocity field at the reported aircraft locations. Their formulation included constraints to ensure the continuality of the velocity field. Then, they defined the complexity of the airspace as low if the optimization problem had a feasible solution. Ishutkina et al. built on this idea and used the topological entropy of the hypothetical velocity field to quantify airspace complexity [44]. However, these techniques do not apply to UTM and UAM related problems. The high-density traffic requires excessive computational resources to solve the hypothetical velocity fields within an acceptable duration.

The traffic management problem is one type of centralized multi-agent control problem [45]–[47]. Hamidi et al. used a multi-agent system framework to analyze and improve ground transportation systems [45] although their work cannot apply to the air transportation system. Hill et al. developed a distributed air traffic control with a multi-agent system architecture [46]. Their work adopted Game Theory to enable the distributed agents to collaborate and converge to unselfish, efficient, and conflict-free solutions [46]. Brittain et al. generated a reinforcement learning model for the distributed agents [47]. Their model enables the distributed agents to avoid collisions [47]. Although both works do not include potential wind perturbations and location measurement errors, which are common environmental perturbations in urban areas, they demonstrate that there might have some metrics from the multi-agent control field for assessing airspace complexity.

Control systems research commonly adopts the information entropy metric to identify the potential trade-off between controller performance and communication requirements. However, the relevant methodologies have not been applied to the airspace complexity assessment problem yet. Weidemann et al. and Touchette et al. used information theory to analyze the communication requirements of a discrete or continuous system [48], [49]. And Li et al. proposed a framework to analyze the relationships between communication requirements and state control uncertainty for a cyber-physical system [50]–[57]. Colonius et al. used the topological entropy to create a mathematical foundation for identifying the minimum invariant entropy and stabilizing an unstable system [58]. Christoph Kawan discussed the relationship between invariant entropy and minimum data rate requirements [59]. Extending the communication channel from sensors to the computed control output can derive both the computational requirements of a controller and the communication requirements between sensors and a controller. Finally, Tanaka et al., Tatikonda et al., and Kostina et al. examined the trade-off between the controller performance and the communication requirements of a linear quadratic Gaussian controller [60]–[62]. With the maximum acceptable cost in the optimal control context, their approaches identified the minimum communication requirements for achieving the desired control performance. These methodologies might help air traffic control problems quantify air traffic conditions and assess communication requirements.

2.5 Summary & Research Gap

Tables 2.1 and 2.2 summarize the identified gaps from the literature review. The literature review includes five distinct topics as follows.

1. **En-Route Airspace Sector Capacity Estimation**: The related research focuses on assessing en-route airspace sector capacity in the NAS. The recent studies show that the bottleneck of limiting air traffic throughput without sacrificing airspace safety is the air traffic controller workloads. Hence, these studies focus on developing frameworks for identifying correlations between traffic throughput, traffic patterns, and workloads of traffic controllers. However, their methodologies are not applicable for AAM traffic. There is no historical data to identify the correlations of air traffic controller workloads and novel mission profiles.

2. **Physics-related Quantities for Quantifying Traffic Complexity**: Regarding 1-D highway traffic as a 1-D continuous flow, the related research derived the physics-related quantities for analyzing highway traffic. However, their methodologies do not apply to air traffic because aerial traffic is a 3-D flow and violates the continuous flow assumption.

3. **Topological Entropy for Quantifying Airspace Complexity**: This methodology generates a hypothetical velocity field based on known vehicle statuses. Then, it applies the topological entropy calculation based on a hypothetical velocity field. However, this methodology can be unstable with wind perturbations and vehicle state measurement errors.

4. **Multi-agent system for Traffic Problems**: Several research groups adopted the methods for a multi-agent system control problem to develop distributed traffic management models. However, the recent related works usually ignored the potential environmental perturbations of the vehicle operations.

5. **Information Entropy & Control Theory**: Multiple research teams attempt to derive the correlations between communication capacities and controller performances

of Cyber-Physical systems. However, some works do not consider the multi-agent problem or the air traffic management problem. Also, their methodologies have not been applied to quantify airspace complexity.

The future AAM traffic includes high density and highly diverse traffic in urban areas, where strong wind perturbations and high measurement errors are more likely to happen. Hence, there is a need to identify airspace complexity metrics, which consider environmental disturbance, various types of AAM aircraft, and diverse flight missions. The aforementioned research topics provide methodologies to solve parts of the problem. And, it lacks a comprehensive study considering the identified factors.

Table 2.1. Summary of Literature Review and Identified Gaps Part 1

Topic	Literature	Proposed Methodology	Gaps
En-Route Airspace Sector Capacity Estimation	[22], [38]	• Use simulations to assess ATC workloads under different traffic patterns • Use survey for tuning simulation parameters	• Air traffic controllers may not be the bottleneck with the introduction of autonomous systems • Diverse mission requirements and profiles can create different work tasks and loading
Physics-related Quantities for Quantifying Traffic Complexity	[39]–[41]	• Analyze highway traffic as a 1-D continuous traffic flow and derive physics-related quantities	• AAM traffic is a 3-D non-continuous flow problem, which violates their basic assumptions • Their methodologies do not include the impacts from wind perturbations or state measurement errors
Topological Entropy for Quantifying Airspace Complexity	[43], [44]	• Use an optimization approach to create a hypothetical velocity field to match with known vehicle statuses • Quantify airspace complexity with the topological entropy analyzing the hypothetical velocity field	• The optimization problem is computationally expensive with high-density urban AAM traffic • The methodology is unstable with wind perturbations and measurement noises

Table 2.2. Summary of Literature Review and Identified Gaps Part 2

Topic	Literature	Proposed Methodology	Gaps
Multi-agent System for Traffic Problems	[45]–[47]	• Develop models for distributed traffic managements with multi-agent system architectures	• Does not consider environmental perturbations
Information Entropy & Control Theory	[48], [49], [51]–[60]	• Identify relationships between controller performances and communication requirements	• Some methodologies do not apply to multi-agent system problems • These methods have not been applied to quantify airspace complexity

3. ENTROPY-BASED SYSTEM UNCERTAINTY ESTIMATION & MANAGEMENT

The previous chapter identifies gaps between research questions and current research progress. In this study, the proposed entropy-based traffic management framework and two metrics for quantifying airspace status should fill the identified gaps. The following section will illustrate the framework. Subsequently, the derivations of the two metrics are presented.

3.1 Entropy-based Traffic Management Framework

Section 1.3 lists the research questions of this study. Before defining the metrics to assess airspace safety levels under various sources of uncertainty, it is important to identify the information flow between air vehicles and air traffic authorities. The information flow should illustrate the available information of air vehicles and air traffic authorities at each time step. Moreover, it should present the sequence of actions of air vehicles and air traffic authorities.

In this study, airspace is composed of several airspace sectors. In each airspace sector, there are one or more control authorities, which are named air traffic authorities (ATA), monitoring and managing air traffic. The ATAs do not have active sensing radar for airspace surveillance. The ATAs passively monitor air traffic by receiving telemetry data from air vehicles. Therefore, the air vehicles inside an airspace sector periodically broadcast their flight telemetry data to neighboring vehicles and the ATAs. The vehicle telemetry data are inaccurate due to the message dropping, GPS signal interference, or wind perturbations. The ATAs should also identify any near-miss events, which occur when two vehicles are too close, and take actions to resolve near-miss events.

Figure 3.1 shows the flowchart of the proposed information flow of the air traffic management framework. The diamond shape in the figure shows information, while the square box presents actions. By starting from the air vehicle box, an air vehicle requires three pieces of information to estimate its state. The three pieces of information are the air vehicle dynamic model, the collision avoidance model, and the localization system specification. The air vehicle dynamic model should describe the vehicle behaviors under the nominal condition. The collision avoidance model illustrates vehicle responses to avoid mid-air collision against other vehicles or obstacles. And the localization system specification describes the location estimation accuracy. The air vehicles use these pieces of information to generate air vehicle telemetry data with uncertainty estimations.

The ATA is responsible for monitoring the airspace sector. And it receives the vehicle telemetry data from all vehicles in the airspace. The ATA also predicts the states of air vehicles in the airspace sector with weather information and assumptions that all vehicles follow the nominal operations. Moreover, the ATA fuses the predicted vehicle states with the received telemetry for generating the estimated vehicle states with lower uncertainty levels. Subsequently, the ATA evaluates airspace metrics based on the estimated air vehicle telemetry. The following sections will introduce the airspace metrics. Finally, the ATA determines actions to manage the air traffic for ensuring airspace safety and compliance to given airspace regulations. The ATA's actions should include sending commands to certain air vehicles to avoid adverse conditions.

3.2 Statistical Physics, Information Theory, and Kalman Filter

Rudolf Clausius proposed the concept of entropy for describing the observations of irreversible energy flows [63]. The application of this concept to statistics roots from the work of Ludwig Boltzmann [64] in 1866. Entropy can explain ample physics phenomena from classical physics, statistical mechanics, and quantum physics [65]. In 1948, Claude Shannon adopted this concept to communication technologies [66], which built up the foundation of modern communication theory. His work quantified the maximum communication channel capacity and the information entropy of transmitted information [66]. Although the term "information" creates multiple discussions about whether this theory is applicable beyond communication research, Prof. Leon Brillouin published a book and reviewed the successful applications of information theory in physics fields [67]. In 1957, Jaynes proved that information entropy and statistical entropy are equivalents [68]–[70]. This section consists of two parts for building the foundation of the derivations of the proposed metrics. The first part

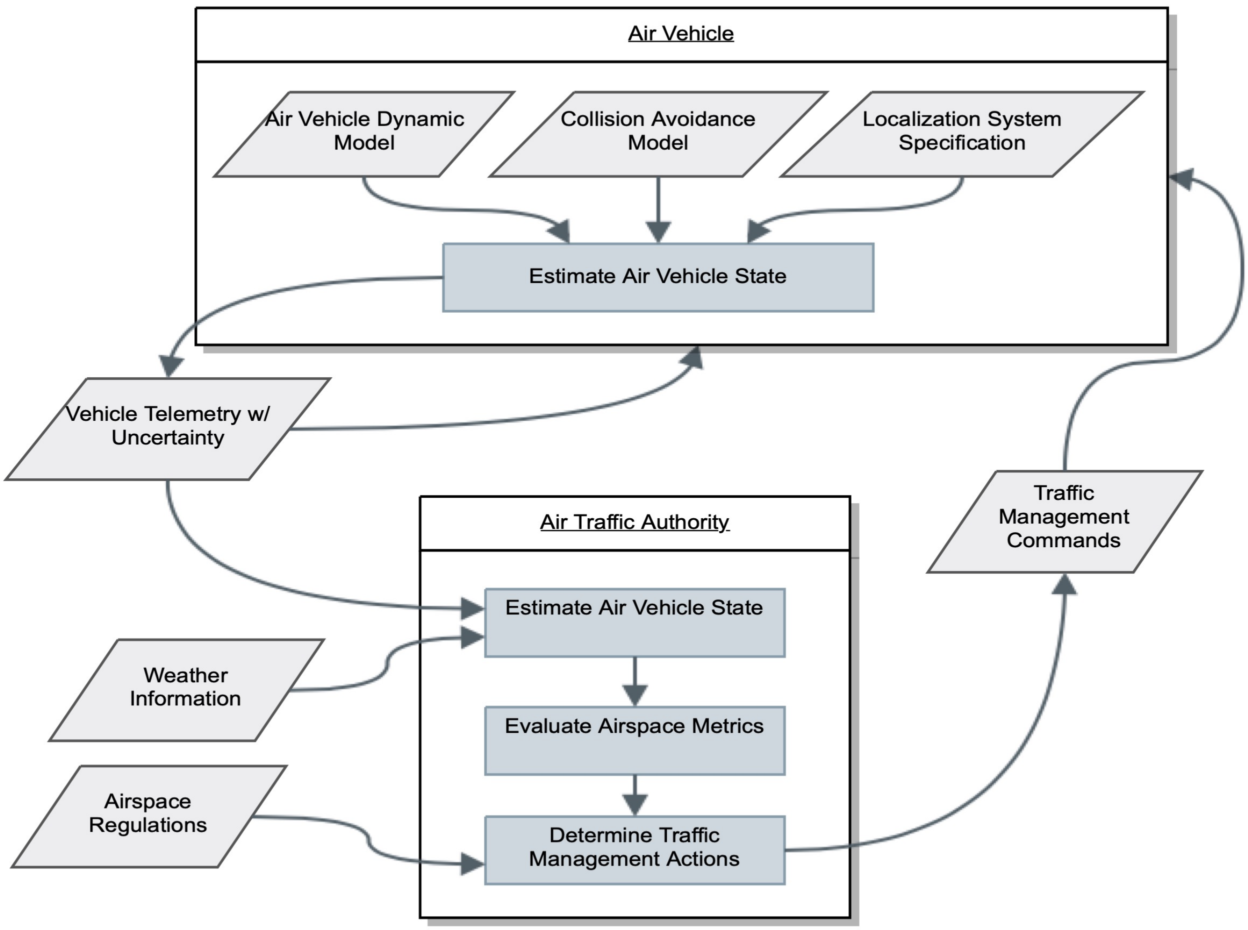

Figure 3.1. Information Flow of Air Traffic Management Framework

reviews Jaynes' work. The second part revisits the derivation of the Kalman filter and the related information entropy.

Two sets of parameters, which are micro-parameters and macro-parameters, can describe a physics system. For a physics system including multiple particles, there are two ways to describe the system's behaviors. Firstly, researchers can track the positions and velocities of each particle in the system. The parameters related to the state of each particle are the micro-parameters. On the other hand, macro-parameters describe the collective system properties, such as temperature, pressure, volume, etc. Macro-parameters are not associated with any specific particle, but they are related to the collective behaviors of all particles. Tracing the state of every particle in the system is infeasible due to the large number of particles. The only practical way to describe the system is by using the statistical properties of all particles in the system. For example, temperature and pressure are common statistical properties. These statistical properties are the macro-parameters of the system. Both macro-parameters and micro-parameters can describe the behaviors of the systems. The micro-parameters can illustrate the fundamental interactions between the particles, while the macro-parameters can capture the collective behaviors of the systems.

Jaynes' work in 1957 [68] showed that using the maximum entropy principle can derive a fundamental state distribution function by formulating an information entropy maximization problem (Eq. 3.1). The objective function in the information entropy maximization problem (Eq. 3.1a) shows the information entropy of the state distribution function ($P(\mathbf{x})$) and is scaled by the Boltzmann constant (k_B). And $\mathbf{x}_j$ is a discrete random variable representing the concatenated states of all particles. The subscription j indicates one of the possible drawn outcomes from the probability function.

The maximization problem also includes the constraints for ensuring that (1) the state distribution function is a legit probability function (Eq. 3.1b) and (2) the expectation values of mapping functions match with the measured values, such as pressure or temperature (Eq. 3.1c). $\mathscr{I} \in [1, I]$ indicates all expected system quantities, while the mapping function ($f_i(\mathbf{x}_j)$) maps the instance of particle states to the system quantity (i) value. $\langle f_i(\mathbf{x}_j)\rangle$ indicates the expected value of the mapping function.

$$\max_{P(\mathbf{x})} -k_B \sum_j P(\mathbf{x}_j) \ln P(\mathbf{x}_j) \tag{3.1a}$$

subject to

$$\sum_j P(\mathbf{x}_j) = 1 \tag{3.1b}$$

$$\sum_j P(\mathbf{x}_j) f_i(\mathbf{x}_j) = \langle f_i(\mathbf{x})\rangle, \forall i \in \mathscr{I} \tag{3.1c}$$

The Lagrange multiplier method can solve this maximization problem. Equation 3.2 shows the generic solution of the state distribution in terms of Lagrangian multipliers (μ_i) and the mapping functions ($f_i(\mathbf{x}_j)$). $\boldsymbol{\mu}$ is the collection of the Lagrangian multipliers in a vector form ($\boldsymbol{\mu} = (\mu_0, \mu_1, \cdots)$). To satisfy the normalization constraint in Eq. 3.1b, Jaynes [68] derived μ_0 and defined a partition function ($Z(\boldsymbol{\mu})$) in Eq. 3.3. In statistical physics, the partition function depends on the particle state distribution and is associated with the number of randomly drawn states (j) to achieve the same expected system quantity, which is shown in the derived partition function in Eq. 3.3.

The Lagrange multiplier method also shows that every system quantity has a conjugated Lagrangian multiplier. Equation 3.4a is from Eq. 3.1c and shows the relationships between the expected system quantity and the Lagrangian multiplier. The value of the expected value function is the derivation of the partition function with the conjugated Lagrangian multiplier. Equation 3.4a also shows that the partition function includes the system properties, which are the collective behaviors of the constituted particles.

Eq. 3.4b shows the relationship between physics entropy (S), Lagrange multipliers, and the expected values of the mapping functions. Physics entropy is one of the properties of the system and only depends on the Lagrangian multipliers and the values of the expected mapping functions. From information perspective, physics entropy is information entropy related to the state distribution function and is scaled by the Boltzmann constant (Eq. 3.4b). Physics entropy relies on the collective behaviors of the systems, while information entropy depends on the state distribution of the constituent particles. The ratio of the physics entropy to the information entropy is just the Boltzmann constant.

$$P\left(\mathbf{x}_j|\boldsymbol{\mu}\right) = \exp\left(-\mu_0 - \sum_{i\in\mathscr{I}} \mu_i f_i\left(\mathbf{x}_j\right)\right) = \frac{1}{\exp\left(\mu_0\right)} \exp\left(-\sum_{i\in\mathscr{I}} \mu_i f_i\left(\mathbf{x}_j\right)\right) \tag{3.2}$$

$$Z\left(\boldsymbol{\mu}\right) = \sum_j \exp\left(\sum_{i\in\mathscr{I}} -\mu_i f_i\left(\mathbf{x}_j\right)\right) = \exp\left(\mu_0\right) \tag{3.3}$$

$$\begin{aligned} \langle f_i\left(\mathbf{x}\right)\rangle &= \sum_j P\left(\mathbf{x}_j\right) f_i\left(\mathbf{x}_j\right) \\ &= \frac{1}{Z\left(\boldsymbol{\mu}\right)} \sum_j \exp\left(\sum_{i\in\mathscr{I}} -\mu_i f_i\left(\mathbf{x}_j\right)\right) f_i\left(\mathbf{x}_j\right) \\ &= -\frac{\partial}{\partial \mu_i} \ln Z\left(\boldsymbol{\mu}\right), \forall i \in \mathscr{I} \end{aligned} \tag{3.4a}$$

$$S = k_B \left(\mu_0 + \sum_{i \in \mathscr{I}} \mu_i \left\langle f_i\left(\mathbf{x}\right)\right\rangle \right) = k_B \left(-\sum_j P\left(\mathbf{x}_j\right) \ln P\left(\mathbf{x}_j\right) \right) \tag{3.4b}$$

Although the derivation only uses discrete random variables (x_j), the aforementioned derivations can be applied to continuous variables without modification except for Eq. 3.4b [69]. Eq. 3.4b shows that physics entropy equals the multiplication of the information entropy and the Boltzmann constant. However, by replacing the probability function $(P(x_j))$ with a probability density function $(p(x_j))$, Eq 3.4b is not invariant under coordinate transformation and is not strictly positive. Jaynes discretized a continuous random variable and applied the information entropy equation [69] for addressing this issue. The information entropy of continuous random variables follows Eq. 3.5 [69], where n is the number of discretization cells, and $m(\mathbf{x})$ shows the distribution of the discretization cells. Finally, multiplying Eq. 3.5 with a Boltzmann factor results in the physics entropy for continuous random variables.

$$S_{info}^{C} = \ln n - \int p\left(\mathbf{x}\right) \ln \left(\frac{p\left(\mathbf{x}\right)}{m\left(\mathbf{x}\right)} \right) d\mathbf{x} \tag{3.5}$$

$$S = S_{info}^{C} k_B \tag{3.6}$$

The number of particles that a parameter is associated with can determine if it is a micro-parameter or a macro-parameter. For example, the state vector $\mathbf{x}_j$ from the previous deviations is a micro-parameter because each element in the state vector only relates to one dimension of the state of one particle. On the other hand, scientists usually set the system quantity mapping function as the Hamiltonian function, which represents the system's total energy and depends on the collective behaviors of all particles. Hence, the Hamiltonian function and the associated Lagrangian multiplier are macro-parameters.

Macro-parameters summarize properties of air traffic in airspace and are beneficial to decision-makers of airspace for assessing airspace-related policies and monitoring airspace statuses. From the ATA's perspective, the traffic management problem is a multi-agent control problem. The air vehicles in the airspace are the constituted agents. And the goal of the ATA is to control the system to the desired state. Due to the high dimensions of the system state vector, summarizing the system status of a multi-agent system is difficult. If the goal of a study is to understand the collective behaviors of the whole system, macro-parameters can reduce the difficulties by reducing the number of variables, which describe the behaviors of a system. Since both physics systems and multi-agent systems compose multiple particles/agents, researchers can use Jaynes' derivation to derive macro-parameters associated with a multi-agent system. Then, the macro-parameters related to air traffic can summarize properties of airspace and help decision-makers assess different airspace management options.

Researchers can use Jaynes' derivation to identify a probability distribution about the statuses of the constituted particles. On the other hand, due to the measurement uncertainty and wind perturbation, the exact locations of air vehicles in the airspace are unknown. Hence, researchers can use the same approach to derive the probability distribution about the statues of air vehicles in the airspace. The derived probability distribution should match with the probability distributions from other algorithms in control theory.

The Kalman filter is a common algorithm for estimating system states under state measurement noises and environmental perturbations. The Kalman filter generates expected system states with a corresponding covariance matrix for describing estimation uncertainty. The definition of an estimation state error is the difference between a true system state to an expected system state. The Kalman filter assumes that estimation state errors, measurement noises, and environmental perturbations independently follow multivariate normal distributions. The probability density function of the true state follows Eq. 3.7 with a given expected state vector ($\hat{\mathbf{x}}$). $\mathbf{P}$ is the covariance matrix of the estimation state errors, while $\mathbf{x}$ is the true system state. Afterwards, rearranging Eq. 3.7 to a form similar to Eq. 3.2 can identify the system quantity mapping functions.

$$\begin{aligned} p\left(\mathbf{x}|\hat{\mathbf{x}},\mathbf{P}\right) &= \det\left(2\pi\mathbf{P}\right)^{-\frac{1}{2}}\exp\left(-\frac{1}{2}\left(\mathbf{x}-\hat{\mathbf{x}}\right)^{T}\mathbf{P}^{-1}\left(\mathbf{x}-\hat{\mathbf{x}}\right)\right) \\ &= \exp\left(-\frac{1}{2}\ln\left(\det\left(2\pi\mathbf{P}\right)\right)-\frac{1}{2}\left(\mathbf{x}-\hat{\mathbf{x}}\right)^{T}\mathbf{P}^{-1}\left(\mathbf{x}-\hat{\mathbf{x}}\right)\right) \end{aligned} \tag{3.7}$$

Rearranging the second term on the right-hand side of Eq. 3.7 based on the exponents of $\mathbf{x}$ results in Eq. 3.8. Subsequently, the definitions of the Lagrangian multipliers and mapping functions of the system quantities are shown in Eq. 3.9, where n_x is the number of elements in the state vector (x). The mapping functions and conjugated Lagrangian multipliers are micro-parameters because they depend on the state of one agent in the system.

$$p\left(\mathbf{x}|\hat{\mathbf{x}},\mathbf{P}\right)=\exp\left(-\frac{1}{2}\left(\ln\left(\det\left(2\pi\mathbf{P}\right)\right)+\hat{\mathbf{x}}^{T}\mathbf{P}^{-1}\hat{\mathbf{x}}\right)-\frac{1}{2}\mathbf{x}^{T}\mathbf{P}^{-1}\mathbf{x}-\left(-\hat{\mathbf{x}}^{T}\mathbf{P}^{-1}\mathbf{x}\right)\right) \tag{3.8}$$

$$\mu_0=\frac{1}{2}\left(\ln\left(\det\left(2\pi\mathbf{P}\right)\right)+\hat{\mathbf{x}}^{T}\mathbf{P}^{-1}\hat{\mathbf{x}}\right) \tag{3.9a}$$

$$\mu_{1,i}=-\sum_{j}\left(\mathbf{P}^{-1}\right)_{j,i}\hat{\mathbf{x}}_j,\forall i\in\left[1,n_x\right] \tag{3.9b}$$

$$\mu_{2,i,j}=\frac{1}{2}\left(\mathbf{P}^{-1}\right)_{i,j},\forall i\in\left[1,n_x\right],j\in\left[1,n_x\right] \tag{3.9c}$$

$$f_{1,i}=x_i,\forall i\in\left[1,n_x\right] \tag{3.9d}$$

$$f_{2,i,j}=x_ix_j,\forall i\in\left[1,n_x\right],j\in\left[1,n_x\right] \tag{3.9e}$$

$$Z\left(\boldsymbol{\mu}\right)=\exp\left(\mu_0\right)=\exp\left(\frac{1}{2}\hat{\mathbf{x}}^{T}\mathbf{P}^{-1}\hat{\mathbf{x}}\right)\det\left(2\pi\mathbf{P}\right)^{\frac{1}{2}} \tag{3.9f}$$

3.2.1 Traffic Entropy

Evaluating the statistical entropy from the Kalman filter requires the definition of discretization cells based on Eq. 3.6 and Eq. 3.5. The first term on the right-hand side of Eq. 3.5 is the number of discretization cells. And the second term is the Kullback-Leibler divergence, which is the relative entropy of the probability density function of the discretization cell distribution $m(\mathbf{x})$ to the probability density function of the state vector distribution $p(\mathbf{x})$.

There is a need for understanding the meanings of the discretization cell probability distribution and the state vector probability distribution before illustrating the meaning of the continuous statistical entropy. The discretization cell distribution shows the initial guess of the state vector distribution before any measurements. Without prior knowledge about the state vector distribution, it is logical to use the uniform distribution as the discretization cell distribution. In other words, the uniform discretization distribution says that the measurement of the vehicle state can be any value because no information can help the ATA estimate the air vehicle state.

The ATA can estimate the potential state of the air vehicle by using the Kalman filter algorithm with the vehicle state measurement data. The state vector distribution shows that the true vehicle state should be somewhere nearby the state measurement. Hence, the state vector distribution has a much lower vehicle state uncertainty than the discretization cell distribution, which has no prior knowledge about the air vehicle state. The ATA can gain some information from the vehicle state measurement and reduce the vehicle state estimation uncertainty. And the relative entropy can be used to quantify the information gain.

The continuous statistical entropy quantifies the uncertainty of system statuses by using the discretization cell distribution as the baseline. The extra information gained from the vehicle state measurement reduces the continuous statistical entropy because it reduces the uncertainty level of the vehicle state estimation. Hence, the continuous statistical entropy presents the uncertainty level of the vehicle state distribution.

Without any prior information, it is reasonable to assume the discretization cells uniformly distribute in the phase space of the state vector. The phase space is the space that all potential state vectors exist in. If the definition of the state vector includes both locations and velocities, the phase space is the product of the location space and the velocity space. Hence, the statistical entropy follows Eq. 3.10, where V_d is the volume of the phase space. And the last term in Eq. 3.10 is the differential entropy of a multivariate normal distribution. Even though the differential entropy could be negative, the first two terms in Eq. 3.10 can ensure that the statistical entropy is positive.

Eq. 3.10 defines traffic entropy, which equals statistical entropy. Researchers need to determine the number of discretization cells and the volume of phase space for applying Eq. 3.10 to quantify airspace uncertainty. The discretization cells should be small enough to have enough resolutions to present the probability distribution of the state vector. Additionally, the discretization cells should cover the entire phase space for including any potential vehicle state measurement. The phase space volume of an air vehicle is the product of the physical volume of airspace (V_{space}) and the velocity space volume ($\prod_{i\in[x,y,z]}(v_{i,\max}-v_{i,\min})$). Consequently, the total phase space volume equals the product of the phase space volume of an air vehicle through all vehicles in the airspace (Eq. 3.11), where AC indicates the set of the types of the air vehicle.

$$S_{\mathbf{x}|\hat{\mathbf{x}}} = k_B \left(\ln n - \ln V_d + \frac{1}{2} \ln \left(\det \left(2\pi e \mathbf{P} \right) \right) \right) \tag{3.10}$$

$$V_d = \prod_{ac\in AC} \left(V_{space} \times \prod_{i\in[x,y,z]} \left(v_{ac,i,\max} - v_{ac,i,\min} \right) \right) \tag{3.11}$$

This work illustrates the properties of the Kalman filter from statistical mechanics and information theory perspectives. From the statistical mechanics perspective, a Lagrange multiplier is a conjugate variable to the corresponding macro-parameter mapping function. Together, the macro-parameter mapping functions and the conjugated Lagrange multipliers can summarize the properties of the multi-particle system with fewer variables than the micro-parameters. From the Kalman filter perspective, the Lagrange multipliers and the system quantity mapping function from Eq. 3.9 are associated with each dimension of each constituted agent under a multi-agent system context. The system quantity mapping functions and the Lagrange multipliers are still micro-parameters, but it is possible to rearrange the system quantity mapping function to deduce macro-parameters. The next section shows the derivation of macro-parameters, which are analogous to energy and temperature from statistical mechanics.

Statistical Entropy Parameter Setting

Equation 3.10 should always be higher than zero since statistical entropy is always positive. However, the last term in Eq. 3.10 is the differential information entropy of a multivariate normal distribution. The last term can be negative if the uncertainty level of a multivariate normal distribution is low. For example, if a vehicle uses GPS measuring its location with measurement error last than 1 meter and the measurement error follows a multivariate normal distribution, the differential information entropy should be negative, as shown in Eq. 3.12.

$$\ln\det\left(\begin{bmatrix}\sigma_x^2 & 0 & 0\\ 0 & \sigma_y^2 & 0\\ 0 & 0 & \sigma_z^2\end{bmatrix}\right) = \ln\det\left(\begin{bmatrix}0.9 & 0 & 0\\ 0 & 0.9 & 0\\ 0 & 0 & 0.9\end{bmatrix}\right) = \ln\left(0.9^3\right) = -0.3162 \tag{3.12}$$

The number of discretization cells is critical for ensuring positive statistical entropy. Before using this metric, researchers should estimate the minimum covariance matrix and the size of phase space from their systems. The minimum number of discretization cells should be high enough to ensure the statistical entropy is positive.

3.2.2 Traffic Safety Severity & Traffic Temperature

In statistical mechanics, there is no restriction on how to construct a system quantity mapping function. Scientists commonly use the Hamiltonian of all particles as the system quantity. In a multi-agent system, the system quantities from the previous section relate to each dimension of the state vector. Hence, it is possible to rearrange system quantities to derive a new system quantity mapping function, which summarizes system behavior, reduces the dimension of interesting variables, and keeps the state distribution function from the Kalman filter intact.

The regrouped system quantities should present the collective behaviors of the system. This study uses the quadratic cost function from optimal control theory as a system quantity mapping function. First, the cost function quantifies the quality of system states and control actions into a single number. Furthermore, the quadratic cost function can preserve the estimated state distribution from the Kalman filter algorithm. Equation 3.13 shows the quadratic cost function ($J(\mathbf{x}|\mathbf{Q})$), where $\mathbf{Q}$ is a semi-positive matrix and determines the weights of each dimension of the state vector. And the conjugated Lagrangian multiplier of the quadratic cost function is defined as β, as shown in Eq. 3.14a.

$$J(\mathbf{x}|\mathbf{Q}) = \mathbf{x}^T \mathbf{Q} \mathbf{x} \tag{3.13}$$

To derive a macro-parameter related to the cost function, it is necessary to insert the multiplication of the cost function and the conjugated Lagrange multiplier in Eq. 3.8. The following section shows the procedure for inserting the multiplication in the probability function. Adding and subtracting the multiplication generate Eq. 3.14a. This operation does not influence the estimated state distribution because the last two terms in Eq. 3.14a cancel out each other. Then, the quadratic cost function can replace the last two terms to simplify Eq. 3.14a. Next, merging the second-order state vector term with the second-last term in Eq. 3.14a results in Eq. 3.14b.

Eq. 3.15 shows how the covariance matrix ($\mathbf{P}$) can include two new terms. The first term represents the uncertainty in terms of the quadratic cost function. And the second term ($\mathbf{P'}^{-1}$) shows the reciprocal residual covariance matrix. For evaluating the expected cost function value, the original covariance matrix ($\mathbf{P}$) in Eq. 3.9f replaces the new two terms from Eq. 3.15. Additionally, using Eq. 3.4a can derive the expected cost function as shown in Eq. 3.16b. Finally, since the statistical entropy only depends on the probability density function, the formation of the statistical entropy is the same as Eq. 3.10.

$$\begin{aligned}p\left(\mathbf{x}|\hat{\mathbf{x}},\mathbf{P},\mathbf{Q}\right) = &\exp\left(-\frac{1}{2}\left(\ln\left(\det\left(2\pi\mathbf{P}\right)\right)+\hat{\mathbf{x}}^T\mathbf{P}^{-1}\hat{\mathbf{x}}\right)-\frac{1}{2}\mathbf{x}^T\mathbf{P}^{-1}\mathbf{x}\right.\\&\left.-\left(-\hat{\mathbf{x}}^T\mathbf{P}^{-1}\mathbf{x}\right)+\beta\mathbf{x}^T\mathbf{Q}\mathbf{x}-\beta\mathbf{x}^T\mathbf{Q}\mathbf{x}\right) \qquad (3.14a)\\=&\exp\left(-\frac{1}{2}\left(\ln\left(\det\left(2\pi\mathbf{P}\right)\right)+\hat{\mathbf{x}}^T\mathbf{P}^{-1}\hat{\mathbf{x}}\right)-\frac{1}{2}\mathbf{x}^T\left(\mathbf{P}^{-1}-2\beta\mathbf{Q}\right)\mathbf{x}\right.\\&\left.-\left(-\hat{\mathbf{x}}^T\mathbf{P}^{-1}\mathbf{x}\right)-\beta J\left(\mathbf{x}|\mathbf{Q}\right)\right) \qquad (3.14b)\end{aligned}$$

$$\mathbf{P}^{-1}=2\beta\mathbf{Q}+\mathbf{P}'^{-1} \qquad (3.15)$$

$$Z\left(\boldsymbol{\mu},\beta\right)=\exp\left(\frac{1}{2}\hat{\mathbf{x}}^T\mathbf{P}'^{-1}\hat{\mathbf{x}}+\hat{\mathbf{x}}^T\mathbf{Q}\beta\hat{\mathbf{x}}\right)\det\left(2\pi\left(\mathbf{P}'^{-1}+2\beta\mathbf{Q}\right)^{-1}\right)^{\frac{1}{2}} \qquad (3.16a)$$

$$\begin{aligned}\left\langle J\left(\mathbf{x}|\mathbf{Q}\right)\right\rangle &= -\frac{\partial}{\partial\beta}\ln Z\left(\boldsymbol{\mu},\beta\right)\\&=\hat{\mathbf{x}}^T\mathbf{Q}\hat{\mathbf{x}}+Tr\left(\mathbf{Q}\mathbf{P}\right)\end{aligned} \qquad (3.16b)$$

The role of the cost function in control theory is similar to the role of the Hamiltonian of physics systems in statistical mechanics. The Hamiltonian of physics systems includes all types of energy based on the states of constituent particles, like kinetic energy, electrical potential, etc. The cost function also maps the states of constituted agents to a positive number. When net heat flows in or out of a multi-agent system, it perturbs the system and increases/decreases the value of the cost function. Additionally, if the boundary of the system interacts with the agents in the system, the boundary change influences the cost function. This process is like expanding or compressing gas in a can with a piston. These mechanisms are similar to the first law of thermodynamics, as shown in Eq. 3.17. In this study, the air traffic sector volume is fixed and has no interaction with the air vehicles.

Hence, the volume difference (dV) and the pressure (P) are zero. The impacts from the net heat flow (δQ) equal the cost function difference (dU).

$$dU = \delta Q - PdV \tag{3.17}$$

The entropy from the classical thermodynamics formulation depends on the net heat flow and the system temperature, which is shown in Eq. 3.18 as the first inequality equation. The discussion in the previous paragraph concluded that the net heat flow is related to a change of the cost function values, which is represented by the second and third equality signs in Eq. 3.18. Finally, Eq. 3.19 shows the rearranged version of Eq. 3.18.

$$\begin{aligned} dS &\geq \frac{\delta Q}{T} \\ &= \frac{dU}{T} \\ &= \frac{d\left\langle J\left(\mathbf{x}\right)\right\rangle}{T} \end{aligned} \tag{3.18}$$

$$d\left\langle J\left(\mathbf{x}\right)\right\rangle \leq TdS \tag{3.19}$$

Equation 3.19 shows that the difference of the cost function is less than or equal to the multiplication of the temperature and change of the statistical entropy. The equality sign holds only when the process is reversible. Deriving the definition of the traffic temperature requires defining the initial (i) and final (f) states of the systems. And there is a reversible process from an initial state to a final state to ensure that the equality sign holds.

The study assumes that a conceptual process for creating the system from vacant space to the final system state exists. Because there is no vehicle in the vacant space, the entropy and cost function are zero. Additionally, the conceptual process is assumed to be isothermal, so the traffic temperatures at the initial state and the final state are the same. Subsequently, the traffic temperature in Eq. 3.21 is the ratio between the expected cost function value and the total entropy at the final state.

$$\langle J(\mathbf{x}) \rangle_f - TS_f = \langle J(\mathbf{x}) \rangle_i - TS_i = 0 \tag{3.20}$$

$$\begin{aligned} T &= \frac{\langle J(\mathbf{x}) \rangle}{S} \\ &= \frac{\hat{\mathbf{x}}^T \mathbf{Q} \hat{\mathbf{x}} + Tr(\mathbf{QP})}{k_B \left(\ln n - \ln V_d + \frac{1}{2} \ln \left(\det \left(2\pi e \mathbf{P} \right) \right) \right)} \end{aligned} \tag{3.21}$$

The temperature metric is the second metric proposed by this study. Finally, the numerator, which is the expected cost function, is the third metric. The expected cost function is the traffic safety severity measure, which quantifies the airspace safety level according to the airspace-related regulations. Further discussions will be included in the following sections.

3.2.3 Traffic Temperature Discussion

Figure 3.2 summarizes the flowchart of calculating the traffic temperature metric. The three colors in the flowchart represent the different types of inputs, outputs, and functions for the calculation. The shapes with grey outlines show the policy-related inputs and functions. Under the context of the air traffic management, the cost function in Eq. 3.21 depends on the given airspace regulations and should quantify the traffic safety severity level based on the traffic state. In Fig. 3.2, the cost function is the traffic state safety severity function.

The shapes with blue outlines show that inputs and functions, which are related to vehicle state estimation and prediction. The "data fusion and vehicle state prediction" procedure estimates or predicts the vehicle states based on the air vehicle states and the state covariance matrix. The algorithm does not output a vector to represent the estimated or predicted vehicle state. Instead, the algorithm generates the air traffic state distribution to show the all possible states of all vehicles in the air traffic. Although it is more comprehensive to consider all possible outcomes from the air traffic state distribution, it should have a metric to summarize the traffic condition from the state distribution for helping operators understand the distribution. The traffic temperature metric can summarize the air traffic state distribution.

The shapes with green outlines indicate the steps of calculating the traffic temperature. The traffic safety severity function evaluates the safety severity level of vehicles in the air traffic according to a traffic instance. Subsequently, the expected traffic safety severity uses the air traffic state distribution to calculate the average safety severity. Next, the "state estimation uncertainty evaluation" calculates the traffic entropy of the air traffic state distribution. The higher traffic entropy indicates that there is higher uncertainty on the estimated or predicted traffic state. Finally, the traffic temperature is the ratio of the expected traffic severity over the traffic entropy.

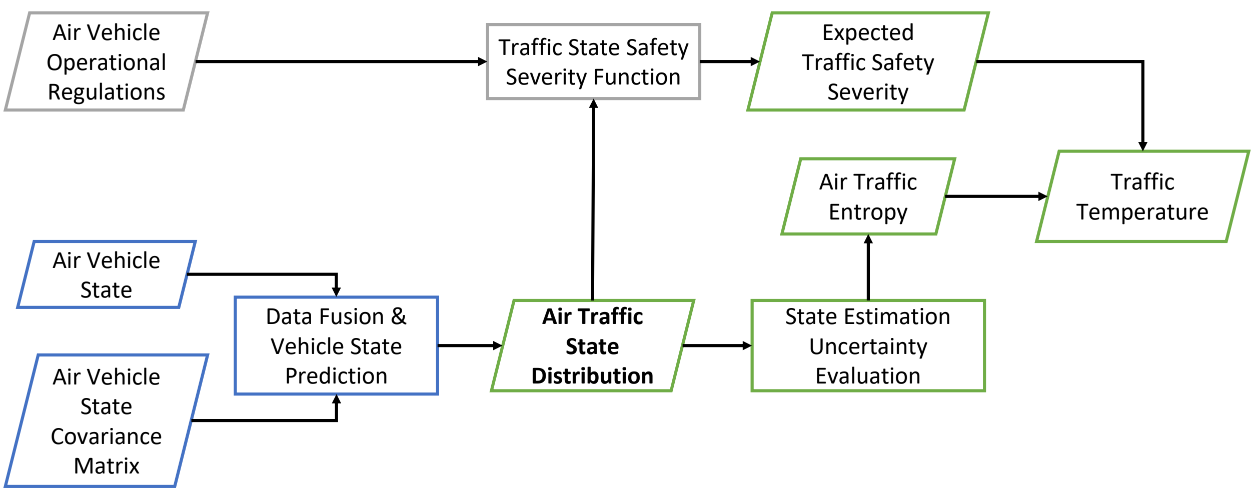

Figure 3.2. Flowchart of Traffic Temperature Evaluation (The shapes with grey outlines indicate policy-related functions and inputs. The shapes with blue outlines show the functions and inputs relate to vehicle state estimation and prediction. The shapes with green outlines present functions and inputs/outputs related to the traffic temperature calculations. The boxes show functions or procedures, while the parallelograms indicate the inputs and outputs of functions.)

The traffic temperature has two convenient properties for air traffic management applications. First, it is suitable for assessing the effectiveness of various airspace technologies in scenarios with various number of vehicles because it is an intrinsic quantity, which does not depend on the number of vehicles in the airspace. Second, the traffic temperature is directly associated with the traffic state safety severity. The traffic temperature increases with a more severe traffic condition and indicates that the behaviors of vehicles in the air traffic are unfavorable based on given airspace regulations.

Although the the traffic state safety severity function and the traffic temperature are similar, they have different interpretations. The traffic state safety severity function quantifies how severely vehicles in air traffic violate given airspace regulations. On the other hands, the traffic temperature quantifies the degree of confidence about how severely air vehicles violate given airspace regulations.

3.3 Charged Particle based Air Vehicle Model

The traffic entropy and the traffic temperature depend on the estimated states of air vehicles in the airspace (Fig. 3.1). Hence, the ATA should predict the behaviors of air vehicles under nominal and contingent conditions. Because this study intends to demonstrate the capability of the airspace metrics instead of realistically modeling the dynamics of the air vehicles, the air vehicle model should be simple enough to reduce simulation complexity. Hence, this study uses a 2-D charged-particle vehicle model to include the following vehicles' activities.

1. **Navigation System**: The vehicle has an onboard navigation system that navigates the air vehicle from its origin to its destination.

2. **Collision Avoidance System**: The vehicle executes collision avoidance maneuvers if the distance to a neighboring vehicle is less than the collision avoidance distance (CAD).

3. **Limited Motor Output**: The vehicle cannot execute aggressive maneuvers due to limited motor outputs.

4. **Telemetry Data Broadcasting**: The vehicle periodically broadcasts its telemetry data to the ATA and neighboring vehicles within the broadcasting range. The default setting of the telemetry data broadcast frequency is 1 second.

5. **State Measurement Error**: The vehicle can measure its state with some state measurement errors.

6. **Wind Perturbations**: The vehicle experiences wind perturbations, which push the air vehicle away from its original course.

The 2-D charged-particle vehicle model can simplify simulation complexity and model the navigation and collision avoidance systems. The vehicle model uses a single point particle with assigned charges (q_i) and masses (m_i) to represent a vehicle without simulating vehicle flight dynamics. The model uses a constant magnitude electric field (E) to represent the strength of the navigation system. In Eq. 3.22a, $\mathbf{r}_d$ represents the distance from the vehicle i to its destination. The electric field points to the destination ($\mathbf{r}_d/\left|\mathbf{r}_d\right|$) and guides the air vehicle while the air vehicle is off course. Repelling forces from the same charges represent the collision avoidance system to keep two or more vehicles apart. In Eq. 3.22b, $\mathbf{r}_{i,j}$ indicates the distance from the neighboring vehicle j to the vehicle i. Additionally, the air vehicle uses motors with limited power output for executing commands from the navigation and collision avoidance systems. Hence, the maximum output from all motors is a g (Eq. 3.22c) in this study.

There is a drag force to slow down the vehicle (Eq. 3.22d) in the simulation. The combined effects of the drag force and the navigation force can determine the cruise speed of the air vehicle. Additionally, the drag coefficient determines how sensitive the air vehicle is to wind perturbations. Wind turbulence is easier to push the air vehicles with a higher drag coefficient.

$$\mathbf{F}_{nav} = \frac{\mathbf{r}_d}{\left|\mathbf{r}_d\right|} E q_i \tag{3.22a}$$

$$\mathbf{F}_{col} = \sum_{j \sim i} \frac{\mathbf{r}_{i,j} q_i q_j}{\left|\mathbf{r}_{i,j}\right|^3} \tag{3.22b}$$

$$\mathbf{F}_{tot} = (\mathbf{F}_{nav} + \mathbf{F}_{col}) \times \frac{\max\left(|\mathbf{F}_{nav} + \mathbf{F}_{col}|, g \times m_i\right)}{|\mathbf{F}_{nav} + \mathbf{F}_{col}|} \tag{3.22c}$$

$$\mathbf{F}_{drag} = -C_d \mathbf{v}_i \tag{3.22d}$$

In this simplified model, both the navigation force and the collision avoidance force are nonlinear. Hence, the Extended-Kalman Filter (EKF) can be used to estimate vehicle state. The Euler integration scheme also helps convert the continuous-time representation to the discrete-time representation.

The magnitude of the charge determines the minimum separation distance between two vehicles. In an ideal situation with a large enough charge setting, the repelling force can stop and drive the air vehicles in the opposite directions to avoid the mid-air collision. In other words, increasing the magnitude of the charge can increase the minimum separation distance.

3.4 Two Proposed Actions for Air Traffic Authority

Figure 3.1 shows that the ATA should determine the actions to manage the air traffic. The ATA's actions should generate commands that the air vehicles can execute. Although the vehicle model from Section 3.3 is simple, it captures the critical behaviors of air vehicles. The ATA's actions include the following mechanisms, which change the simulation parameters of the simplified model.

- **Vehicle Telemetry Broadcast Frequency (VTBF) Adjustment Mechanism**: The estimated state of the air vehicles can be high due to unreliable communication, high state measurement errors, or strong wind perturbation. Hence, the ATA agent can require the air vehicles to increase the telemetry broadcasting frequency for the uncertainty reduction of the estimated vehicle states.

- **Minimum Separation Criterion Adjustment Mechanism**: The ATA should require air vehicles to increase the minimum separation criterion from neighboring vehicles if they have a high likelihood of violating airspace regulations. In this study, the

ATA can increase the magnitude of the vehicle's charge and effectively increase the minimum separation distance.

3.4.1 Entropy-based Trigger for Adjusting Vehicle Telemetry Broadcast Frequency

Equation 3.10 shows that the statistical entropy is the summation of the information entropy and some constants. In information theory, information entropy relates to the channel capacity of a communication channel. Tanaka et al. [60] showed that their Linear-Quadratic-Gaussian (LQG) controller achieves the minimum communication data rate from the plant to the controller. Hence, the ATA can assess if the available communication data rate can support the desired controller performances. Then, the ATA ask for increasing the communication data rate by increasing the vehicle telemetry broadcast frequency.

Review of Information Theory

Equations 3.23 and 3.24 can simplify the derivation of the VTBF adjustment mechanism. Equation 3.23 shows that $\mathbf{x}_t$ is a vector with all elements are at time t. Equation 3.24 shows that $\mathbf{x}^t$ stacks all vectors from time t to time 0 for representing $\mathbf{x}$ revolution.

$$\mathbf{x}_t = [x_{1,t}, x_{2,t}, \cdots]^{\mathrm{T}} \tag{3.23}$$

$$\mathbf{x}^t = \left[\mathbf{x}_0^{\mathrm{T}}, \mathbf{x}_1^{\mathrm{T}}, \cdots, \mathbf{x}_t^{\mathrm{T}}\right]^{\mathrm{T}} = \left[\mathbf{x}^{t-1^{\mathrm{T}}}, \mathbf{x}_t^{\mathrm{T}}\right]^{\mathrm{T}} \tag{3.24}$$

Figure 3.3 presents the relationship between information entropy ($H(\cdot)$), mutual information ($I(\cdot;\cdot)$), and conditional information ($H(\cdot|\cdot)$). In the diagram, both X and Y are stochastic variables. The information entropy of X and Y are shown in the blue and red circles, respectively. The conditional entropy of Y given X is in the red area, while the conditional entropy of X given Y is in the blue region. The intersection between the two circles is the mutual information of X and Y. The mutual information is the shared information between variables X and Y. Finally, the information entropy of X and Y is the area covered by the union of the two circles.

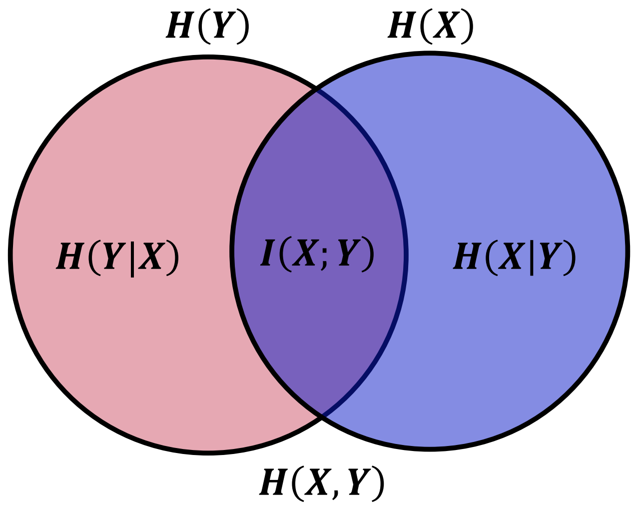

Figure 3.3. Information Venn Diagram shows the relationships between information entropy ($H(\cdot)$), mutual information ($I(\cdot;\cdot)$), and conditional information ($H(\cdot|\cdot)$)

Equation 3.25a shows that the mutual information equals the subtraction of the information entropy of $\mathbf{X}$ from the conditional information entropy of $\mathbf{Y}$ given $\mathbf{X}$. And Eq. 3.25b shows that the total information entropy of both $\mathbf{X}$ and $\mathbf{Y}$ equals the summation of the information entropy of $\mathbf{X}$ and the conditional information entropy of $\mathbf{Y}$ given $\mathbf{X}$. Finally, Eq. 3.25c shows the alternative formulation of the conditional entropy of $\mathbf{X}$ given $\mathbf{Y}$.

$$I(\mathbf{X};\mathbf{Y}) = H(\mathbf{X}) - H(\mathbf{X}|\mathbf{Y}) = H(\mathbf{Y}) - H(\mathbf{Y}|\mathbf{X}) \tag{3.25a}$$

$$H(\mathbf{X},\mathbf{Y}) = H(\mathbf{X}) + H(\mathbf{Y}|\mathbf{X}) = H(\mathbf{Y}) + H(\mathbf{X}|\mathbf{Y}) \tag{3.25b}$$

$$H(\mathbf{X}|\mathbf{Y}) = H(\mathbf{X}) + H(\mathbf{Y}|\mathbf{X}) - H(\mathbf{Y}) \tag{3.25c}$$

Derivation of Upper Bound of Directed Information

Figure 3.4 shows the communication channel from the vehicle telemetry broadcast to the ATA vehicle state estimation. Firstly, the onboard sensor measures the latest vehicle state. And the communication encoder converts the sensor outputs to a message signal (m_t). The encoder-sensor mechanism is in $\mathbb{P}\left(\mathbf{m}_t|\mathbf{x}^t, \mathbf{m}^{t-1}\right)$ and depends on the history of the vehicle state ($\mathbf{x}^t$) and the history of broadcast messages ($\mathbf{m}^{t-1}$). The new message (m_t) travels through a wireless communication channel (shown in dashed line in Fig. 3.4) to the ATA, where l_t indicates the length of the message in binary. The ATA decodes the message as an observation ($\mathbf{y}_t$). Subsequently, the ATA uses the Kalman filter algorithm ($\mathbb{P}\left(\hat{\mathbf{x}}_t|\mathbf{y}^t, \hat{\mathbf{x}}^{t-1}\right)$) to estimate the air vehicle state ($\hat{\mathbf{x}}_t$).

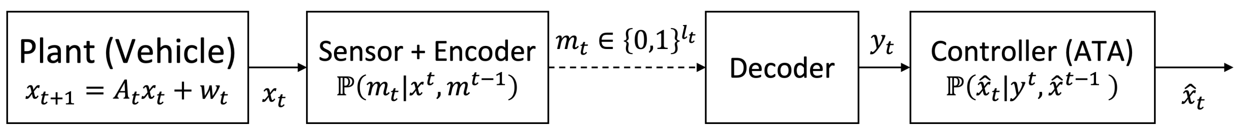

Figure 3.4. Communication Channel from Vehicle State Measurement to ATA Vehicle State Estimation

Tanaka et al. defined that the directed information ($I\left(\mathbf{x}^W \rightarrow \hat{\mathbf{x}}^W\right)$) from the true state ($\mathbf{x}^W$) to the estimated state ($\hat{\mathbf{x}}^W$) of the vehicle (Eq. 3.26) [60]. $I\left(\mathbf{x}^t; \hat{\mathbf{x}}_t|\hat{\mathbf{x}}^{t-1}\right)$ is the summation of the conditional mutual information between the history of the true state and the latest state estimation given the history of the estimated states through each time step. In other words, the directed information quantifies the amount of information shared between the true state and the estimated state. Tanaka et al. also showed that the minimum channel capacity (R) from all channels in Fig. 3.4 should be larger than the average directed information (Eq. 3.27) [60].

$$I\left(\mathbf{x}^W \rightarrow \hat{\mathbf{x}}^W\right) \equiv \sum_{t=1}^{W} I\left(\mathbf{x}^t; \hat{\mathbf{x}}_t|\hat{\mathbf{x}}^{t-1}\right) \tag{3.26}$$

$$DR \equiv \frac{I\left(\mathbf{x}^W \rightarrow \hat{\mathbf{x}}^W\right)}{W} \leq R \tag{3.27}$$

In this study, the air vehicles broadcast their telemetry data to the ATA. Then, the ATA uses the Kalman filter algorithm to estimate the states of the air vehicles. This study assumes that the ATA has enough computational power to execute the Kalman filter algorithm. The only bottleneck from the information pathway is the wireless communication from the air vehicle to the ATA. If the average directed information from the true state of the air vehicle to the estimated state is known, the ATA can identify if extra communication capacity is necessary to help the information flow.

To derive the directed information for this study, it is necessary to review the mutual information at time t from Eq. 3.26. Using the Information Venn Diagram relationships from Fig. 3.3 results in the derivation in Eq. 3.28. The first equality sign holds because of expanding the mutual information by applying the relationship in Eq. 3.25a. By applying Eq. 3.25b, decomposing the information entropy to isolate the state at time t makes the second equality sign hold. Regrouping terms with and without the given true state ($\mathbf{x}_t$) at time t results in the third equality sign. Finally, the items in the same parenthesis follow the definitions of the mutual information.

$$\begin{aligned}
I\left(\mathbf{x}^t; \hat{\mathbf{x}}_t | \hat{\mathbf{x}}^{t-1}\right) =& H\left(\mathbf{x}^t | \hat{\mathbf{x}}^{t-1}\right) - H\left(\mathbf{x}^t | \hat{\mathbf{x}}^{t-1}, \hat{\mathbf{x}}_t\right) \\
=& \left(H\left(\mathbf{x}^{t-1} | \hat{\mathbf{x}}^{t-1}, \mathbf{x}_t\right) + H\left(\mathbf{x}_t | \hat{\mathbf{x}}^{t-1}\right)\right) \\
& - \left(H\left(\mathbf{x}^{t-1} | \hat{\mathbf{x}}^{t-1}, \hat{\mathbf{x}}_t, \mathbf{x}_t\right) + H\left(\mathbf{x}_t | \hat{\mathbf{x}}^{t-1}, \hat{\mathbf{x}}_t\right)\right) \\
=& \left(H\left(\mathbf{x}^{t-1} | \hat{\mathbf{x}}^{t-1}, \mathbf{x}_t\right) - H\left(\mathbf{x}^{t-1} | \hat{\mathbf{x}}^{t-1}, \hat{\mathbf{x}}_t, \mathbf{x}_t\right)\right) \\
& + \left(H\left(\mathbf{x}_t | \hat{\mathbf{x}}^{t-1}\right) - H\left(\mathbf{x}_t | \hat{\mathbf{x}}^{t-1}, \hat{\mathbf{x}}_t\right)\right) \\
=& I\left(\mathbf{x}^{t-1}; \hat{\mathbf{x}}_t | \hat{\mathbf{x}}^{t-1}, \mathbf{x}_t\right) + I\left(\mathbf{x}_t; \hat{\mathbf{x}}_t | \hat{\mathbf{x}}^{t-1}\right)
\end{aligned} \tag{3.28}$$

The first term on the right-hand side of the last equality sign in Eq. 3.28 is related to the information flow of the Kalman filter framework. The Kalman filter framework forms a Markov Chain process shown in Eq. 3.29. The history of the trues state before time t ($\mathbf{x}^{t-1}$) results in the history of the estimated state before time t ($\hat{\mathbf{x}}^{t-1}$) and the latest true state

($\mathbf{x}_t$). Then, the history of the estimated state ($\hat{\mathbf{x}}^{t-1}$) and the latest true state ($\mathbf{x}_t$) can help the Kalman filter algorithm to generate the estimated state vector at time t ($\hat{\mathbf{x}}_t$).

$$\mathbf{x}^{t-1} \rightarrow \left(\mathbf{x}, \hat{\mathbf{x}}^{t-1}\right) \rightarrow \hat{\mathbf{x}}_t \tag{3.29}$$

In Eq. 3.28, the first term on the right-hand side of the last equality sign is the mutual information associated with the Markov Chain process in Eq. 3.29. The mutual information from Eq. 3.28 calculates the mutual information between the first and third terms in Eq. 3.29 given the second term in Eq. 3.29. However, since the values of the second term in Eq. 3.29 are known, there is no shared information between the two end-nodes in the Markov Chain process. In other words, in Eq. 3.28, the first term on the right-hand side of the last equality sign equals 0. Equation 3.30 shows the simplified Eq. 3.28. The term on the right-hand side of Eq. 3.30 describes the shared information between the latest true state and the latest estimated state vector given the history of the estimated state.

$$I\left(\mathbf{x}^t; \hat{\mathbf{x}}_t | \hat{\mathbf{x}}^{t-1}\right) = I\left(\mathbf{x}_t; \hat{\mathbf{x}}_t | \hat{\mathbf{x}}^{t-1}\right) \tag{3.30}$$

The Kalman filter framework also forms another Markov Chain process for describing the estimation step shown in Eq. 3.31. The latest true state ($\mathbf{x}_t$) results in a state measurement vector ($\mathbf{y}_t$). Then, the Kalman filter algorithm uses the state measurement to generate the latest estimated state ($\hat{\mathbf{x}}_t$). During this process, the mutual information between the true state and the estimated state is lower than the mutual information between the state measurement and the estimated state. Hence, this relationship results in the first inequality sign in Eq. 3.32.

$$\mathbf{x}_t \rightarrow \mathbf{y}_t \rightarrow \hat{\mathbf{x}}_t \tag{3.31}$$

The inequality sign in Eq. 3.32 shows the upper bound of the directed information. However, it is still not easy to calculate the right-hand side of the inequality sign. Hence, using Eq. 3.25a from the Information Venn Diagram (Fig. 3.3) results in the second row. Using Eq. 3.25c can decompose the second term on the right-hand side of the first equality sign in Eq. 3.32 and result in the second equality sign. In the third row, the first term on the right-hand side of the equality sign can cancel out with the first term in the parenthesis. The simplified form is in the last row of Eq. 3.32.

$$\begin{aligned}
I\left(\mathbf{x}_t; \hat{\mathbf{x}}_t | \hat{\mathbf{x}}^{t-1}\right) \leq & I\left(\mathbf{y}_t; \hat{\mathbf{x}}_t | \hat{\mathbf{x}}^{t-1}\right) \\
= & H\left(\mathbf{y}_t | \hat{\mathbf{x}}^{t-1}\right) - H\left(\mathbf{y}_t | \hat{\mathbf{x}}^{t-1}, \hat{\mathbf{x}}_t\right) \\
= & H\left(\mathbf{y}_t | \hat{\mathbf{x}}^{t-1}\right) - \left(H\left(\mathbf{y}_t | \hat{\mathbf{x}}^{t-1}\right) + H\left(\hat{\mathbf{x}}_t | \mathbf{y}_t, \hat{\mathbf{x}}^{t-1}\right) - H\left(\hat{\mathbf{x}}_t | \hat{\mathbf{x}}^{t-1}\right)\right) \\
= & H\left(\hat{\mathbf{x}}_t | \hat{\mathbf{x}}^{t-1}\right) - H\left(\hat{\mathbf{x}}_t | \mathbf{y}_t, \hat{\mathbf{x}}^{t-1}\right)
\end{aligned} \tag{3.32}$$

The first term on the right-hand side of the last equality sign in Eq. 3.32 represents the information entropy of the prior state from the Kalman filter framework. Additionally, the second term is the information entropy of the posterior state from the Kalman filter framework. In other words, the upper bound of the directed information is based on the difference of the information entropy between the prior state and the posterior state (Eq. 3.33).

$$I\left(\mathbf{x}^W \to \hat{\mathbf{x}}^W\right) \leq \sum_{t=1}^{W} H\left(\hat{\mathbf{x}}_t | \hat{\mathbf{x}}^{t-1}\right) - H\left(\hat{\mathbf{x}}_t | \mathbf{y}_t, \hat{\mathbf{x}}^{t-1}\right) \tag{3.33}$$

Telemetry Broadcast Rate Adjustment Mechanism

Figure 3.5 shows the flowchart of the mechanism for adjusting the VTBF. This mechanism requires three settings. First is the **measurement window** (W). The ATA counts the number of the received messages from the air vehicle (n_{rcv}) within the measurement time window. Additionally, the measurement time window can derive the average upper bound of the directed information. The second setting is the **message length** (l_m) about the vehicle state information in binary. And, the last setting is the **upper limit of VTBF**.

The ATA evaluates the communication channel capacity and the upper bound of the directed information based on Eq. 3.34 in Fig. 3.5. Subsequently, the ATA checks if the inequality constraint holds. If the upper bound of the directed information exceeds the communication channel capacity, the ATA doubles the broadcast frequency of the air vehicle.

Then, the ATA checks if the new broadcast frequency exceeds the upper limit setting. The ATA sends the new broadcast frequency command to the air vehicle if the new broadcast frequency is below the upper limit.

$$R = n_{rcv} l_m \geq \frac{1}{W} \sum_{t=T-W}^{W} H\left(\hat{\mathbf{x}}_t | \hat{\mathbf{x}}^{t-1}\right) - H\left(\hat{\mathbf{x}}_t | \mathbf{y}_t, \hat{\mathbf{x}}^{t-1}\right) \tag{3.34}$$

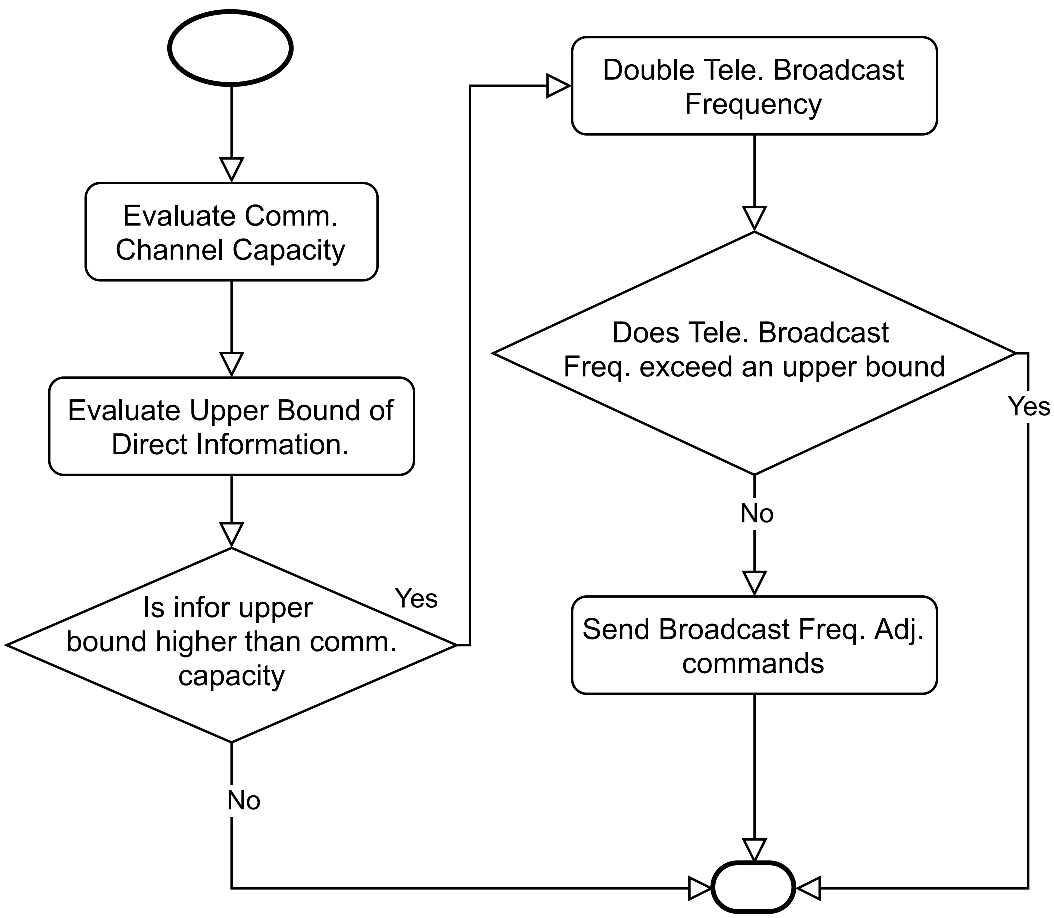

Figure 3.5. Flowchart of Entropy-based Vehicle Telemetry Broadcast Frequency (VTBF) Adjustment Mechanism

3.4.2 Temperature-based Trigger for Adjusting Minimum Separation Criterion

Figure 3.6 shows the temperature-based trigger for adjusting the minimum separation criterion. This mechanism depends on the traffic temperature metric for identifying when and which vehicles to send the commands to. And this mechanism requires two settings. The first setting is the **temperature trigger threshold**, which triggers the adjustment of the minimum separation criterion if the traffic temperature is high enough. The second one is the **charge multiplier**, which defines what the new minimum separation criterion is.

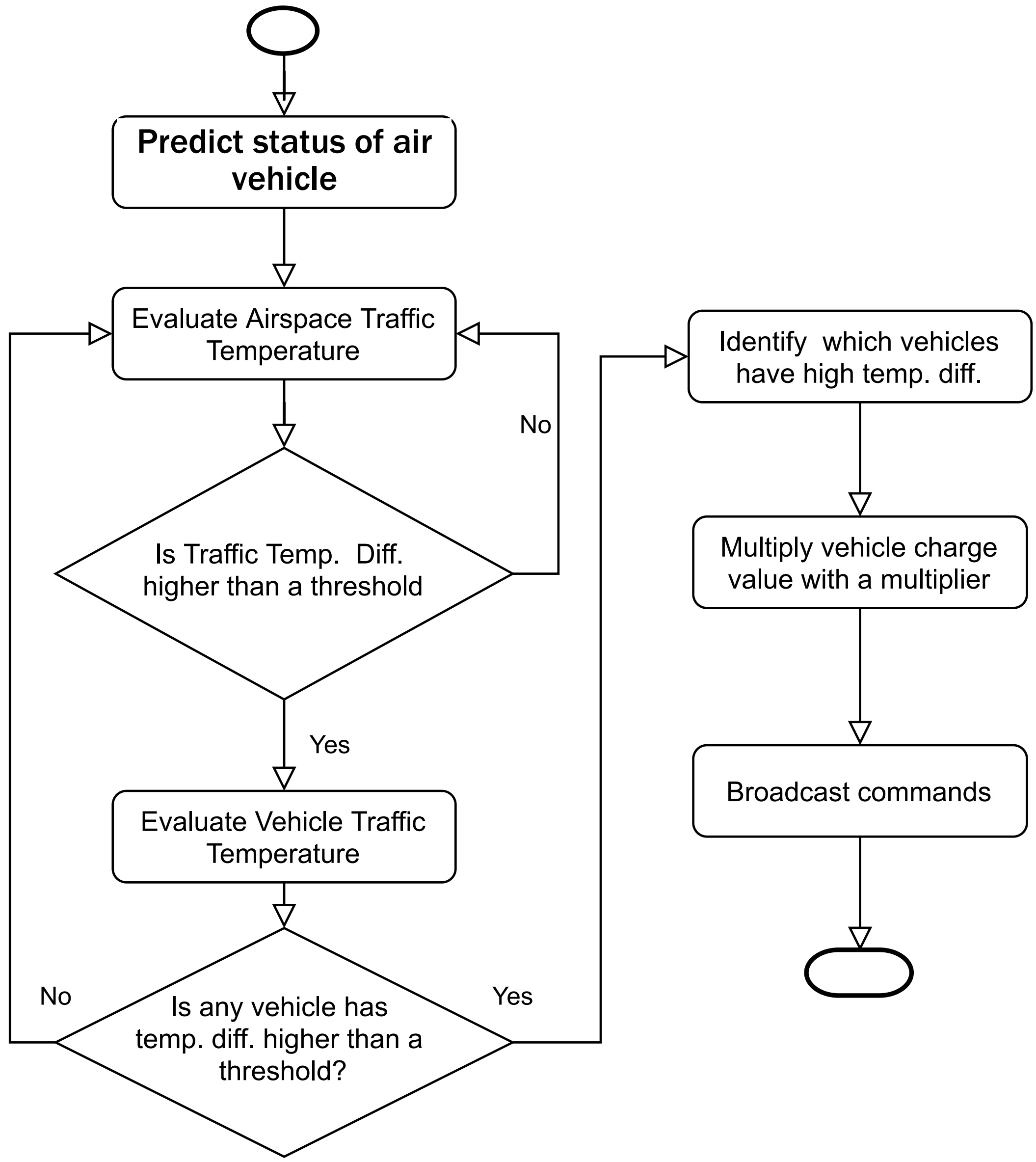

Figure 3.6. Flowchart of Temperature-based Trigger for Adjusting Minimum Separation Criterion Mechanism

Because the goal of this mechanism is to prevent the minimum separation distance violation, the ATA has to look ahead to the status of the air vehicles at a certain period. The ATA agent can use the Kalman filter prediction algorithm to predict the states of all air vehicles with the predicted state distributions. According to Fig. 3.6, the airspace traffic temperature depends on the predicted state distributions. Then, the ATA calculates the difference of the airspace traffic temperatures of the current and previous time step. If the difference of the airspace traffic temperature is higher than the temperature trigger threshold, the ATA evaluates the temperature difference of every air vehicle.

The calculations of the traffic temperatures for each vehicle is similar to the one for the airspace. First, the ATA agent identifies which air vehicles belong to the same collision avoidance cluster. Based on the expected state of all air vehicles, two air vehicles with a relative distance less than the CAD belong to the same group. Then, the ATA calculates the distance between either one of the vehicles from the group to a third vehicle. If any one of the relative distances is less than the CAD, the third vehicle belongs to the same group. The ATA continuous this procedure until it examines all air vehicles in the airspace.

The ATA evaluates the vehicle temperature for each vehicle in each cluster. Since the safety severity function is the total vehicle energy. The vehicle safety severity includes the kinetic energy and the electric potential energy of the vehicle. For the vehicle entropy, the ATA calculates the statistical entropy of the cluster. Then, the cluster entropy is split according to the ratio of the vehicle uncertainty level to the cluster uncertainty level. Finally, the vehicle temperature is the ratio of the vehicle safety severity to the vehicle uncertainty.

The ATA marks all vehicles with a traffic temperature difference higher than the temperature trigger threshold. Subsequently, the ATA increases the minimum separation criterion of these vehicles by multiplying the charges of the marked air vehicles with the charge multiplier setting. Then, the ATA sends commands with the new charge values to all marked vehicles and waits for their acknowledgment. If the ATA does not receive an acknowledgment signal from any marked vehicle within one second, it will resend the command until an acknowledgment is received.

4. RESULTS & DISCUSSION

This study designs three experiments to understand the properties of traffic temperature and traffic entropy. The first experiment includes scenarios with two air vehicles traveling in opposite directions and experiencing environmental perturbations containing wind disturbance, unreliable communications, and degraded GPS signals. This experiment intends to understand how traffic temperature and entropy evolve with different environmental conditions. The setups of the second experiment include multiple vehicles with various traffic patterns. The design of this experiment intends to show how ATA can use the temperature metric to reveal the properties of different traffic patterns. Finally, the third experiment models scenarios with hypothetical UAM traffic in the Chicago metropolitan area. The goal is to show the potential applications of the temperature metric on air traffic monitoring and airspace structure design.

4.1 Computational Analysis of Temperature Metric

This section presents a simplified computational model for testing the relationships of the temperature metric with the vehicle states and the state estimation errors. The computational model includes two stationary points and respective state estimation uncertainty. Figure 4.1 shows four setups of location and state estimation uncertainty of the points. The blue dots indicate the expected location of the points. And the blue areas depict one standard deviation of the probability distribution. The upper left plot shows the baseline setup, in which both points have the same state estimation standard deviation on the x-axis and y-axis. The computational model assumes that the state estimation error follows a multivariate normal distribution. Additionally, the traffic safety severity function (Eq. 4.1) is four over the relative distance between the two points. The following discussions will show that this definition of the safety severity function causes the variance in different directions to have unequal contributions to the temperature.

$$J\left(\vec{x}_1, \vec{x}_2\right) = \frac{4}{|\vec{x}_1 - \vec{x}_2|} \tag{4.1}$$

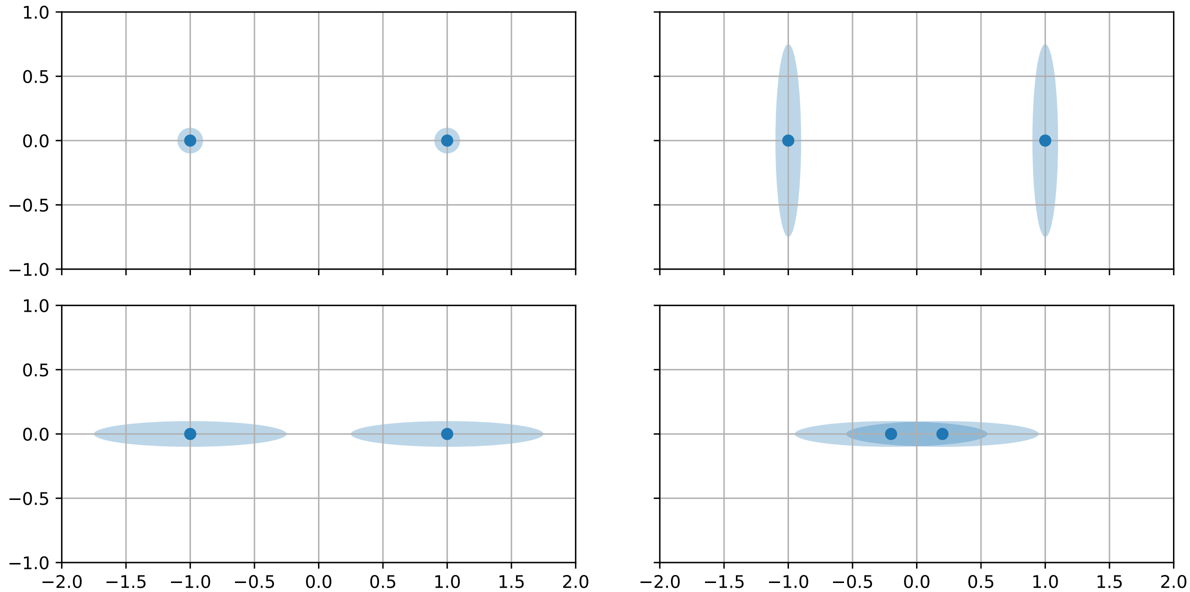

Figure 4.1. Four Different Relative Distance and State Estimation Uncertainty Setups. (The blue dots indicate the expected locations of the points. The blue areas indicate one standard deviation area. The upper left plot shows the baseline setup. The lower left figure indicates the experiment by varying the standard deviation on the x-axis, while the upper right figure shows the testing by changing the standard deviation on the y-axis. Finally, the lower right plot shows the setup by changing the relative distance between two points.)

The lower left plot in Fig. 4.1 shows the setup obtained by changing the standard deviation on the x-axis. The two points are at -1 and 1 on the x-axis, respectively. The relative distance based on the expected point locations is 2. Additionally, the y-axis standard deviation is 0.2. Figure 4.2 shows the simulation results corresponding to this setup. The horizontal axis is the variance along the x-axis, in logarithmic scale, varying from $10^{-}2$ to 10.

This study uses the Monte Carlo Integration for calculating the temperature, the expected relative distance (r_{mean}), and the expected safety severity function (J_{mean}). The first step of the Monte Carlo Integration samples the locations of the two points based on the given probability distribution function. Then, the second step uses the sampled point to calculate the metrics. Finally, the expected values of the metrics are the mean of the sampled points.

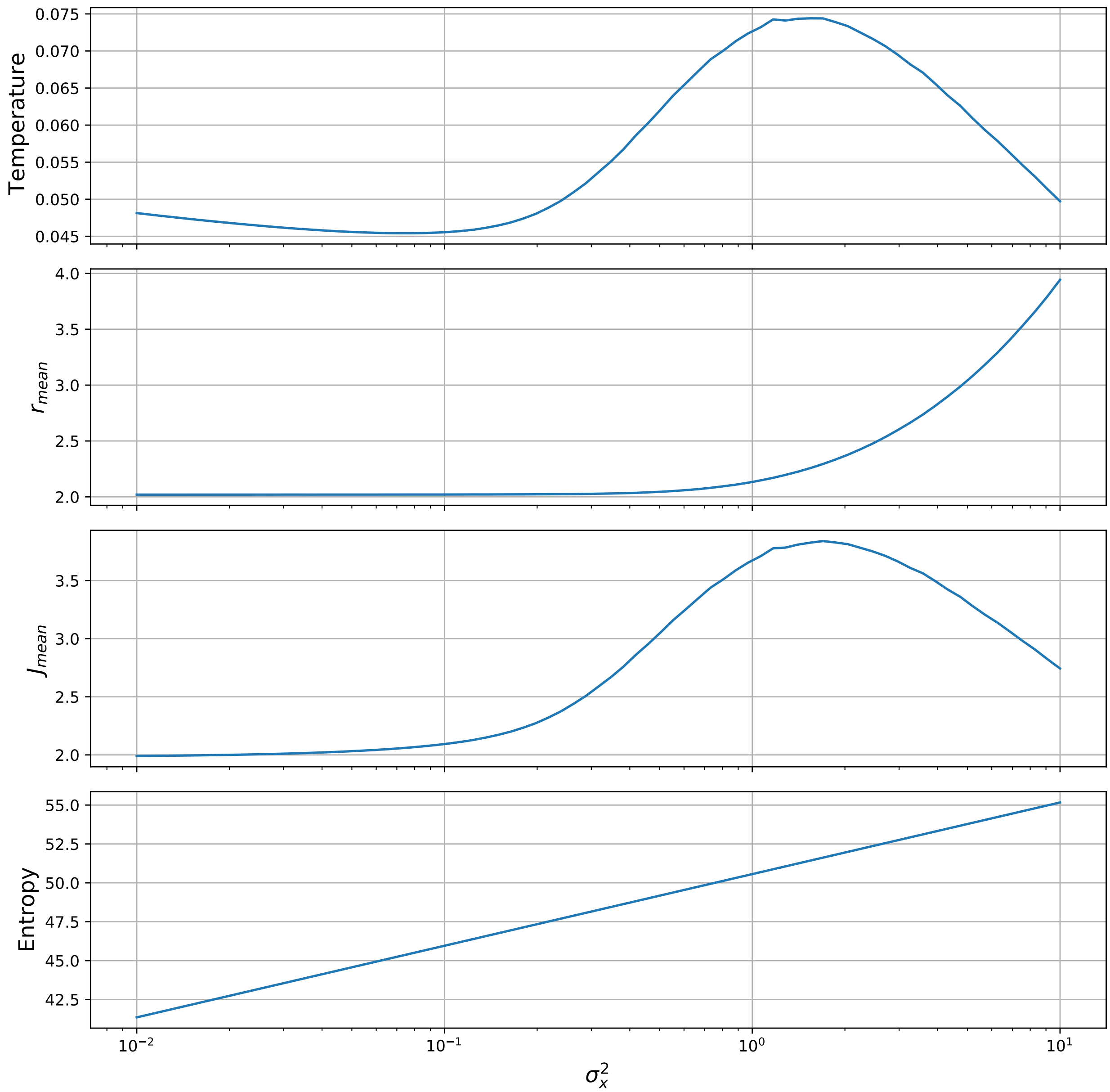

Figure 4.2. Results of the experiment by changing the x-axis variance. (The x-axis shows the variance in the logarithmic scale. The first plot shows the trend of the temperature metric, while the second plot presents the expected relative distance between the two points. The third plot shows the trend of the expected safety severity. Finally, the last plot shows the entropy.)

When the x-axis variance is small, the sampled points surround the expected locations. Hence, the expected relative is slightly higher than 2 (Fig. 4.2). During the Monte Carlo Integration process, when the sampled points lie in the region between two points, the relative distance value is lower and positive. The relative distance increases when the sampled points are outside the inner area. Hence, the expected relative distance is slightly higher than the relative distance based on the expected locations because the relative distance is always positive. The increasing variance on the x-axis also makes the expected relative distance increase.

The expected safety severity function has a different trend from the expected relative distance. The expected safety severity function also increases as the x-axis variance reaches the peak value when the x-axis variance is about 2. When the x-axis variance increases, the sampled points between the two points have a higher chance of getting closer to each other and increasing the expected traffic safety severity. The peak value occurs because the regions of one standard deviation from both points start overlapping when the x-axis variance is over 1. Then, the expected safety severity function reaches the maximum value. The overlapping standard deviation region increases further as the x-variance increase, so chances that the sampled points with a short relative distance decrease due to increasing expected relative distances. And, this phenomenon drives down the expected safety severity.

The entropy has a simple relationship with the x-axis variance. It increases linearly with the logarithm of the x-axis variance. In other words, the higher variance on the x-axis corresponds to the higher uncertainty levels of expected point locations.

The temperature is defined as the ratio of the expected safety severity to the entropy. In the region where the change of the expected safety severity is small ($10^{-2} \leq \sigma_x^2 \leq 10^{-1}$), the temperature slightly decreases as the x-axis variance increases. The safety severity function gives a relatively higher weight to the instance that the sampled points are closer to each other. On the other hand, the temperature takes a higher weight in cases where the sampled points are farther apart. Hence, the temperature identifies that the condition with a slightly higher variance is better. As the x-axis variance increases further, the temperature follows a similar trend in the region.

Figure 4.3 shows the experiment by varying the y-axis variance, shown in the upper right plot in Fig. 4.1. The expected relative distance increases with the increasing y-axis variance. Instead, the expected safety severity decreases as the y-axis variance increases. The increasing y-axis variance results in more sampled points with longer relative distance and a lower safety severity. Furthermore, the entropy follows the same trend in Fig. 4.2 and increases linearly with the logarithm of the y-axis variance. Finally, the temperature follows a similar trend as the expected safety severity. The reduction rate of the temperature is faster than the expected safety severity because the temperature puts higher weighting on the instance further away.

Figure 4.4 shows the results of changing the relative distance between two points (lower right plot in Fig. 4.1). The expected relative distance increases almost linearly when the expected locations of the two points increase. Furthermore, the expected safety severity and the temperature decrease with the same trend because the entropy is constant, due to the fixed covariance matrix.

These results show that the variances on different axes have inequivalent influences on the temperature. The traffic safety severity function defines the primary axis that distinguishes variances on different axes. The temperature function and traffic safety severity function have different trends when the variance in the primary axis increases. On the other hand, the temperature monotonically decreases if the increasing standard deviations are on the axes normal to the principal axis. Additionally, these results show that the temperature gives more weight on the instance that two points are apart, while the safety severity function emphasizes conditions where points are close to each other.

4.2 Metric Property Analysis with Two-Vehicle Simulation

This experiment includes scenarios with two air vehicles traveling in opposite directions from the opposite sides of a virtual world. The region at the center of the virtual world is characterized by more severe wind perturbations, more unreliable communications, and more vehicle state measurement errors. The experiment's goal is to understand how the traffic temperature and the traffic entropy change when the air vehicles are at different conditions.

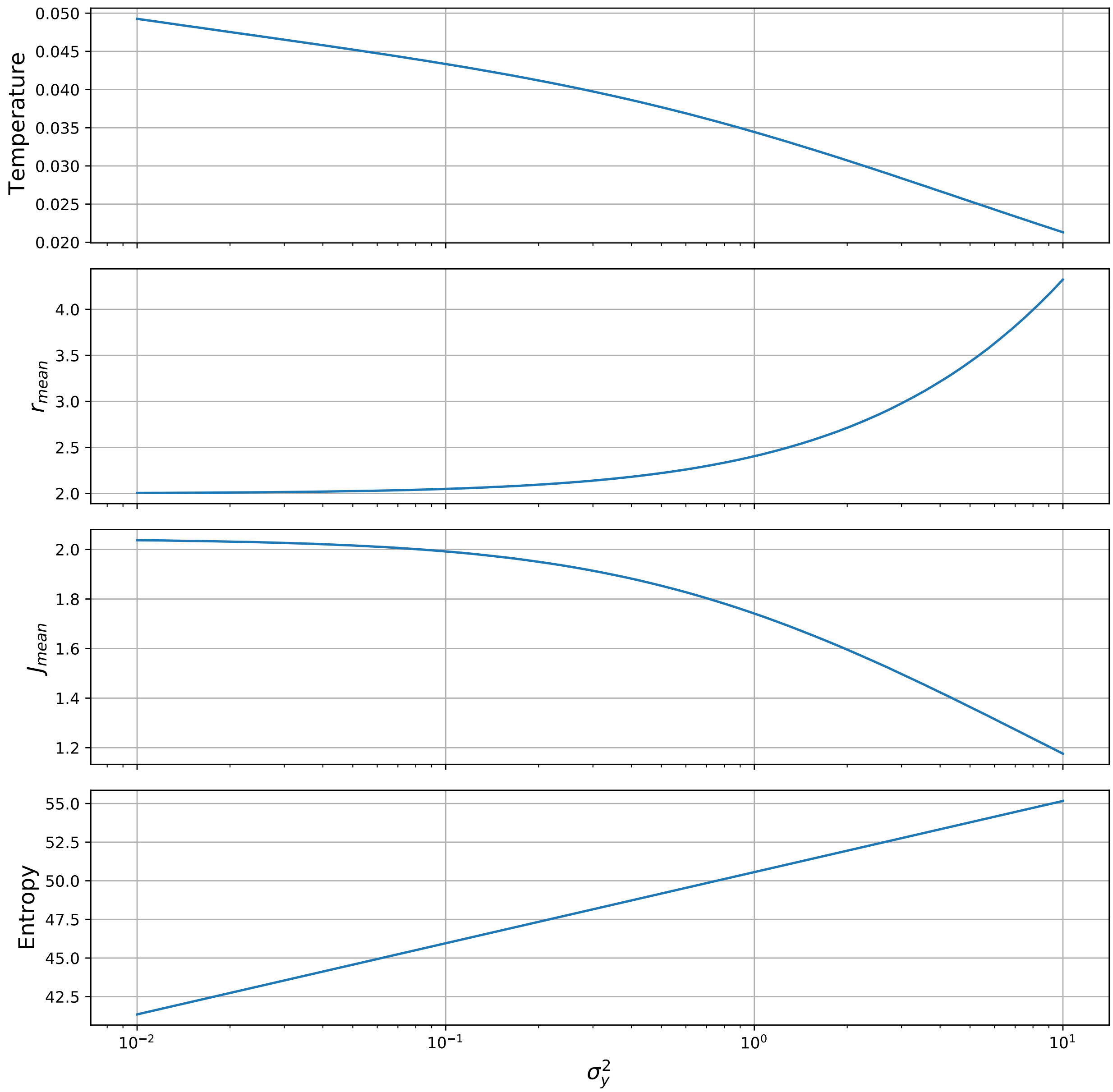

Figure 4.3. Simulation results of the experiment by changing the standard deviation on the y-axis. (The x-axis shows the variance in the logarithmic scale. The first plot shows the trend of the temperature metric, while the second plot presents the expected relative distance between the two points. The third plot shows the trend of the expected traffic state safety severity function. Finally, the last plot presents the entropy.)

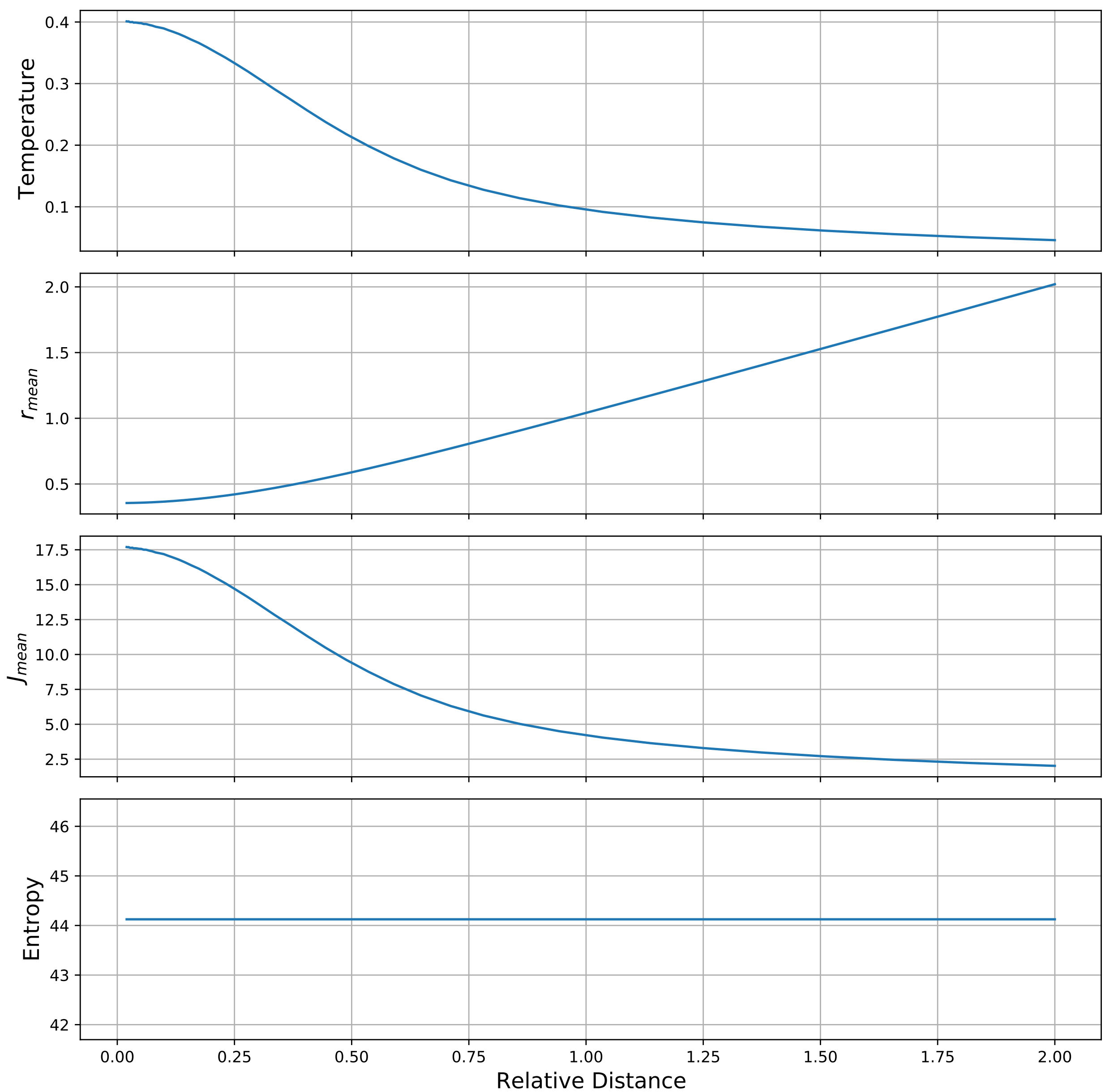

Figure 4.4. Simulation results of the experiment by changing the relative distance between the two points. (The x-axis shows the relative distance between two points. The first plot shows the trend of the temperature metric, while the second plot presents the expected relative distance between the two points. The third plot shows the trend of the expected traffic state safety severity function. Finally, the last plot presents the entropy.)

4.2.1 Two-Vehicle Simulation Description

This simulation includes a 2-D virtual world with two air vehicles traveling from the opposite sides of the map (Fig. 4.5). The 2-D virtual world is a square with 6000 meter-long edges. At the center of the virtual world, this experiment implements a rectangular area, shown as a green box in Fig. 4.5, that centers around the y-axis, and measuring 2000 meters in width and 6000 meters in length. Inside the green area, the air vehicles experience severer wind perturbations, more unreliable communications, or more localization measurement errors. In the simulation, one air vehicle (blue trajectories in Fig. 4.5) travels from the left-hand side of the map to the right-hand side. Another vehicle (red trajectories in Fig. 4.5) travels from the right-hand side of the map to the left-hand side. Without corrections, the air vehicles have a very high chance of experiencing a near-miss event at the center of the map.

Defining a function for traffic safety severity is necessary to use the traffic temperature metric. In this study, the safety severity function is the total energy of all vehicles (Eq. 4.2). The first term in Eq. 4.2 shows the kinetic energy of vehicle ac_i, where AC is a set of vehicles in the airspace. The second term is the electric potential between vehicles ac_i and ac_j, where NV_{ac_i} is the set of the neighboring vehicles of the vehicle ac_i, whose distances from the vehicle ac_i are lower than the collision range (r_{col}). Finally, $\mathbf{r}_{ac_i,ac_j}$ is the estimated relative distance from vehicle ac_i to vehicle ac_j. The safety severity function shows that the air traffic measures a lower safety severity if air vehicles fly slower and are further apart.

$$J\left(\mathbf{x}\right) = \sum_{ac_i \in AC} \left(\frac{m_{ac_i} \left|\mathbf{v}_{ac_i}\right|^2}{2} + \sum_{ac_j \in NV_{ac_i}} \frac{q_{ac_i} q_{ac_j}}{2\left|\mathbf{r}_{ac_i,ac_j}\right|} \right) \tag{4.2}$$

The experiment consists of two parts. In the first part of the experiment, the ATA actions are not put into place, so the experiment results reveal how the traffic temperature and the traffic entropy evolve according to the conditions of both vehicles. The wind perturbation and the state measurement error follow the multivariate normal distribution with 0 mean and given covariance matrix (Table 4.1). The ATA's actions are active in the second part of the experiment to understand how effective the mechanisms are. For both parts of the

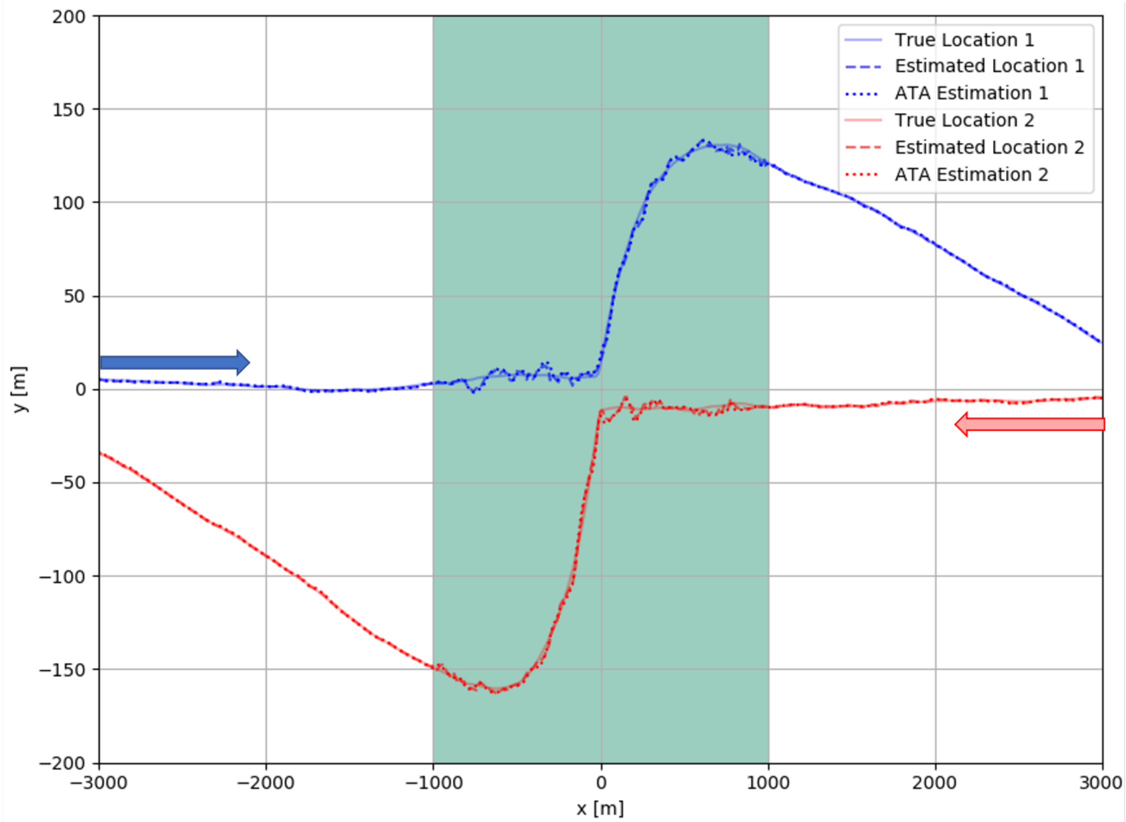

Figure 4.5. Example of 2-D Simulation Environment with Vehicle Trajectories (The blue vehicle comes from left to right, while the red vehicle travels from right to left. The solid lines show the true vehicle trajectories; the dashed lines show the estimated trajectories by the vehicles; the dotted lines show the estimated trajectories by the ATA.)

test, the baseline settings related to the air vehicles are shown in Table 4.2. Table 4.1 shows the baseline settings of the diagonal elements of the covariance matrices for the wind perturbation and the state measurement error.

Table 4.1. Baseline Measurement and Wind Perturbation Variance Settings

Measurement Error Variance		**Wind Perturbation Variance**	
σ_x^2	1.00 [m^2]	σ_{wx}^2	0.50 [(m/s)^2]
σ_y^2	1.00 [m^2]	σ_{wy}^2	0.50 [(m/s)^2]
σ_{vx}^2	2.00 [(m/s)^2]		
σ_{vy}^2	2.00 [(m/s)^2]		

Table 4.2. Simulation Parameter Settings

Parameter	**Value**	**Parameter**	**Value**
m_i	1.00 [kg]	q_i	81.8392 [C]
E	0.01 [V/m]	Cruise Speed	10.00 [m/s]
r_{col}	600 [m]	Broadcasting Range	1500 [m]

The goal of the first part of the experiment is to reveal how the traffic entropy and the traffic temperature respond to environmental perturbations and LOS. This study introduces uncertainty multipliers to increase the strength of uncertainty for wind perturbations and state measurement errors. The wind perturbation multiplier affects the baseline wind perturbation covariance matrix, while the measurement error multiplier influences the measurement error covariance matrix. Additionally, since both air vehicles and the ATA rely on the broadcast telemetry from air vehicles, the unreliable broadcast system can influence airspace safety. This study also sets the message reception rate for modeling unreliable communications. Table 4.3 lists the uncertainty multipliers and message reception rate settings.

Table 4.3. Variance Multipliers and Receiving Rate Settings

Variable	**Values**
Measurement Error Multiplier	[1.0, 20.0, 40.0]
Wind Perturbation Multiplier	[1.0, 20.0, 40.0]
Message Reception Rate	[1.0, 0.66, 0.33]

The goal of the second part of the experiment is to assess the impacts of the ATA's traffic management mechanisms. This study focuses on three mechanism settings, turning on/off the VTBF adjustment, changing the temperature trigger threshold, and changing the charge multiplier. The setting of the temperature trigger threshold depends on the results of the first part of the experiment. Table 4.4 summarizes the settings of the ATA traffic management mechanisms for this study.

For each combination of the variance multipliers, receiving rate, and TA Traffic Management Mechanism setting, 50 runs of the simulation are conducted. The simulation results and discussion are in the following sections.

Table 4.4. Setting for ATA Traffic Management Mechanisms

Parameter	**Values**	
VTBF Adjust. Mechanism	[On, Off]	
Temp. Trigger Threshold	Off	[0.005, 0.01, 0.05]
Charge Multiplier	Off	[1.2, 1.5, 1.8]

4.2.2 Metric Property Analysis

The first part reveals how the metrics evolve under different environmental conditions for both vehicles. Figures 4.6 to 4.8 show the evolution of the metrics based on real-time vehicle state estimations under different variance multipliers and receiving rate settings. The solid lines indicate the mean values of the metrics from the simulation results, while the shaded areas present the regions covered by one standard deviation of the simulation results.

The Kalman filter algorithm makes the three metrics converge to stable values within 50 seconds. Then, both vehicles stay in the region of higher variance or low message reception rate from about 200 to 400 seconds. Within this region, both air vehicles start executing collision avoidance behaviors from about 275 to 350 seconds. They reach the point with the shortest relative distance at about 300 seconds. Finally, they continue their journeys without further maneuvers after 400 seconds. The entropy metric quantifies the uncertainty level and increases when either vehicle enters the region of high variance or low message reception rate. The safety severity function quantifies how severely both air vehicles violate given airspace regulations and increases when both air vehicles get too close to each other. Finally, the traffic temperature is the ratio of the two metrics and indicates the level of confidence of how severely vehicles violate airspace regulations.

Figure 4.6 shows the evolution of the three metrics when varying the message reception rate. When both vehicles enter the low message reception rate region, the entropy increases between 200 and 425 seconds. In the same period, the traffic temperature drops a little bit because the ATA has less confidence in the situations of both vehicles due to the dropped messages. When both air vehicles are at the minimum relative distance, the entropy also reaches the highest value due to the collision avoidance system. Since the collision avoid-

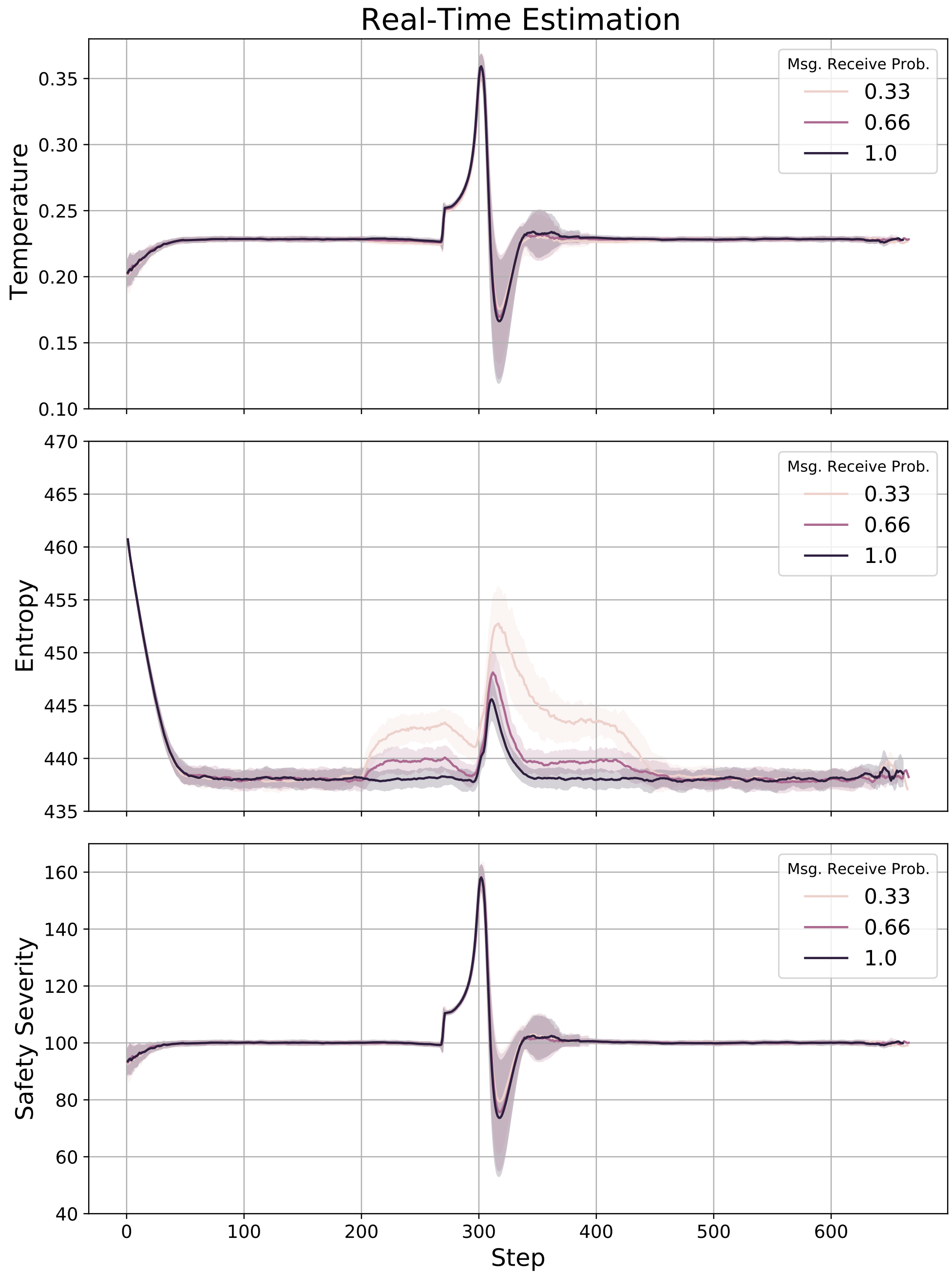

Figure 4.6. Metrics Evolution according to Real-Time Vehicle State Estimations with Changing **Message Reception Rate** (The plots from the top row to the bottom row show the temperature, the entropy, and the safety severity evolution. The solid lines show the mean of the results, while the shaded areas show the one-standard-deviation regions.)

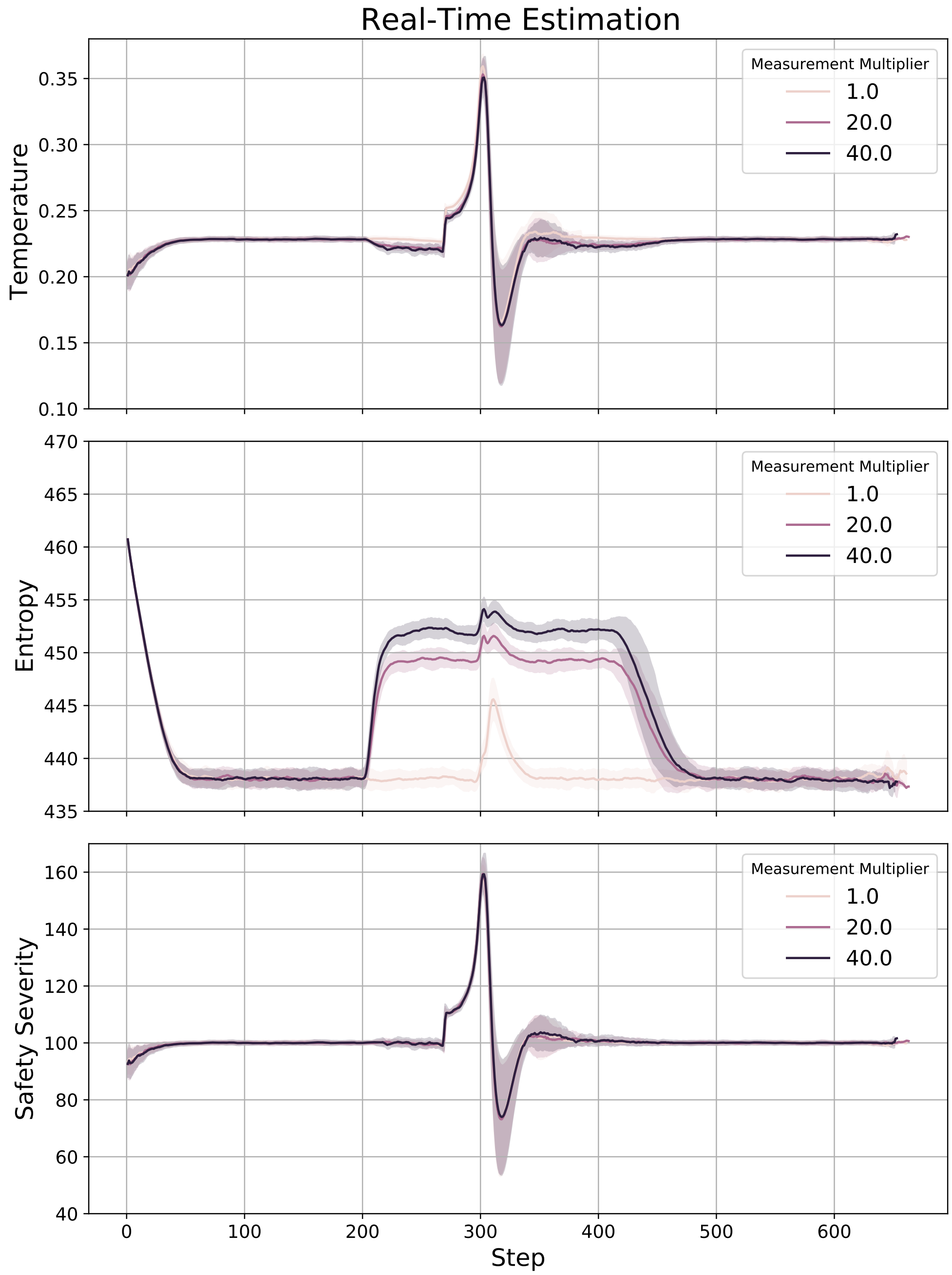

Figure 4.7. Metrics Evolution according to Real-Time Vehicle State Estimations with Changing **Measurement Noise Multiplier** (The plots from the top row to the bottom row show the temperature, the entropy, and the safety severity evolution. The solid lines show the mean of the results, while the shaded areas show the one-standard-deviation regions.)

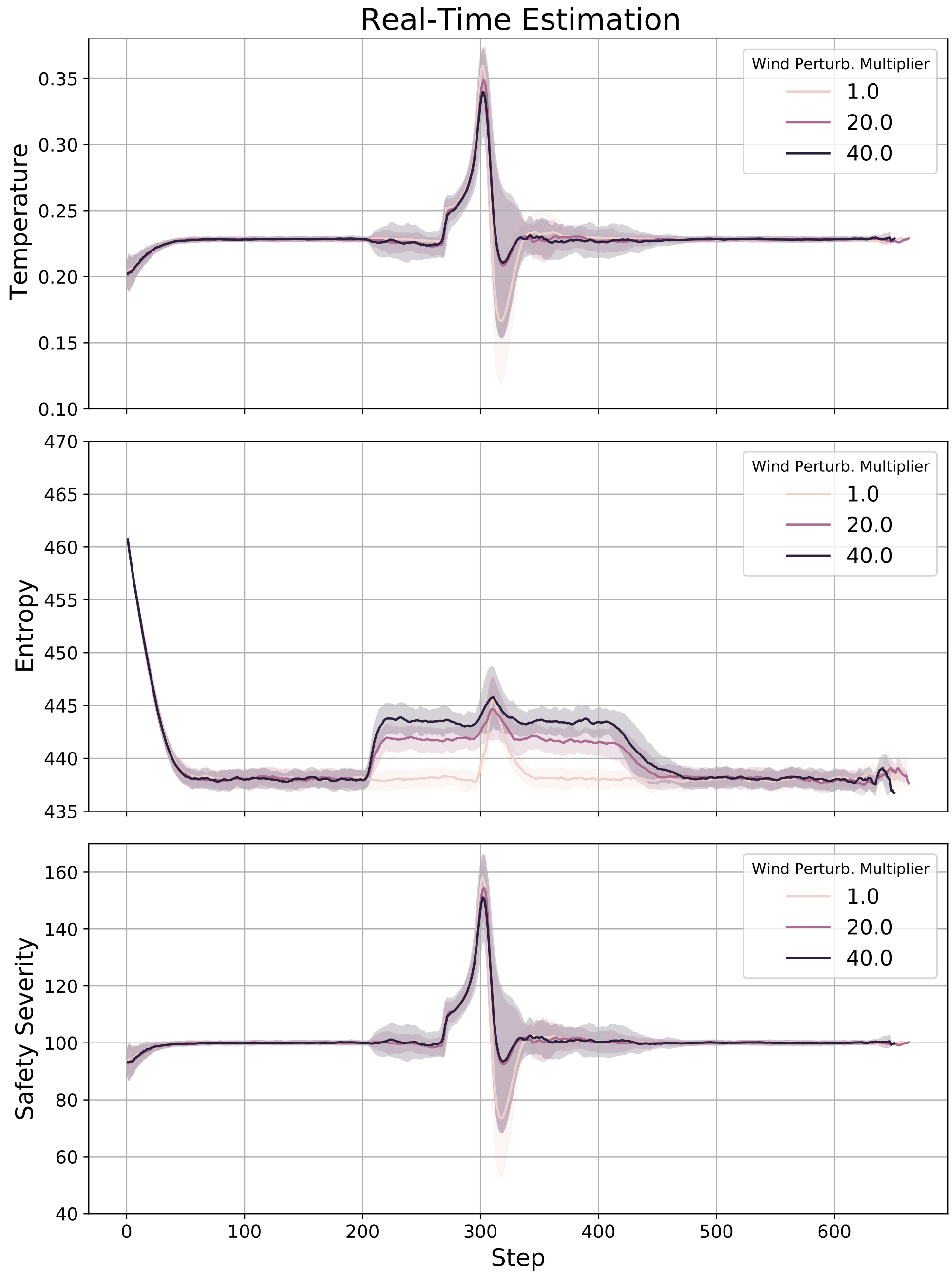

Figure 4.8. Metrics Evolution according to Real-Time Vehicle State Estimations with Changing **Wind Perturbation Multiplier** (The plots from the top row to the bottom row show the temperature, the entropy, and the safety severity evolution. The solid lines show the mean of the results, while the shaded areas show the one-standard-deviation regions.)

ance system relies on the estimated states of both vehicles, the uncertainty from one air vehicle influences the uncertainty level of the other. At the same time, the safety severity increases and reaches peak values. Due to the increasing severity of the traffic conditions, the temperature also increases even if the vehicle state uncertainty is high.

Similar phenomena also happen in the scenarios by changing the measurement error multipliers (Fig. 4.7). The main difference is the impact of the measurement error multiplier on the entropy evolution. Since the measurement error directly influences vehicle state estimations, a higher measurement error multiplier significantly increases the uncertainty level of vehicle state estimations. Additionally, the traffic temperature gives a higher weighting to the instance with safe traffic conditions. The high uncertainty levels of vehicle state estimations indicate that the true states of air vehicles might be farther away from the expected vehicle states. Also, the traffic temperature metric takes the true air vehicle states as stochastic variables and considers all potential random-drawing outcomes. For each time step, the temperature value with a higher measurement error multiplier is lower than the temperature with a lower measurement error multiplier. Nonetheless, the temperature reaches a similar peak value regardless of the measurement error setting when the two vehicles are at the minimum distance condition. Since the two air vehicles are at the minimum distance condition, all random-drawing instance has unfavorable traffic condition and makes the temperature reach a similar peak value.

The wind perturbation multiplier results in similar behaviors of the three metrics (Fig. 4.8) as other results. The wind perturbation pushes/pulls air vehicles and increases the standard deviation of the safety severity and the traffic temperature. The impact level of the wind perturbation multiplier on the entropy is as significant as the impact of the measurement error multiplier. Additionally, the traffic temperature slightly drops when both vehicles enter the high wind perturbation region. Then, when the relative distance between air vehicles is less than the collision avoidance distance, the traffic temperature increases and indicates that both vehicles are under a more unsafe condition.

The metrics based on the vehicle state prediction with a 20-second window (from Figs. 4.9 to 4.11) have similar trends as the metrics based on the real-time state estimation. The main difference from the metrics based on real-time state estimation is that the peaks lead to about

20 seconds. Based on the predicted vehicle state, the Kalman filter algorithm can identify if a near-miss event happens. And, the near-miss event increases the traffic temperature value because the Kalman filter has higher confidence that both vehicles are in unsafe conditions.

The predicted vehicle state comes with a high uncertainty value. Comparing plots from Figs. 4.6 to 4.11, the entropy metric based on the predicted vehicle state has higher entropy than the value based on the real-time estimation. This phenomenon indicates that the predicted vehicle state has a higher uncertainty than the real-time estimation. Additionally, the traffic temperature based on the predicted vehicle state is lower than the temperature based on real-time state estimation. The traffic temperature shows a lower level of confidence based on how severe the conditions between vehicles are.

The simplified simulation scenarios can help understand the metrics. The safety severity quantifies the safety level of the conditions of all vehicles. However, it is not sensitive to the uncertainty levels of the vehicle state estimations and predictions. Instead, the entropy value can represent the uncertainty level of the vehicle state estimations and predictions. When there is a higher uncertainty setting in the simulation, the entropy metric can truthfully quantify the uncertainty level of the vehicle state estimations and predictions. Finally, the traffic temperature is the ratio between the safety severity to the entropy. It can represent the level of confidence of how severe the traffic condition is. Although the traffic temperature decreases with a higher uncertainty setting, it can truthfully represent the near-miss event by reaching peak values. Hence, the temperature peak value detection can be an accurate trigger to identify if a near-miss event happens. Figure 4.12 shows the difference of a metric value with the value at the previous time step based on the 20 seconds vehicle state prediction.

The first row of Fig. 4.12 shows the difference of the traffic temperature based on 20 seconds vehicle state prediction. The first dip at around 200 seconds indicates that vehicles enter the high uncertainty region. The first peak happens at around 250 seconds when the Kalman filter algorithm estimates that the relative distance between the vehicles is less than the collision avoidance distance. Hence, the traffic safety severity function starts to include the electric potential energy part. Then, the second peak happens at around 280 seconds when the Kalman filter algorithm predicts that the vehicles are at the minimum distance

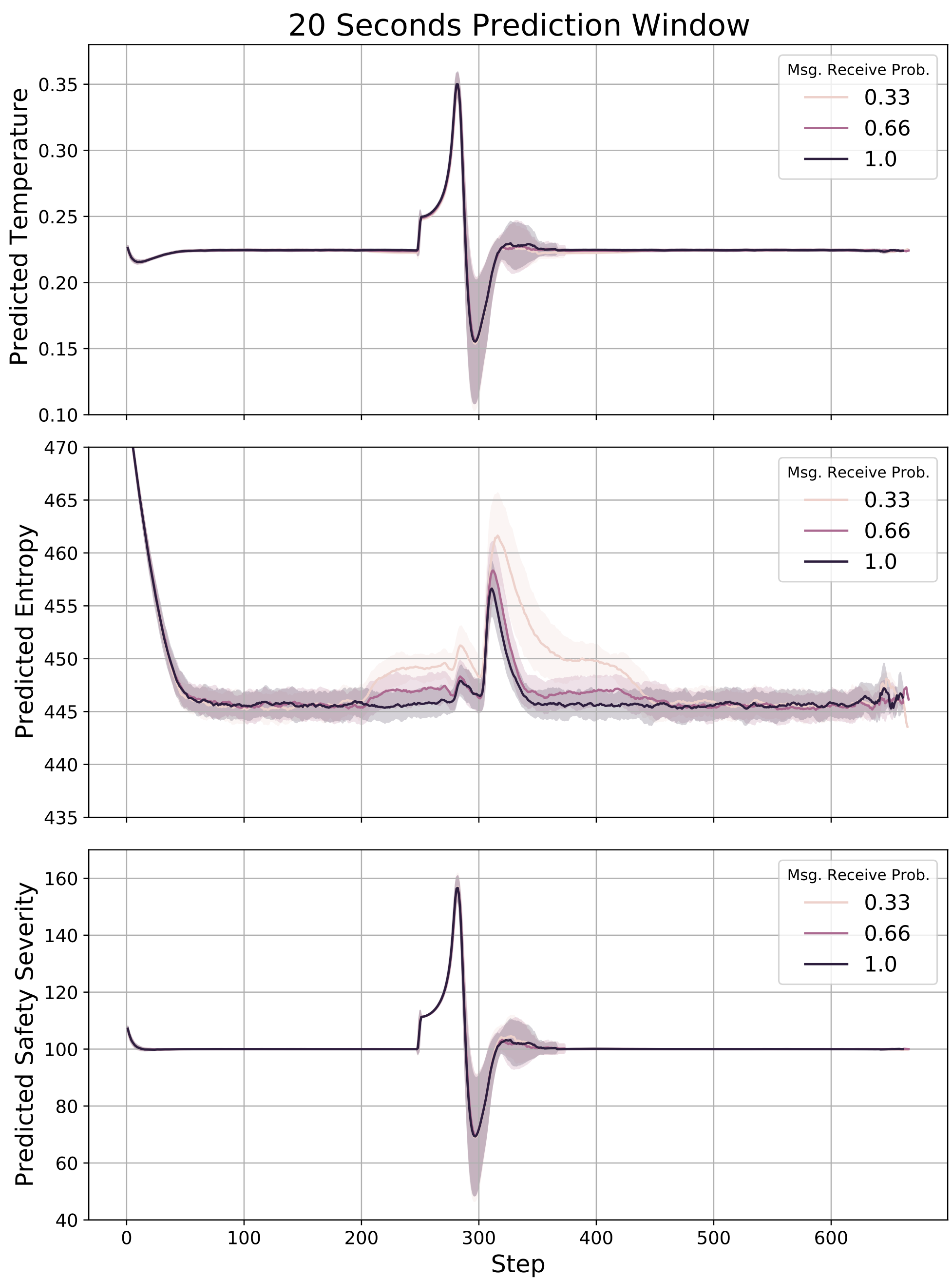

Figure 4.9. Metrics Evolution based on 20 Seconds State Predictions with Changing Variance Multipliers and Receiving Rate Settings — **Message Receiving Probability**

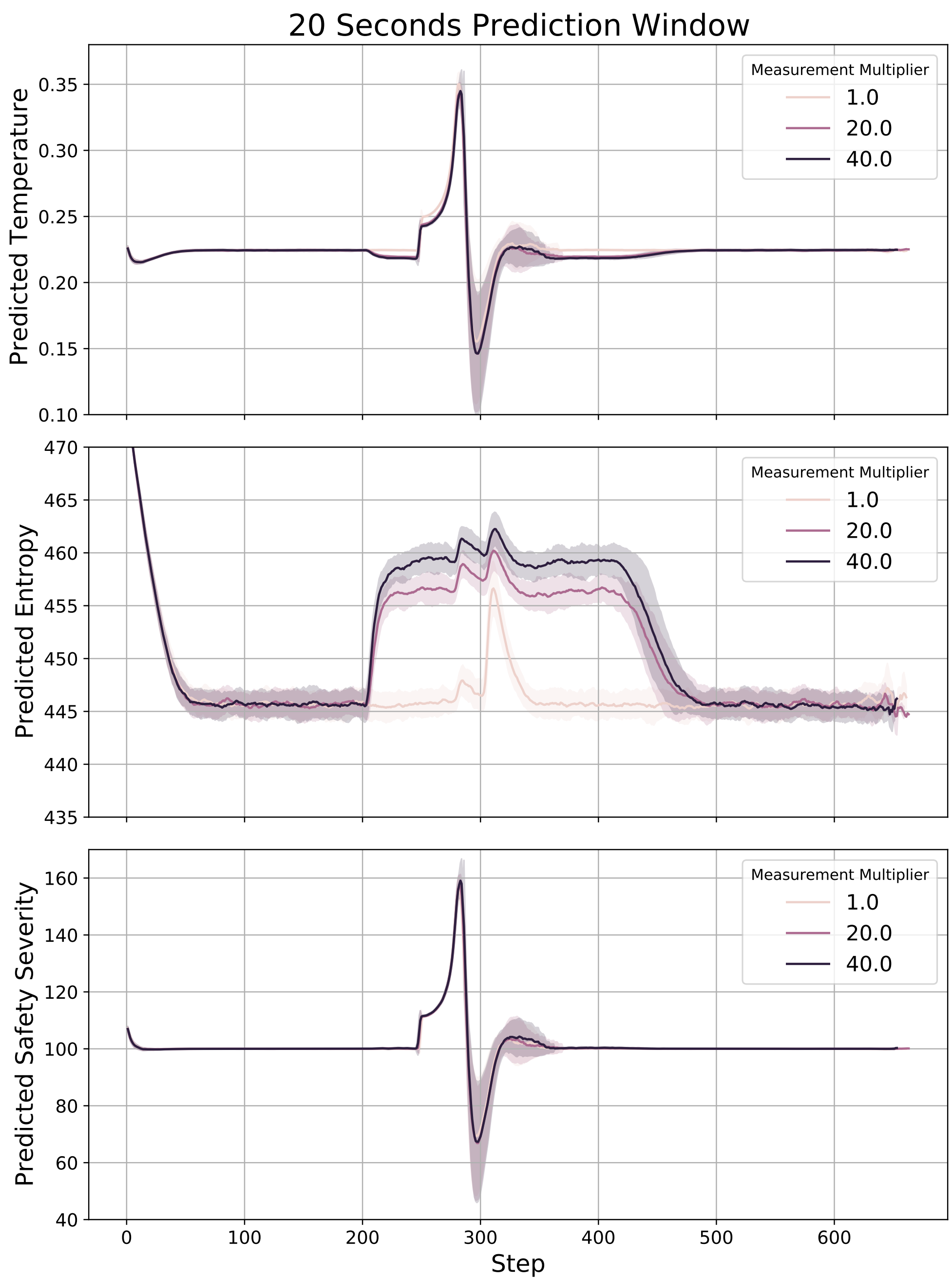

Figure 4.10. Metrics Evolution based on 20 Seconds State Predictions with Changing Variance Multipliers and Receiving Rate Settings — **Measurement Noise Multiplier**

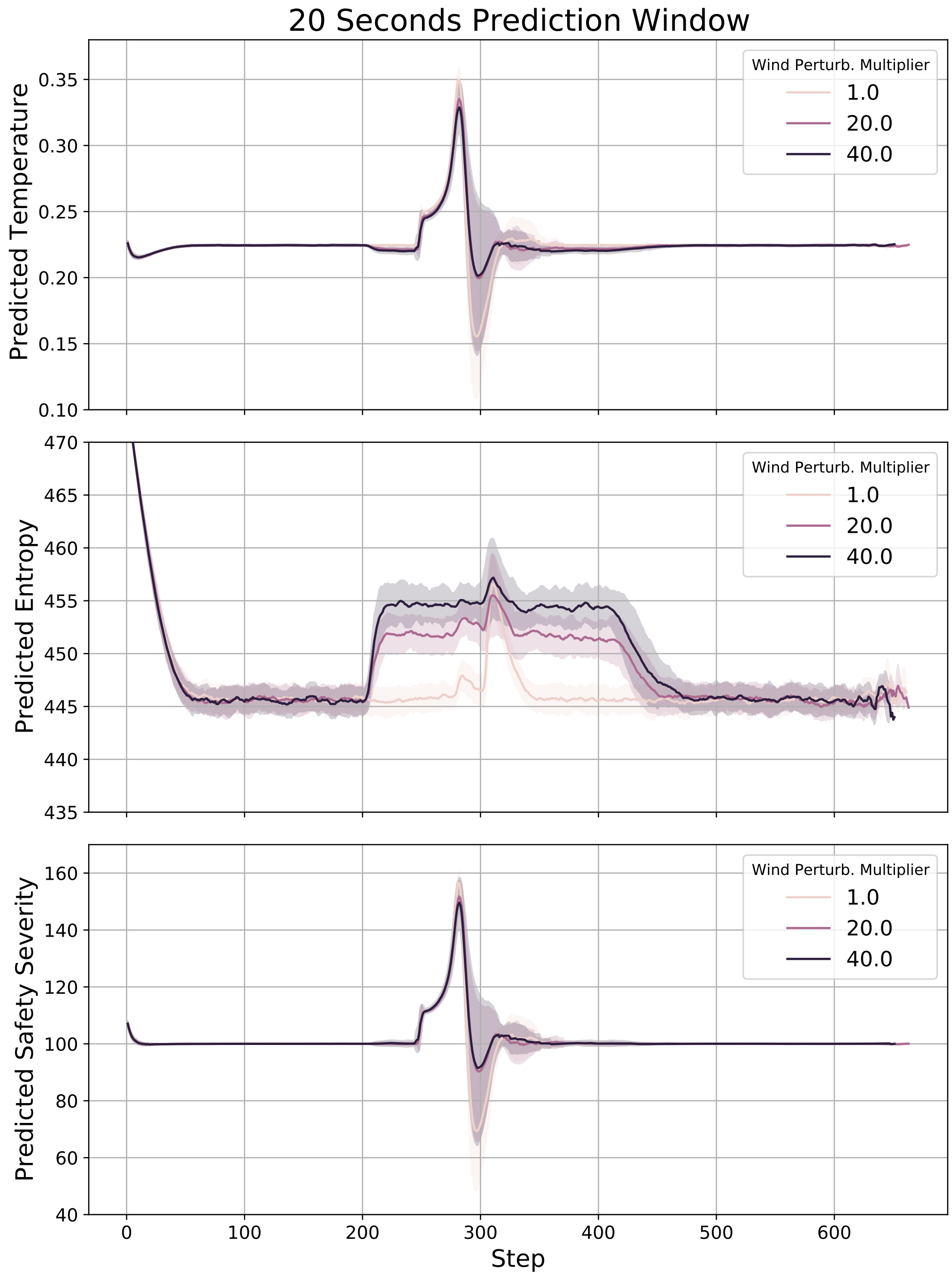

Figure 4.11. Metrics Evolution based on 20 Seconds State Predictions with Changing Variance Multipliers and Receiving Rate Settings — **Wind Perturbation Multiplier**

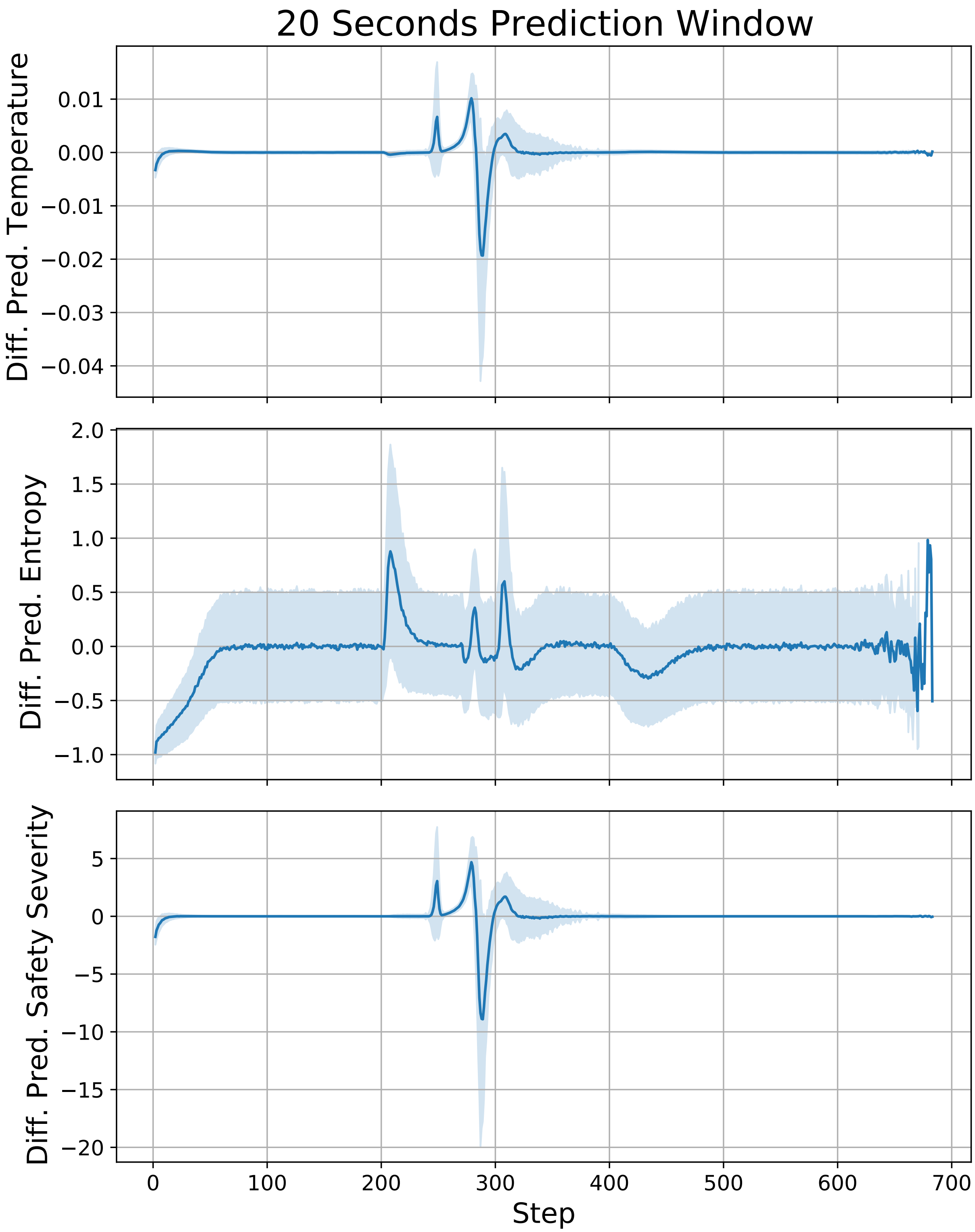

Figure 4.12. Difference of Metrics based on 20 Seconds State Prediction (Solid lines show the average value from the results. The shaded areas are the regions cover by 95% of the confidence interval.)

point. Finally, the second dip happens about 290 seconds because the Kalman filter predicts that both air vehicles will slow down and depart from each other.

The entropy plot in the second row of Fig. 4.12 tells a similar story. Both vehicles enter the high uncertainty region at around 200 seconds. Then, the second peak happens at around 280 seconds because the Kalman filter predicts that both air vehicles will reach the minimum relative distance 20 seconds later. The collision avoidance system makes both air vehicles rely on each other's locations. The state estimation uncertainty from one vehicle immediately influences the state estimation accuracy of another. Hence, the collision avoidance drives up the vehicle state estimation uncertainty. Subsequently, the third peak happens at around 300 seconds because the vehicles reach the point of the minimum distance. The Kalman filter algorithm cannot predict vehicle states with low uncertainty levels due to the design of the collision avoidance system.

The safety severity plot in Fig. 4.12 includes three peaks at around 250 seconds, 280 seconds, and 300 seconds. The first peak happens because the collision avoidance system starts to activate. The second peak happens when the vehicles reach the minimum distance point. The third peak occurs when the collision avoidance system pushes the vehicles away from each other.

The one-step difference of the three metrics is eligible as the near-miss event trigger. The next section shows the results with the trigger using the Closest Point of Approach (CPA) as the baseline. The following section includes the comparison of the CPA trigger with triggers based on the differences of the three proposed metrics.

4.2.3 Temperature-based Trigger Performance Analysis

The CPA generates two outputs, which are the time to the closest point of approach (t_{CPA}) and the minimum distance. The near-miss trigger activates if both outputs are lower than pre-set respective thresholds. This study also uses 20 seconds as the threshold for t_{CPA}. The minimum distance threshold for the CPA is adjustable to influence the sensitivity of the near-miss event trigger based on the CPA.

A near-miss event happens when two vehicles are too close to each other. Under an ideal scenario without any perturbation or message dropping, the near-miss event would never happen. Figure 4.13 shows the vehicle trajectories in 1-D space with the setting of the ideal scenario. The y-axis of Fig. 4.13 shows the evolution of the time, while the x-axis shows the position of the vehicles. The blue vehicle travels from the left-hand side of the space to the right-hand side, while the red vehicle moves in the opposite direction. Fig. 4.13 is based on the settings in Table 4.2. The resulting minimum distance between the two air vehicles is about 46 meters. In the following results, a near-miss event happens when the relative distance between two air vehicles is less than 46 meters.

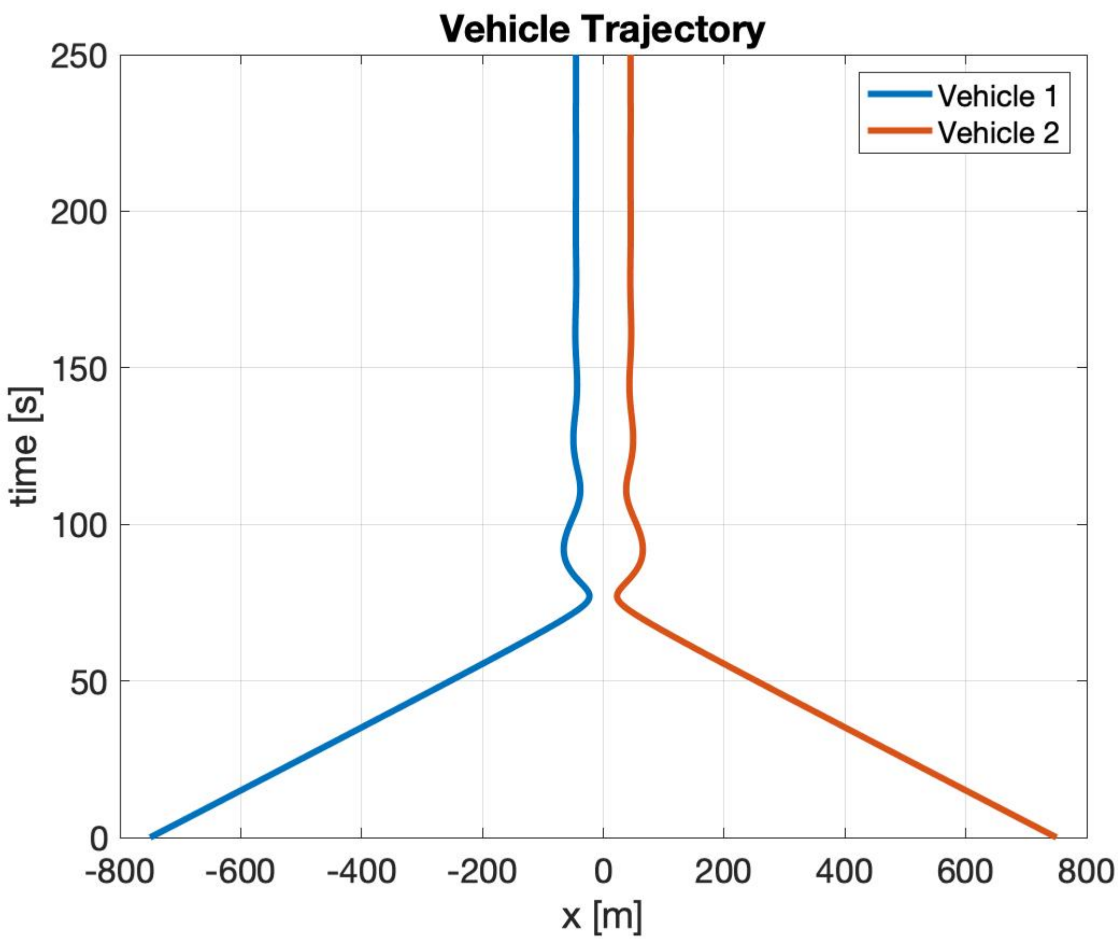

Figure 4.13. Trajectories of Vehicles with the Charged Particle Dynamic Model (Blue vehicle moves from left to right, while the red vehicle travels from right to left. The x-axis shows the locations, while the y-axis shows time.)

The near-miss event triggers based on the one-time step differences of the three metrics need a threshold setting to adjust their sensitivity. A high threshold setting requires a sudden change of the metric value to trigger a near-miss event warning. Although a high threshold setting can reduce the false-positive alarm, the high threshold setting can also reduce the true-positive alarm.

An ideal trigger should reach a 100% true-positive rate and a 0% false-positive rate. However, based on threshold settings, both true-positive rates and false-positive rates vary between 0% and 100%. The Receiver Operation Characteristic (ROC) is a line showing the relationship between the true-positive rate (y-axis) and the false-positive rate (x-axis) of a trigger (Fig. 4.14) by varying the trigger threshold. A commonly used metric to quantify the performance of a trigger is the Area Under the ROC Curve (AUC), which is the shaded area in Fig. 4.14. The ideal trigger (with a 100% true-positive rate and a 0% false-positive rate) will have an AUC score of 1.00.

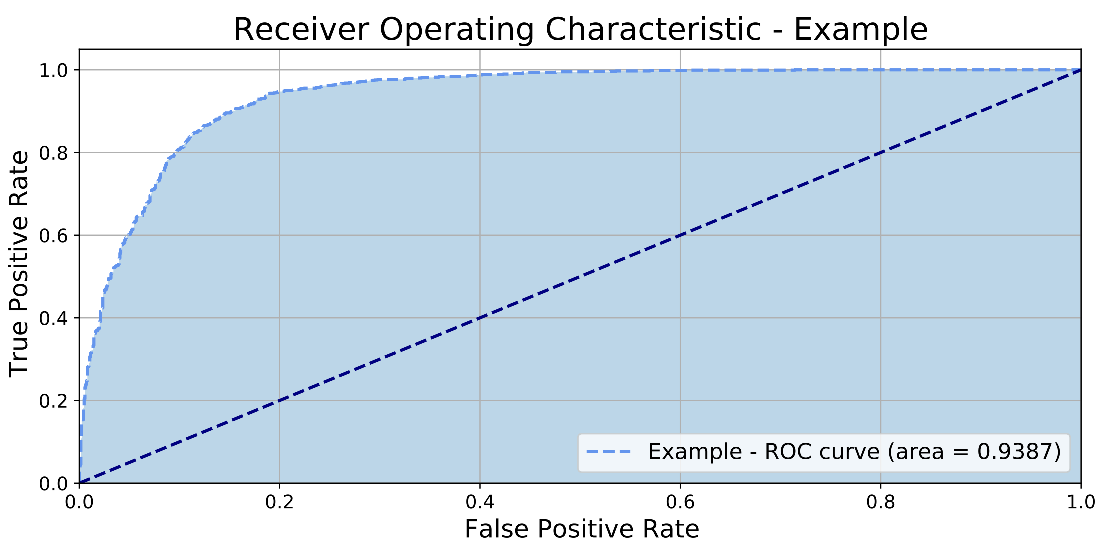

Figure 4.14. Example of Receiver Operation Characteristic (ROC) and Area Under the Curve (AUC) (The ROC is the light blue dashed line, while the AUC is the shaded area under the blue line.)

Figure 4.15 shows the ROC curves and lists AUC scores for the triggers based on the CPA and differences of the three metrics. The CPA-based near-miss event trigger has an AUC score of 0.9435. The trigger based on the difference of the traffic temperature has an

AUC score of 0.9422, which is close to the CPA-based trigger. The trigger based on the difference of the safety severity has an AUC score of 0.9410, which is also marginally worse than the CPA-based trigger. Finally, the trigger based on the difference of the entropy has the worst performance with an AUC score of 0.4417.

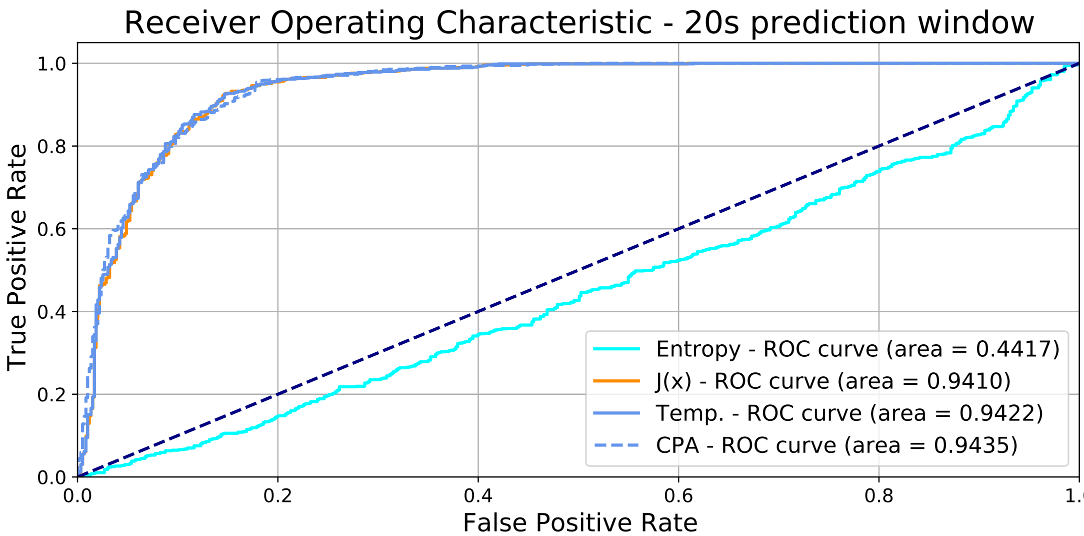

Figure 4.15. Receiver Operating Characteristic (ROC) and Area Under the Curve (AUC) for Trigger based on Metrics and Closest Point of Approach (CPA) (The solid light blue line and the solid orange line shows the ROC of entropy-based and safety-severity-based triggers, respectively. The blue solid line shows the ROC of the temperature-based trigger. The dashed blue line presents the ROC of the CPA-based trigger.)

The trigger based on the difference of the entropy has the worst performance among the chosen three triggers. The difference of the entropy values in Fig. 4.12 shows three peaks indicating three different events between both air vehicles. The first peak happens when either vehicle enters the high uncertainty region. Although the second peak is associated with the predicted near-miss event based on the Kalman filter algorithm, the first peak is much higher than the second one and shadows the performance of the entropy-based trigger.

Results in Fig. 4.15 are based on the assumption that the setting of the high uncertainty region is unknown. However, since there are different possible combinations of the settings in the high-uncertainty region, the performance of the trigger changes. Figure 4.16 shows the distributions of the AUC scores based on different settings for the high uncertainty region. The AUC score distributions of the triggers based on the temperature difference and the safety severity difference are similar and consistent. The AUC score distribution of the CPA-based trigger is more consistent than the triggers based on the temperature difference or the safety severity difference, but it is more skewed towards lower values of AUC. Finally, the trigger based on the entropy difference is consistently lower than the other three triggers.

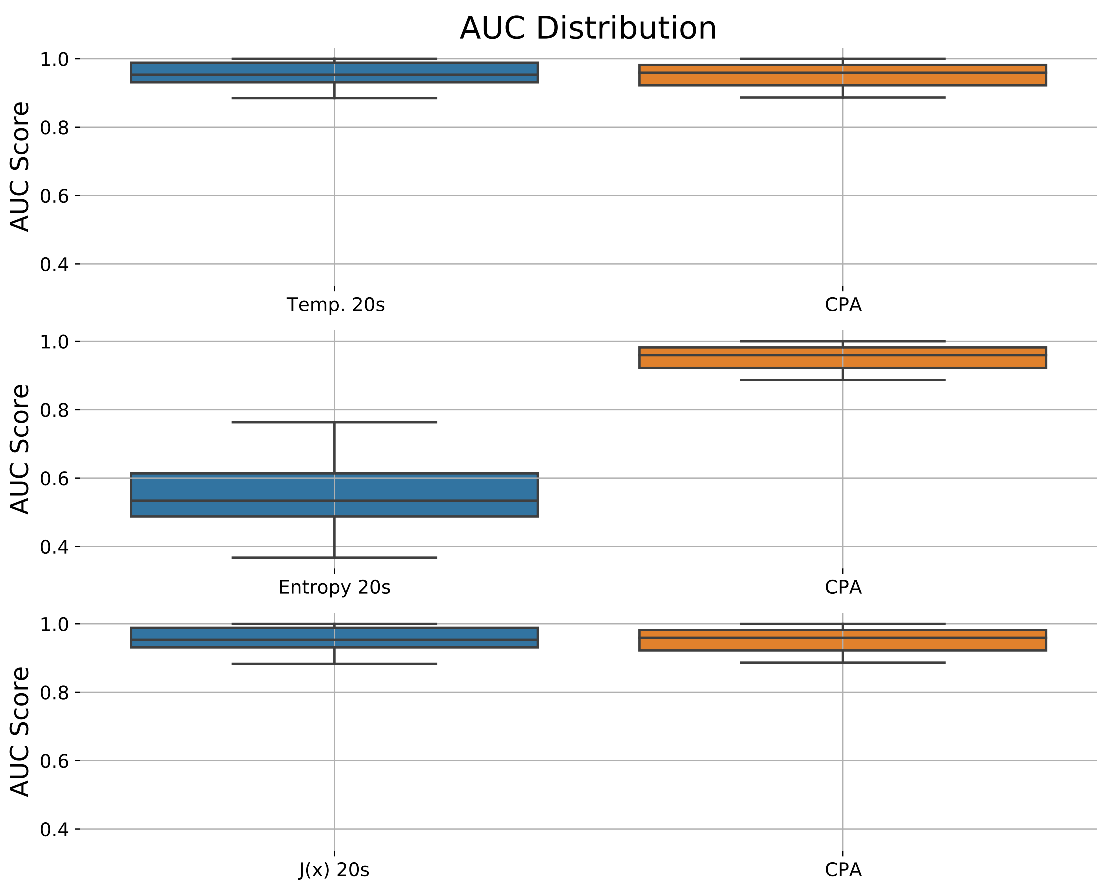

Figure 4.16. AUC Score Distribution based on Various Environmental Perturbation Setting

The results show that the trigger based on the traffic temperature difference should be sufficient for the near-miss event detection. The optimal threshold of the trigger is the temperature difference threshold corresponding to the sum of the true-positive rate and the false-positive rate equals one. The resulting threshold is about 0.019.

4.2.4 Effectiveness of ATA Traffic Management Mechanisms

This section describes results to assess the effectiveness of the ATA traffic management mechanisms. Table 4.5 shows the near-miss rate based on various combinations of the settings of the traffic management mechanisms, assuming that the settings of the high uncertainty region are unknown. The baseline scenario, which disables all traffic management mechanisms, has 56% of the near-miss rate. Based on the setting of the traffic management mechanisms, the lowest near-miss rate is 21.7% when the broadcast rate adjustment mechanism is inactive and the scenario has a low-temperature trigger threshold (0.005) and high charge multiplier (1.8) settings. Subsequently, the results include the near-miss rate based on the combination of settings of the traffic management mechanisms and of the high uncertainty region. This study also includes a linear regression model to understand the relationships between the near-miss rate and the settings of the traffic management mechanisms.

Equation 4.3 shows the linear regression model to identify the effectiveness of the traffic management mechanisms. $R_{\text{Near-Miss}}$ shows the near-miss rate, while $C(\cdot)$ indicates the variable inside this function is a categorical variable. $S_{\text{broadcast}}$ indicates if the VTBF adjustment mechanism is active or not. $S_{\text{trigger}} : S_{\text{multiplier}}$ shows a combination of the temperature trigger threshold and the charge multiplier settings. Finally, Table 4.6 shows the coefficients and p-values of the linear regression model based on Eq. 4.3.

$$R_{\text{Near-Miss}} \sim C\left(S_{\text{broadcast}}\right) + C\left(S_{\text{trigger}} : S_{\text{multiplier}}\right) \tag{4.3}$$

Table 4.6 reveals the different properties of the two traffic management mechanisms. The VTBF adjustment can reduce the near-miss rate by about 1.78%. But the effectiveness of VTBF adjustment is statistically insignificant. Results also show how the minimum separation criterion adjustment mechanism is only effective with certain combinations of the settings. The mechanism is effective when the temperature threshold is low enough (0.005) and the charge multiplier is high enough (1.2). In these cases, the minimum separation criterion adjustment mechanism can reduce the near-miss rate by about 12% to 34%.

Figure 4.17 shows the average traffic temperature based on real-time state estimation through each simulation run, with the mechanism combination shown in Table 4.5. The

Table 4.5. Near-miss Rate Associated with Different Settings for ATA Traffic Management

Broadcast Rate Adjustment	Temperature Trigger Threshold	Charge Multiplier	Near-Miss Rate
False	None	None	56.07%
	0.005	1.2	45.26%
		1.5	30.74%
		1.8	21.70%
	0.010	1.2	52.52%
		1.5	38.00%
		1.8	24.30%
	0.050	1.2	55.78%
		1.5	55.63%
		1.8	57.48%
True	None	None	56.22%
	0.005	1.2	42.59%
		1.5	28.30%
		1.8	21.93%
	0.010	1.2	48.22%
		1.5	34.97%
		1.8	24.96%
	0.050	1.2	53.19%
		1.5	54.44%
		1.8	54.89%

effective combination of ATA traffic management mechanism settings should reduce the average traffic temperature. The VTBF adjustment mechanism just slightly reduces the mean of the traffic temperature, as can be observed by comparing the bars with the active

Table 4.6. Coefficient of Linear Regression Model for Eq. 4.3

Variable	Coefficient.	p-value
Baseline	57.04%	0.000
$S_{\text{broadcast}}$ [True]	-1.78%	0.259
$S_{\text{trigger}} : S_{\text{multiplier}}$ [0.005:1.2]	-12.22%	0.001
$S_{\text{trigger}} : S_{\text{multiplier}}$ [0.005:1.5]	-26.63%	0.000
$S_{\text{trigger}} : S_{\text{multiplier}}$ [0.005:1.8]	-34.33%	0.000
$S_{\text{trigger}} : S_{\text{multiplier}}$ [0.01:1.2]	-5.78%	0.101
$S_{\text{trigger}} : S_{\text{multiplier}}$ [0.01:1.5]	-19.67%	0.000
$S_{\text{trigger}} : S_{\text{multiplier}}$ [0.01:1.8]	-31.52%	0.000
$S_{\text{trigger}} : S_{\text{multiplier}}$ [0.05:1.2]	-1.67%	0.636
$S_{\text{trigger}} : S_{\text{multiplier}}$ [0.05:1.5]	-1.11%	0.752
$S_{\text{trigger}} : S_{\text{multiplier}}$ [0.05:1.8]	0.04%	0.992
Adj. R-square	0.287	

VTBF against the inactive one. When the temperature trigger threshold is low enough (0.01 and 0.005), the higher charge multipliers can reduce the average traffic temperature. The higher charge multiplier effectively increases the minimum separation distance and reduces the safety severity of the traffic conditions.

In conclusion, although the VTBF adjustment mechanism can reduce the near-miss rate, its impact is marginal according to the statistical analysis results and on the average traffic temperature. The adjustment of the minimum separation criterion is an effective mechanism for resolving a near-miss event when the traffic temperature threshold is low enough.

4.3 Temperature Property Analysis with Multi-Vehicle Simulation

This section investigates how the temperature can help an ATA identify unsafe air traffic situations. The first part of the section will discuss the simulation scenario setups. Then, the following section will show the simulation results.

4.3.1 Multi-Vehicle Simulation Description

This section includes two traffic patterns for investigating how the temperature metric responds to different traffic conditions. The structured corridor airspace contains two chan-

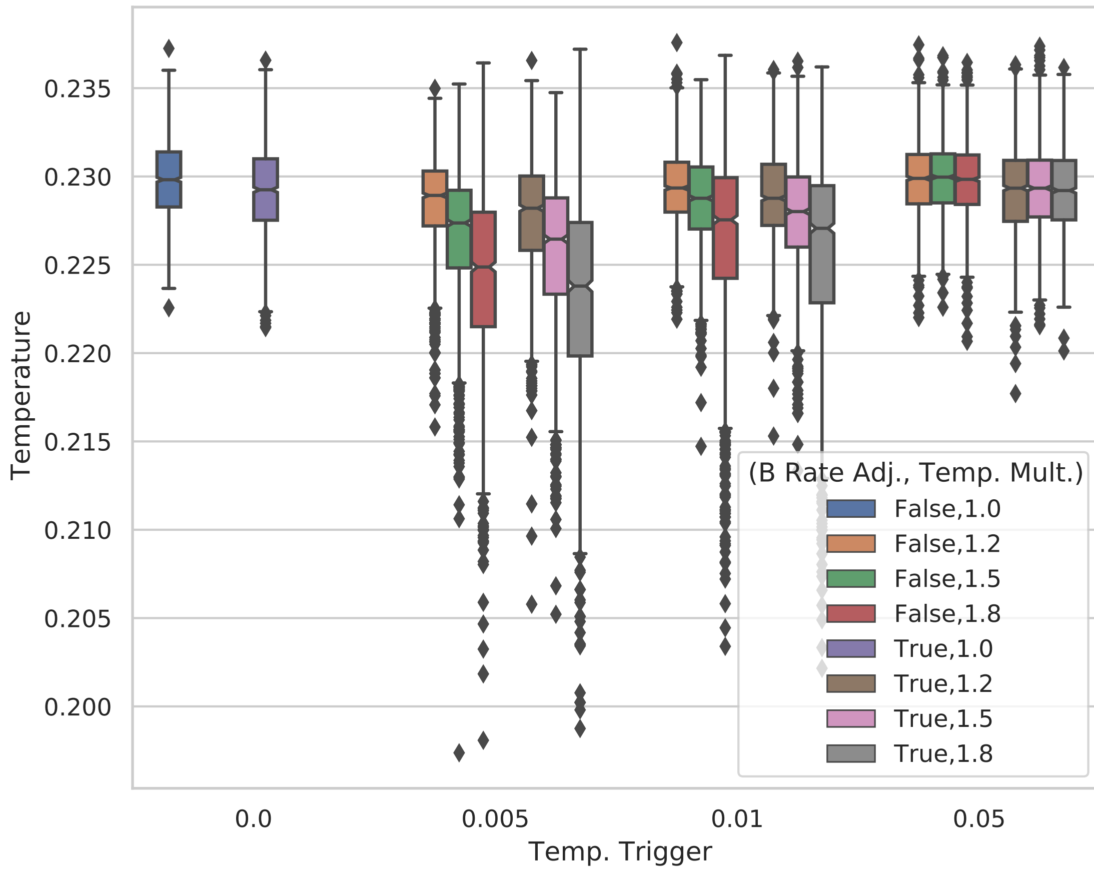

Figure 4.17. Average Temperature Value Distribution based on Various ATA Traffic Management Mechanism Settings

nels with vehicles flying in opposite directions (Fig. 4.18). The green triangles in Fig. 4.18 show the origin locations of the air vehicles, while the grey lines show their trajectories through the simulation. The air vehicles in the upper half of the airspace travel from the left-hand side of the map to the right-hand side. The air vehicles in the lower half of the airspace go from the right-hand side to the left-hand side. The maximum distance between the origin locations of the air vehicles in the same corridor is 600 meters. If there are more than five vehicles in the same channel, the air vehicles are evenly placed across the width of the corridor. Finally, the goal of the air vehicles is to travel to the opposite side of the map.

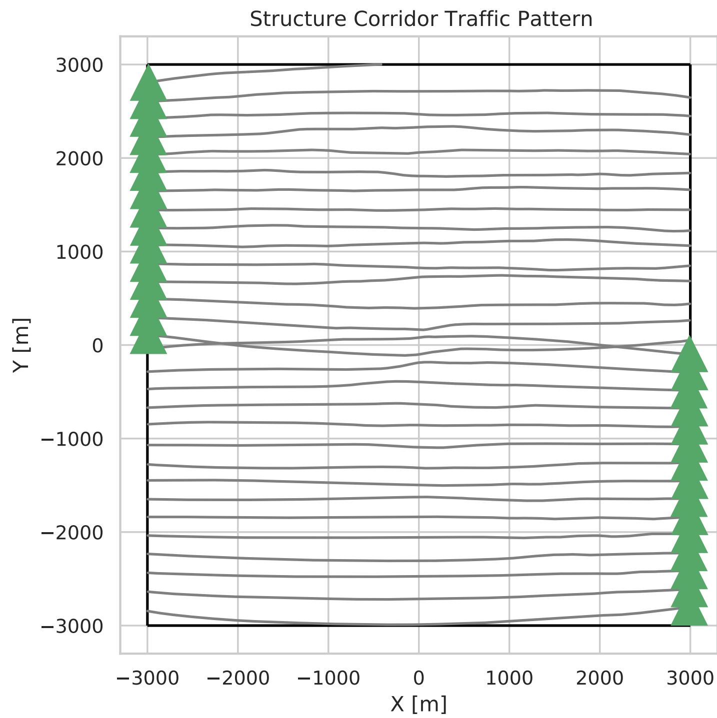

Figure 4.18. Structured Corridor Traffic Pattern (Vehicles can only fly from left-to-right on the upper half of the map, while they can only travel from right-to-left on the bottom half of the map. Green triangles indicate origins of air vehicles, while the grey solid lines show their trajectories.)

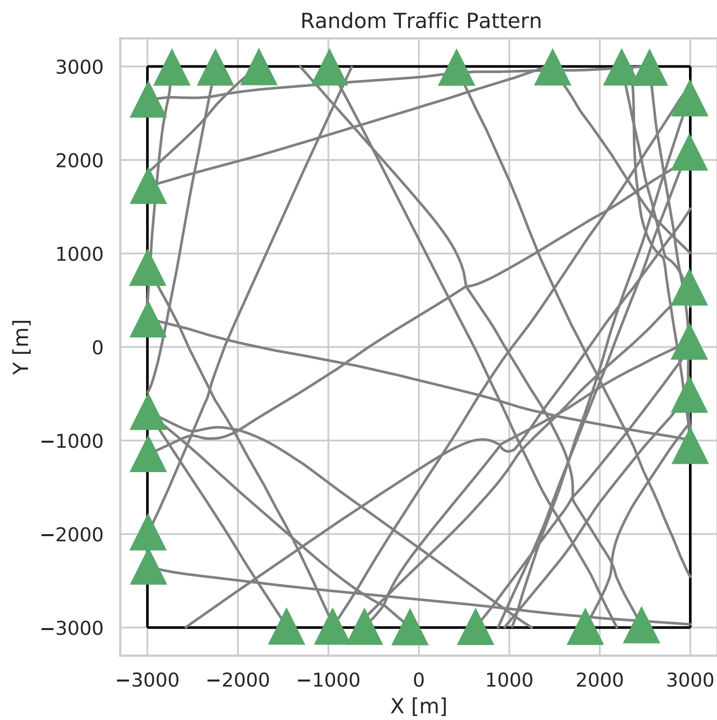

Figure 4.19. Random Traffic Pattern (Vehicles randomly start on either one of the edges of the map to another random place on the other side of the map. Green triangles indicate origins of air vehicles, while the grey solid lines show their trajectories.)

In the random airspace, the origins and destinations of the air vehicles are randomly distributed on the edges of the virtual world (Fig. 4.19). If the relative distance between any two origins is less than the collision avoidance distance (600 meters), the simulation randomly generated two new starting points for ensuring that no air vehicle is in the contingent situation at the beginning of the simulation.

In both types of airspace, there are regions with either a higher measurement error multiplier, a higher wind perturbation multiplier, or a lower message reception rate. These high uncertainty regions can mutually overlap and result in different combinations and sizes of the high environmental uncertainty areas. The list of the multipliers and message reception rate settings for the high uncertainty regions are as follows.

- **Measurement Error Multiplier**: 40
- **Wind Perturbation Multiplier**: 40
- **Message Reception Rate**: 0.5

The air vehicle in the multiple vehicle simulation follows the same setting in Table 4.2. The number of air vehicles in the airspace can be either 6, 10, 20, or 30. Each simulation uses a different combination of the ATA traffic management mechanism settings in Table 4.7 and the number of air vehicles. For each combination of the simulation setting, the simulation repeats 40 times with different random seeds. The following section shows the analyzed simulation results.

Table 4.7. Setting for ATA Traffic Management Mechanisms for Multi-vehicle Simulation

Parameter	**Values**	
Broadcast Freq. Adjust Mechanism	[On, Off]	
Temp. Trigger Threshold	Off	[0.005, 0.01, 0.05]
Charge Multiplier	Off	[1.2, 1.5, 1.8]

4.3.2 Comparison of Different Traffic Patterns

The traffic temperature can represent the level of confidence of how severely the air traffic violates airspace regulations. Figure 4.20 shows the average temperature evolution based on different traffic patterns and the activation of the VTBF adjustment mechanism. The blue lines show the results with the random traffic pattern setting. And the orange lines present the structured corridor traffic pattern results. The solid lines indicate the scenario without activating the VTBF adjustment mechanism, while the dashed lines show the runs with the activated VTBF adjustment mechanism. Additionally, the shaded area indicates the one standard deviation range of the traffic temperature. Each plot in Fig. 4.20 shows the runs with the different numbers of the air vehicles.

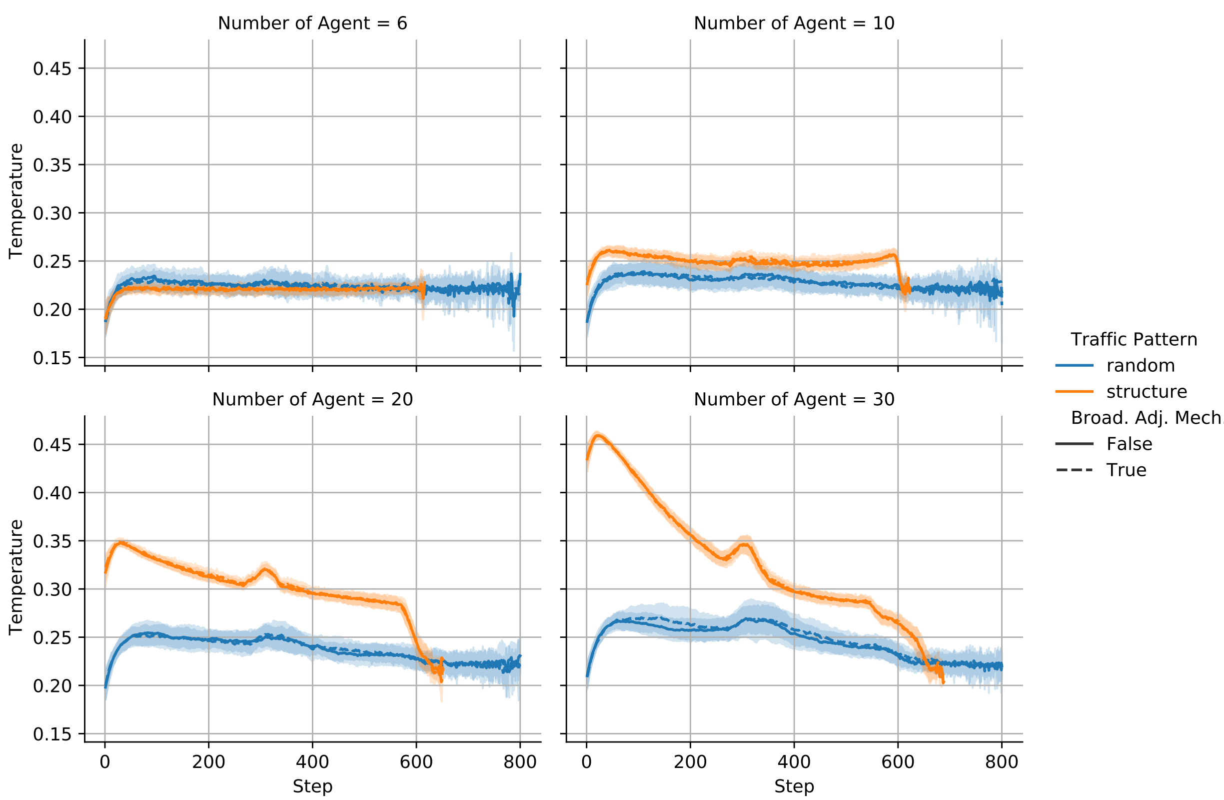

Figure 4.20. Traffic Temperature Evolution with Different VTBF Adjustment Mechanism Settings (The blue and orange lines show the scenarios with random and structured traffic pattern settings, respectively. The solid and dashed lines show the scenario with active and inactive VTBF settings. Each plot shows the simulation results with a different number of vehicles.)

The simulation results show that the number of vehicles influences the evolution of the traffic temperature. With six air vehicles, the traffic temperature from the structured traffic pattern is lower than the temperature from the random traffic pattern. Additionally, the random traffic pattern results in higher traffic temperature variation than the structured traffic pattern. When the number of vehicles increases, the temperature from the random traffic pattern slightly increases. Because there are higher chances that air vehicles in the random traffic pattern have conflicted flight paths, the increasing temperature responses to the higher confidence that the air vehicles are in an unsafe situation.

The average temperature from the structured traffic pattern increases faster than the random traffic pattern as the number of air vehicles increases. Due to the design of the structure corridor, air vehicles in the same channel get closer to accommodate more air vehicles. Although all air vehicles in the same corridor travel in the same direction, they need to pay more attention to the nearby air vehicles to ensure no near-miss situation would happen. Hence, the ATA has a higher and more consistent level of confidence that the air traffic in the structure airspace is more dangerous than the random airspace.

As the simulation proceeds in the structured traffic pattern, the vehicles from the opposite traveling direction corridors meet at the center of the map. Hence, the collision avoidance system of the air vehicles at the center of the map has to be aware of the nearby air vehicles and the vehicles traveling toward them as a temperature peak occurs at around 300 seconds in Fig. 4.20. Similar phenomena also happen in the simulation with the random traffic pattern. Since all vehicles start from the map boundary, they converge to the center of the virtual world and spread out again as the simulation proceeds. Therefore, the average temperature with the random traffic pattern presents a peak at around 300 seconds.

Air vehicles in the structured traffic pattern are squeezed on the y-axis at the beginning of the simulation. As the simulation proceeds, the air vehicles gradually spread out on the y-axis. Some air vehicles leave from the map due to collision avoidance maneuvers. This phenomenon reduces the vehicle density in the airspace and reduces the traffic safety severity level. Hence, the average temperature of the simulation with the structured traffic pattern reduces along with the simulation.

The VTBF adjustment mechanism has an insignificant impact on the average temperature. Figure 4.20 shows that the average temperature evolution is similar between the scenarios with and without the VTBF adjustment mechanism. The solid lines and the dashed lines almost overlap regardless of the number of air vehicles or the traffic patterns.

The minimum separation criterion adjustment mechanism happens more frequently as the number of air vehicles increases. Figure 4.21 shows the 30 vehicles simulation results with different mechanism settings. The columns show results with different temperature trigger threshold settings. And the rows show results with different charge multiplier settings.

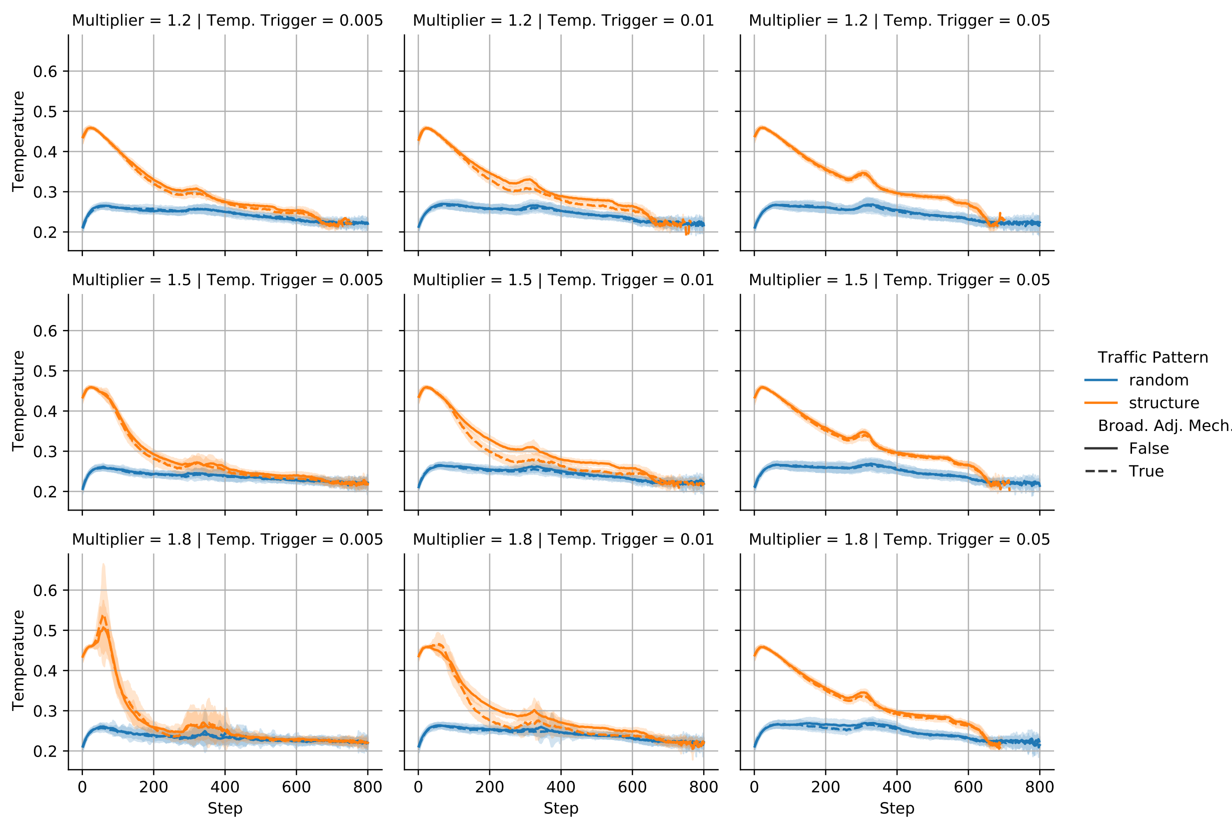

Figure 4.21. 30 Vehicles Traffic Temperature Evolution with Different Settings for Minimum Separation Adjustment Mechanism (The rows from top to bottom show the charge multiplier settings from 1.2, 1.5, and 1.8, respectively. The columns from left to right show results with temperature trigger thresholds from 0.005, 0.01, and 0.05. The blue and orange lines show the results with random and structured traffic patterns, respectively. The solid and dashed lines present the results with and with the VTBF adjustment mechanism.)

The minimum separation criterion adjustment mechanism is effective in the scenarios with a low enough temperature trigger threshold and a high enough charge multiplier setting. First, the separation criterion adjustment mechanism with the temperature trigger threshold of 0.05 is ineffective. The plots on the most right column in Fig. 4.21 are similar to Fig. 4.20. And, the cases with the structured corridor traffic pattern and the low trigger threshold (0.005 and 0.01) have different trends from other scenarios. With the 0.01 temperature trigger threshold, the results with the VTBF adjustment mechanism have a lower average temperature than the result without the VTBF adjustment mechanism. And, with a higher charge multiplier setting, the average temperature drops more quickly from 50 to 200 seconds. Due to the high charge multiplier setting, some air vehicles aggressively spread out and leave the simulation. This phenomenon reduces the number of air vehicles, the traffic safety severity level, and the average temperature. Finally, the air vehicles in the structured traffic pattern have to pay attention to the head-on traffic at around 300 seconds. With a low trigger threshold (0.005) and a high charge multiplier (1.8) setting, the air vehicles may have an aggressive collision-avoidance maneuver and make the average temperature fluctuate.

Figures 4.22 and 4.23 show the example scenario that illustrates the correlations between the temperature metrics, the minimum distance between all vehicles, and the near-miss event. Figure 4.22 shows the temperature evolution based on the real-time state estimation and the minimum distance between air vehicles. The plot shows a local temperature peak whenever the minimum vehicle distance reaches a local minimum. It seems that the two metrics have a negative correlation. Furthermore, Fig. 4.23 shows the temperature evolution based on 20 seconds vehicle state predictions and the number of near-miss events. The plots show that the temperature hits a peak several seconds before the near-miss event occurs. Hence, there should have a positive correlation between the temperature and the number of near-miss events.

The results use cross-correlation to quantify the correlations between the two pairs of the lines in Figs. 4.22 and 4.23. However, the minimum vehicle distance and the temperature based on the real-time state estimations have non-zero auto-correlation. Several research groups show that the auto-correlations influence the assessment of the cross-correlations

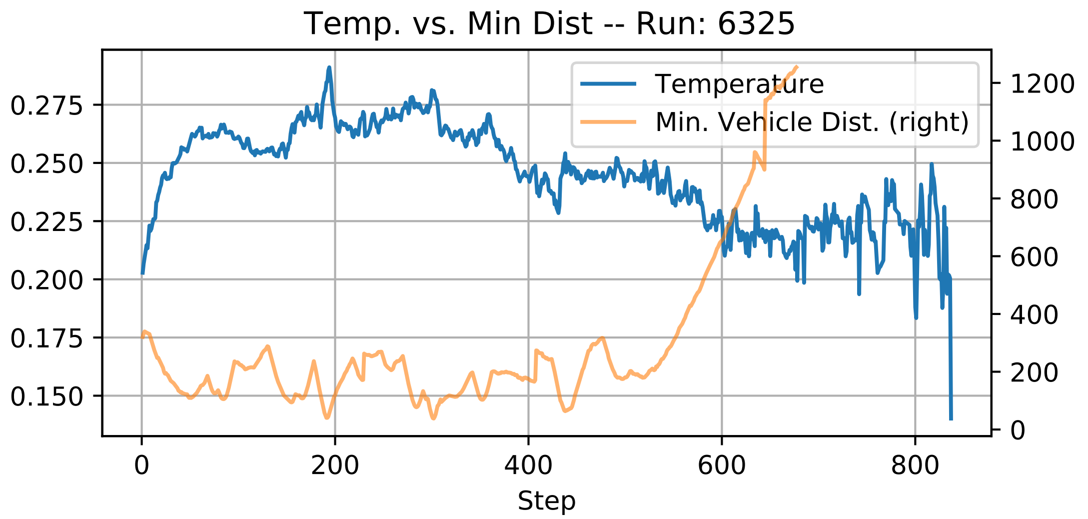

Figure 4.22. Temperature Based On Real-Time State Estimation vs. Minimum Vehicle Distance (The blue lines follow the left-y-axis, while the orange lines go with the right-y-axis.)

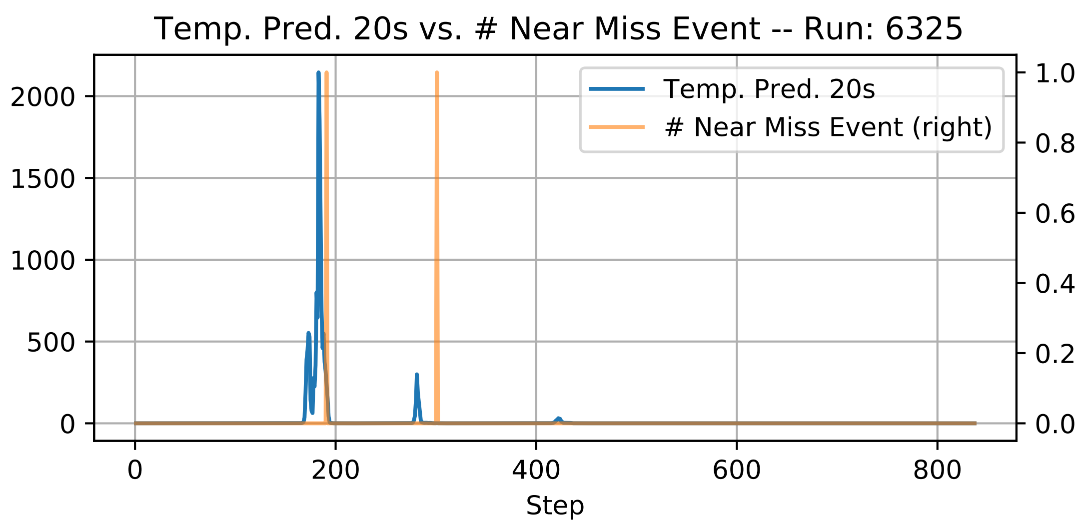

Figure 4.23. Temperature Based on 20 Seconds Vehicle State Prediction vs # Near Miss Event (The blue lines follow the left-y-axis, while the orange lines go with the right-y-axis.)

between two trends [71], [72]. Hence, a pre-whitening procedure is necessary before the cross-correlation calculation.

This study pre-whitens the signals and calculates the cross-correlation between two factors for each simulation run. Figure 4.24 shows the cross-correlation distribution of the minimum vehicle distance and the temperature based on the real-time state estimation. The results show that the median of the cross-correlation is negative and confirms the previous observation from Fig. 4.22. Furthermore, the VTBF adjustment mechanism does not significantly influence the median of the cross-correlation. One of the surprising findings is that the cross-correlation is related to the traffic pattern. The structured traffic pattern results in a wider spread of the cross-correlation distribution than the random traffic pattern.

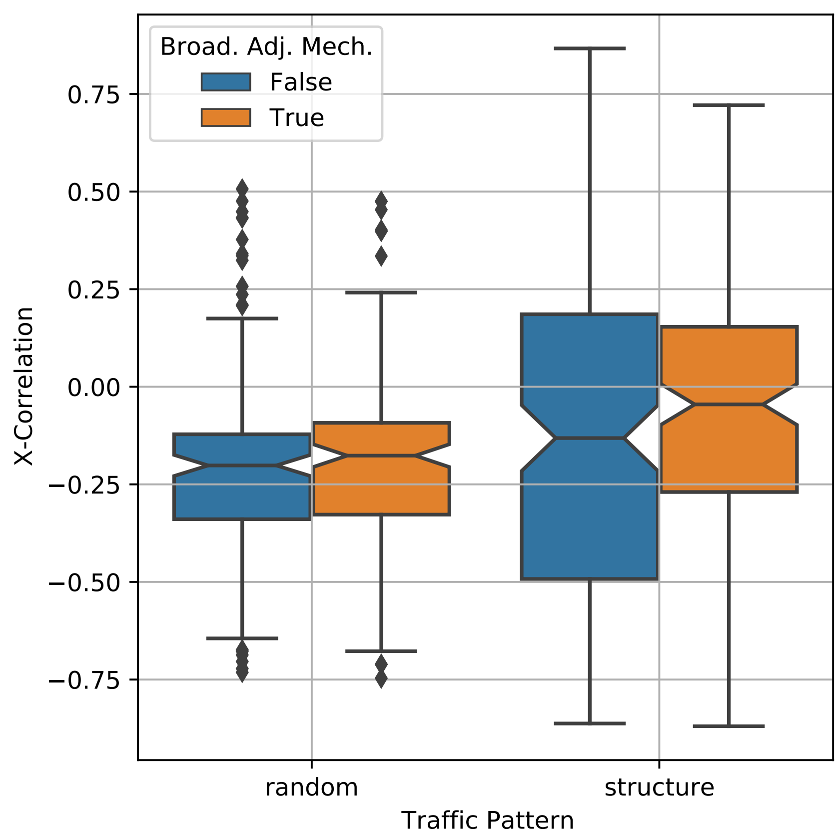

Figure 4.24. Cross-Correlation Distribution of Temperature Based On Real-Time State Estimation vs. Minimum Vehicle Distance (The blue boxes show the results with inactive VTBF adjustment mechanism, while the orange boxes present the results with active VTBF adjustment mechanism. The notches on the boxes show the 95% confidence interval of the median of the correlation.)

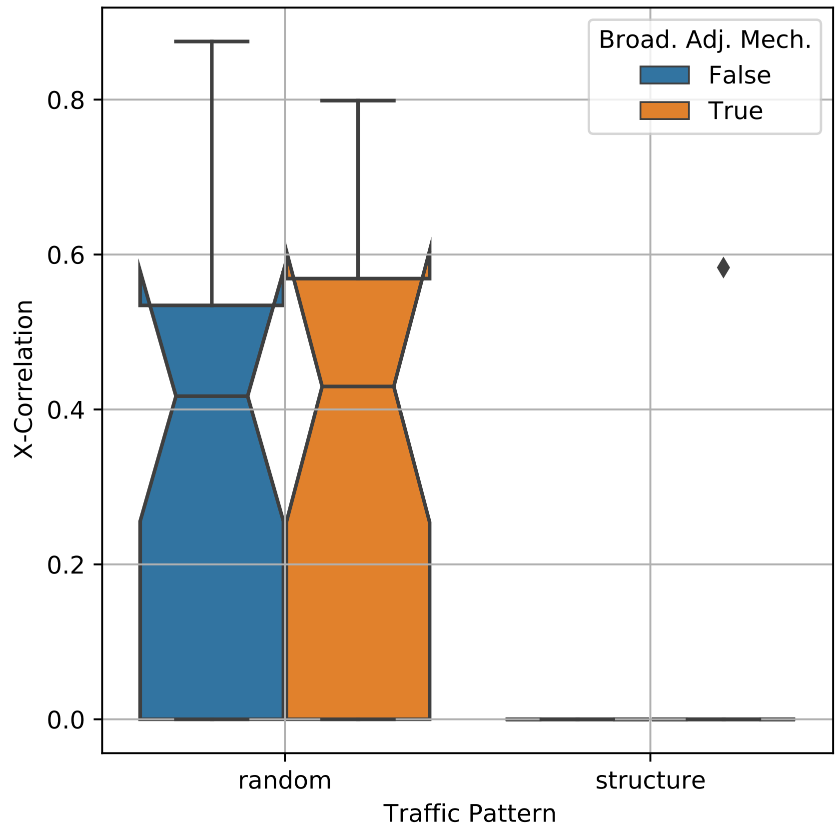

Figure 4.25. Cross-Correlation Distribution of Temperature Based on 20 Seconds Vehicle State Prediction vs Number of Near Miss Event (The blue boxes show the results with inactive VTBF adjustment mechanism, while the orange boxes present the results with active VTBF adjustment mechanism. The notches on the boxes show the 95% confidence interval of the median of the correlation.)

Since there is no auto-correlation for the number of the near-miss trend, there is no need to execute a pre-whitening procedure before the cross-correlation analysis. Figure 4.25 shows the cross-correlation distribution for the number of near-miss and the temperature based on the 20 seconds state predictions. Based on the discussion from the previous section, the temperature based on the 20-second state predictions is a good predictor for the near-miss event. Figure 4.25 confirms the previous findings because it shows the positive cross-correlation between the two factors. However, for the simulation with the structured traffic pattern, the temperature based on the 20 seconds state prediction does not perform well. Because these vehicles are traveling in parallel, it is difficult to predict how a small perturbation pushes an air vehicle away from its course and results in a near-miss event. However, vehicles are traveling in different directions in a random traffic pattern. The headings of the flight courses have a more significant influence on resulting in a near-miss event than any random perturbation.

4.4 Analysis of Chicago Downtown UAM Traffic

The applications of the traffic temperature are real-time airspace monitoring and the airspace structure design assessment. The following sections will use a hypothetical UAM traffic pattern in the Chicago metropolitan area from the works of Maheshwari et al. [73]–[75]. Their work assesses the potential UAM-preferred trip demands distribution through a day based on publicly available data. The UAM-preferred trip demand distribution considers the demographics of the Chicago population, existing highway infrastructures, existing potential UAM vertiports, and commuter demand distribution throughout a typical day. They identified 45 active vertiports and 6,305 UAM-preferred commuter trips from 6,221,968 commuter trips under the no UAM ride-sharing and full-network scenario. Additionally, they provide origin vertiports, destination vertiports, departure times, and arrival times of each UAM-preferred commuter trip.

The real-time airspace monitoring demonstration shows how the traffic temperature metric is associated with the LOS indicator, the minimum distance between vehicles, and the number of vehicles in the airspace. The demonstration also includes scenarios with different environmental uncertainty settings and shows how the traffic temperature responds to various uncertainty conditions. Furthermore, the airspace structure design assessment uses the temperature metric to identify the hot spots with given airspace structures. The airspace structure includes the geographical layouts of flight paths and the ATA's state estimation and commands logic. The decision-makers of the airspace structures can identify any hot spots and assess the airspace structure safety levels.

4.4.1 Chicago Downtown UAM Traffic Scenario Setup

Figure 4.26 shows the trajectories, origin vertiports, and the current locations of the UAM-preferred trips at 6 PM in the Chicago metropolitan area. The blue dots represent the origin vertiports, while the orange dots show the current location of the UAM vehicles. The blue lines show the trajectories of the UAM vehicles, while the blue box shows the study region. The study is a square with 28.8 kilo-meters-long edges. Furthermore, the study region is at a place with enough UAM traffic density and without any vertiports. Finally, Fig. 4.26 only visualizes the flights going through the study region.

Figure 4.27 shows the zoom-in snapshot around the study region. Since there is a high-throughput hub on the right of the study region, multiple UAM traffic converges to it. The hub also creates tremendous UAM traffic in the east-west direction. Due to the city layout, ample UAM traffic goes through the study region in the north-south direction.

Figure 4.28 shows the number of vehicles within the study region from 0:00 AM to 11:59 PM. The figure shows the highest density of the UAM vehicles happens at around 6:00 PM with 41 UAM vehicles in the square with 28.8 km-long edges. The second-highest density happens around 8:30 AM with about 25 UAM vehicles. The first peak represents the work-to-home traffic, while the second peak indicates the home-to-work trips.

The simulation includes three scenarios with different amounts of traffic. A low traffic scenario chooses the traffic condition at 10:30 AM as shown in the box with dotted edges in Fig. 4.28. The low traffic scenario has approximately 8 UAM vehicles in the study region. A mid traffic scenario uses the traffic condition at 8:30 AM as shown in the box with dashed edges in Fig. 4.28. Finally, a high traffic scenario is based on the traffic condition at 5:55 PM as shown in the box with solid edges. Each traffic scenario includes the entry time, the entry locations, and the existing locations of all vehicles traveling through the study region for generating the traffic pattern. The recording of each traffic pattern proceeds for 600 seconds.

The settings of the charged particle model are updated to match with the specification of the modeled UAM vehicle from Maheshwari et al. [73]–[75]. Table 4.8 shows the updated setting of the charged particle model. The cruise speed increases from 10 m/s to 68 m/s to

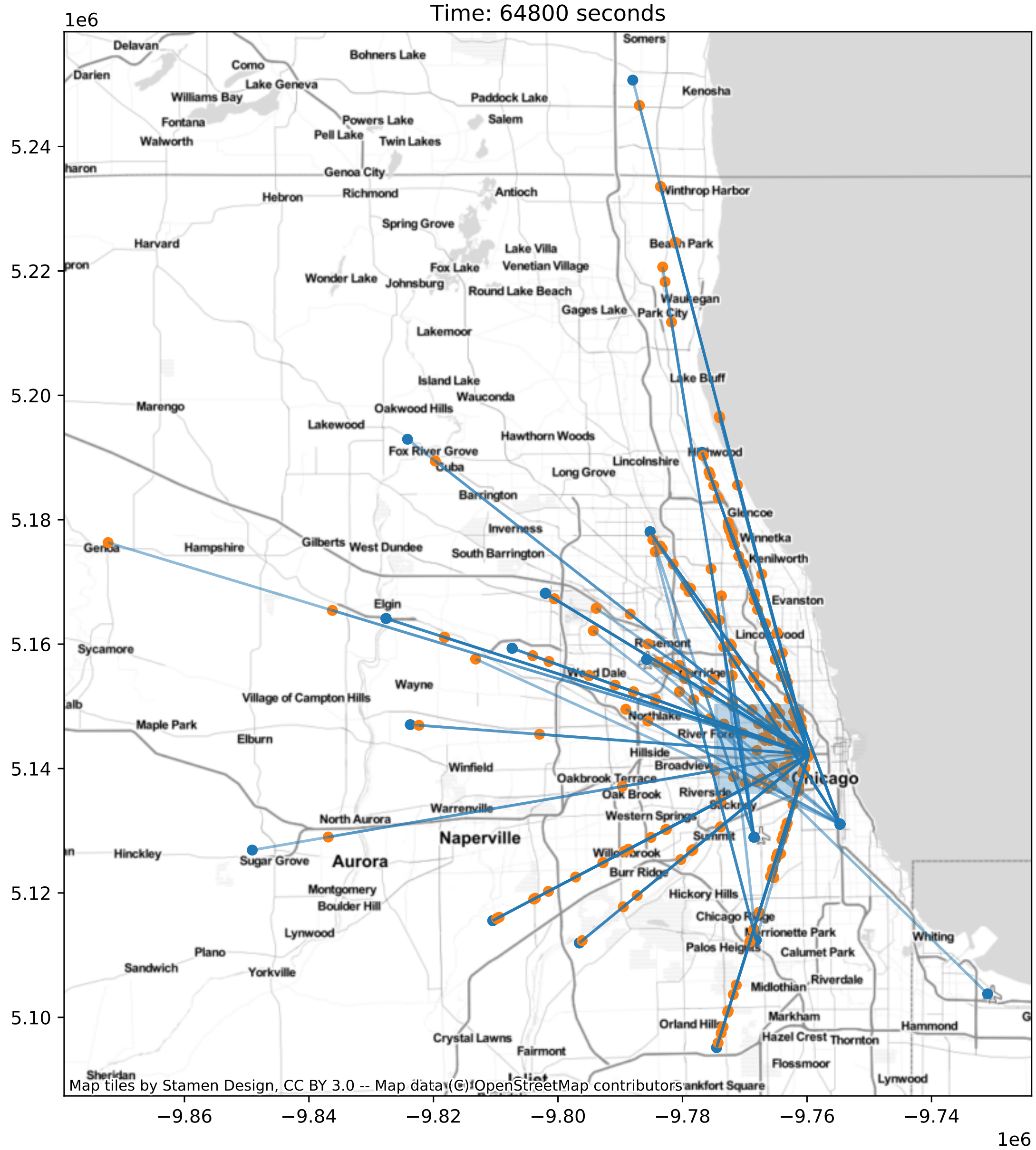

Figure 4.26. Snapshot of Chicago Downtown UAM-preferred Trips at 6 pm

respond to the cruise speed of the modeled UAM vehicle. The simulation also includes a different charge setting of 1043.4498 C to respond to the faster cruise speed and ensure that the collision avoidance system can execute effective collision avoidance maneuvers. Finally, the collision avoidance radius and the telemetry broadcast radius increase to 1500 and 3000 meters, respectively.

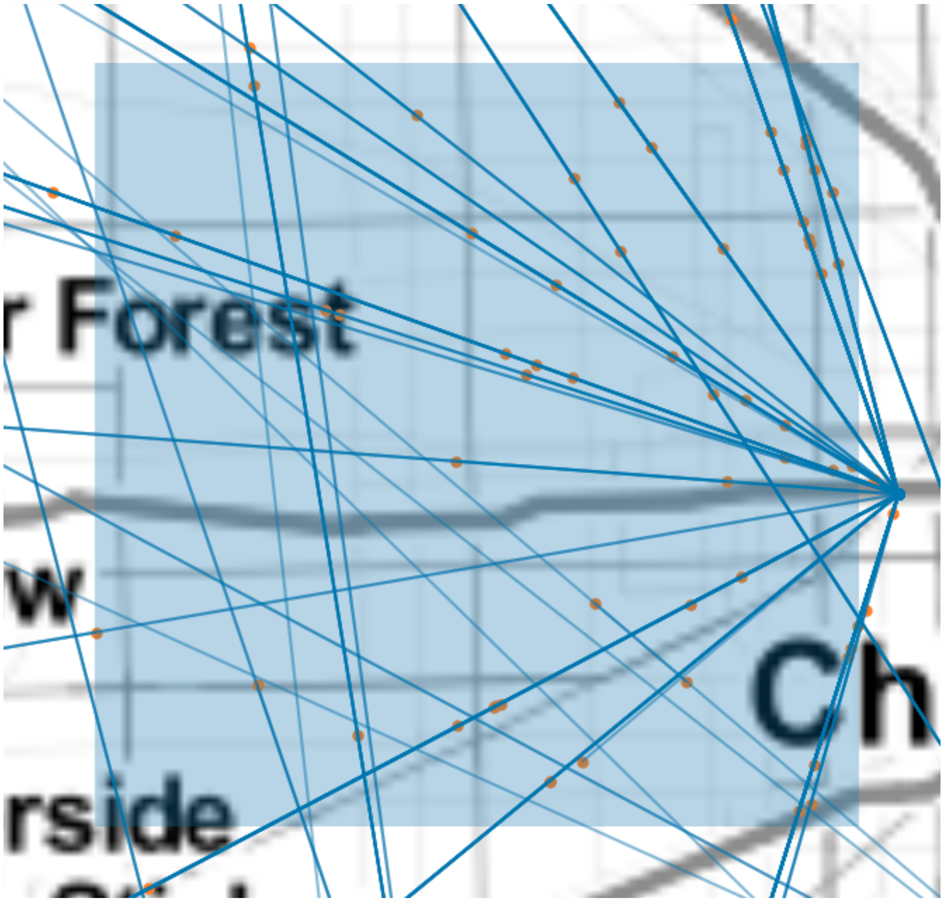

Figure 4.27. Snapshot of Airspace Condition of the Study Region

Table 4.8. Updated Simulation Parameter Settings of Charged Particle Model

Parameter	Value	Parameter	Value
m_i	1.00 [kg]	q_i	1043.4498 [C]
E	0.01 [V/m]	Cruise Speed	68.00 [m/s]
r_{col}	1500 [m]	Broadcasting Range	3000 [m]

The simulation includes two sets of environmental uncertainty settings. Table 4.9 shows the parameters of the Nominal uncertainty setting. Additionally, the High uncertainty scenario involves stronger wind disturbances, higher state measurement errors, and lower message reception rates.

Figure 4.29 shows the trajectories of the flights from the high traffic scenario. The colors of the trajectories are according to the heading angles. The west-to-east traffic is in solid

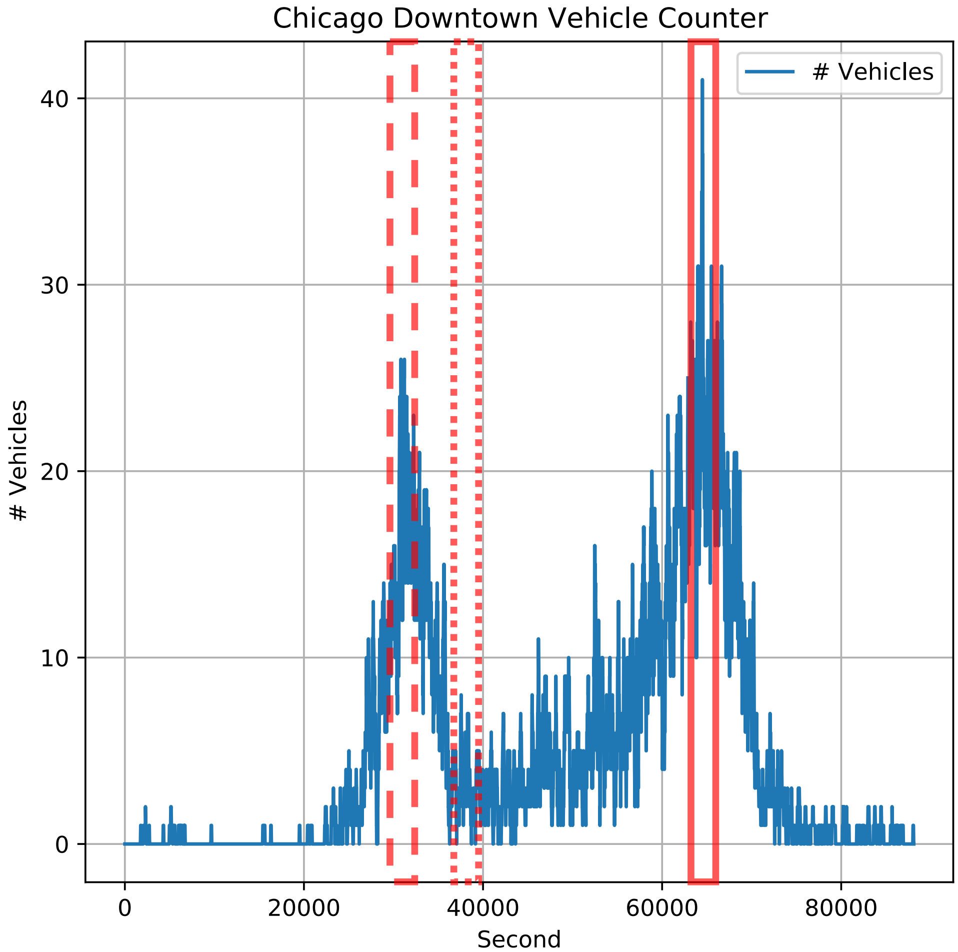

Figure 4.28. Number of Vehicle in Study Region for Every Second Through A Day Since Mid-Night

Table 4.9. Environment Uncertainty Setting

Scenario	Nominal	High
Wind Perturbation Multiplier	1.0	40.0
Measurement Error Multiplier	1.0	40.0
Message Reception Rate	1.0	0.5

lines, while the east-to-west traffic is in dotted lines. Without any manipulation, the west-to-east traffic and the east-to-west traffic overlap with each other. The head-to-head near-miss scenario is inevitable. Hence, there is a need to separate the east-to-west traffic and the west-to-east traffic apart.

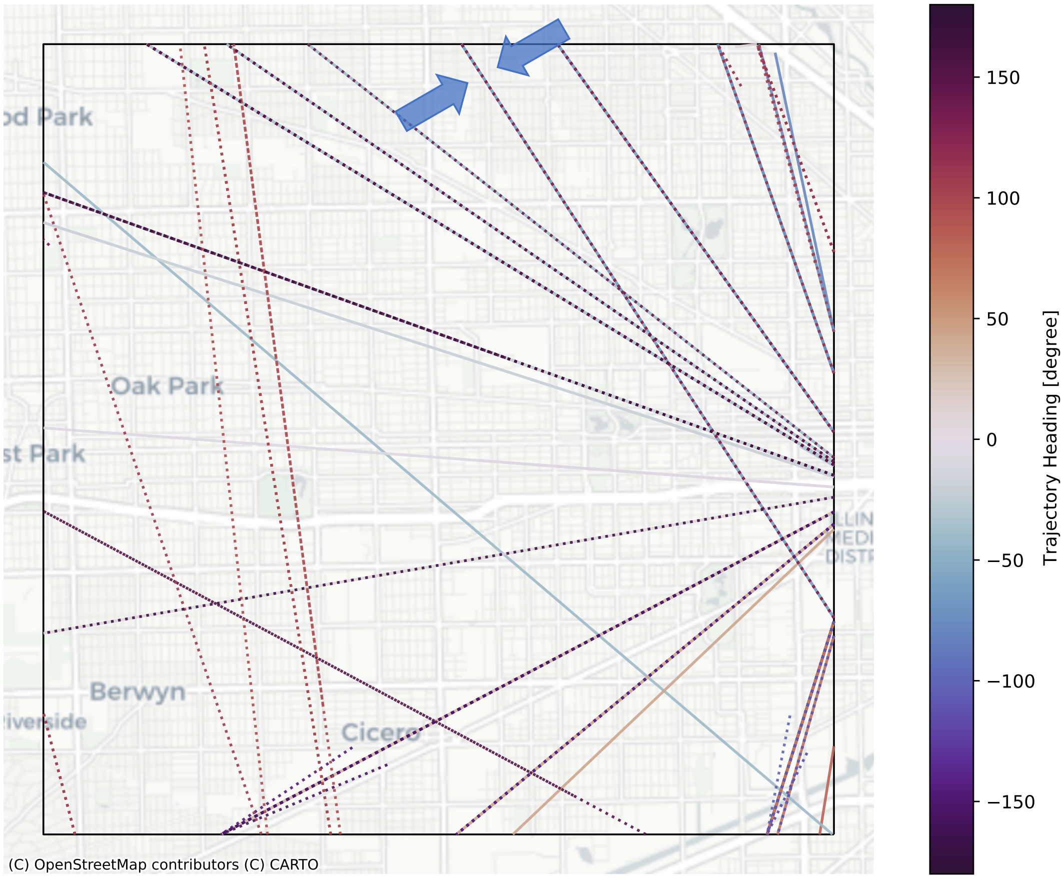

Figure 4.29. Vehicle trajectories of the high traffic scenario in the Chicago downtown area. Vehicle Trajectories are colored based on the heading angles. The west-to-east trajectories are in solid lines, while the east-to-west trajectories are in dotted lines.

The baseline separation structure separates the traffic in opposite directions by 200 meters. Figure 4.30 shows the resulting trajectories in the Chicago urban area. The trajectories pointed by the two blue arrows in Fig. 4.29 are separate apart in Fig. 4.30. The traffic in Figs. 4.31 and 4.32 in the opposite directions from the different traffic scenarios separate from each other in the baseline separation distance.

The study also includes the two extra trajectory separation distance scenario for investigating how the temperature metric responses to the different airspace structure. A loose structure has the increased trajectory separation distance from 200 meters to 800 meters (Fig. 4.33). Although the loose separation distance can reduce the chance of the head-to-hear near-miss event, the structure increases the potential path conflicts with other trajec-

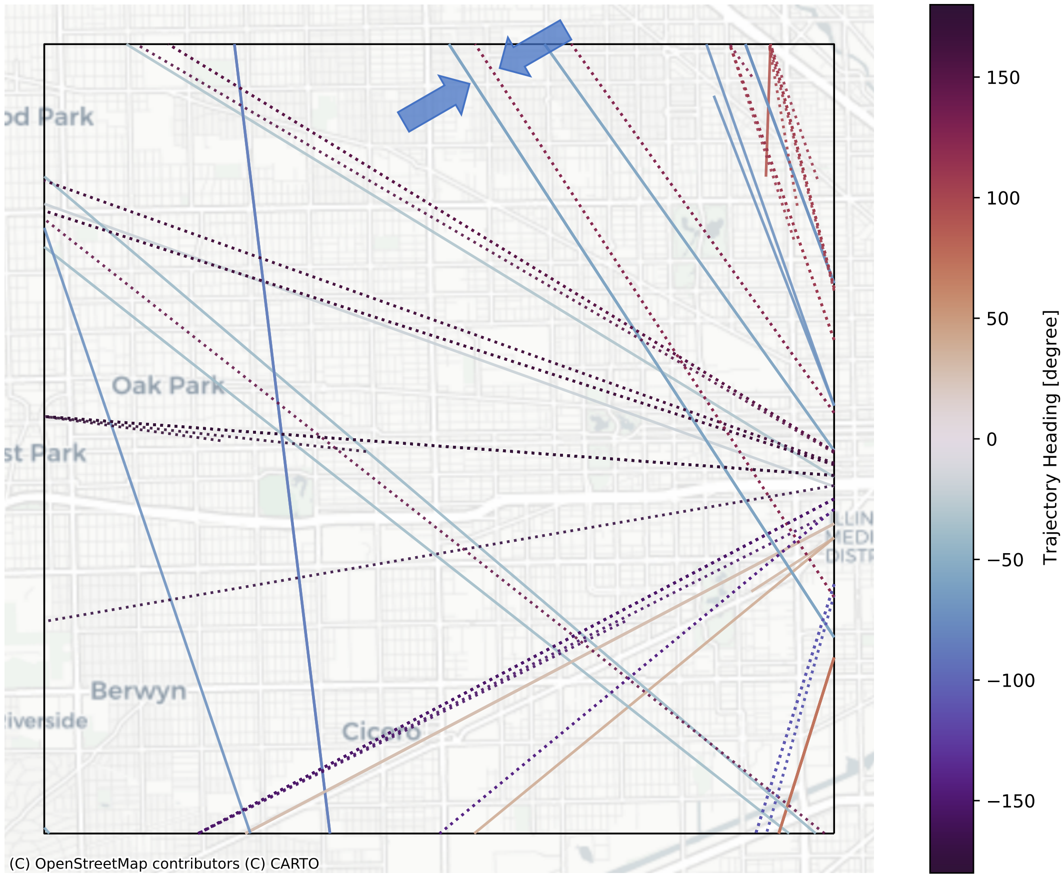

Figure 4.30. Vehicle trajectories of the high traffic scenario in the Chicago downtown area with the Baseline Separation Distance. Vehicle Trajectories are colored based on the heading angles. The west-to-east trajectories are in solid lines, while the east-to-west trajectories are in dotted lines.

tories. On the other hand, a tight structure scenario has the decreased trajectory separation distance from 200 meters to 100 meters (Fig. **??**). The tight structure reduces the chances of the path conflict with other trajectories, but it increases the chance of the head-to-head near-miss events.

This study intents to investigate how the temperature metric responds to (1) different amount of air traffic, (2) different types of ATA mechanism, and (3) various airspace structure. Table 4.10 summarizes the setting of the fixed factor and control factors of simulation scenarios. The expected results of the simulation scenario are as follows.

1. **Traffic Throughput Scenario**: Since the temperature metric is an intrinsic variable, it should not depend on the number of vehicles in the airspace. In other words, the

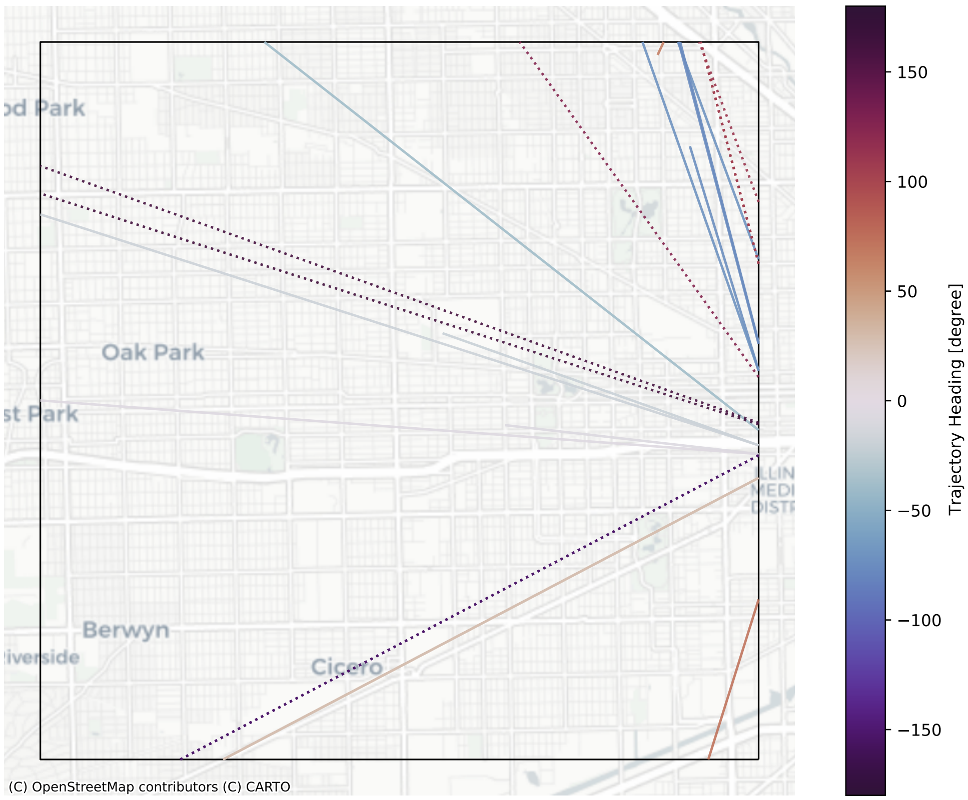

Figure 4.31. Vehicle trajectories in the Chicago downtown area with the Baseline Separation Distance and Low Traffic Scenario (Vehicle Trajectories are colored based on the heading angles. The west-to-east trajectories are in solid lines, while the east-to-west trajectories are in dotted lines.)

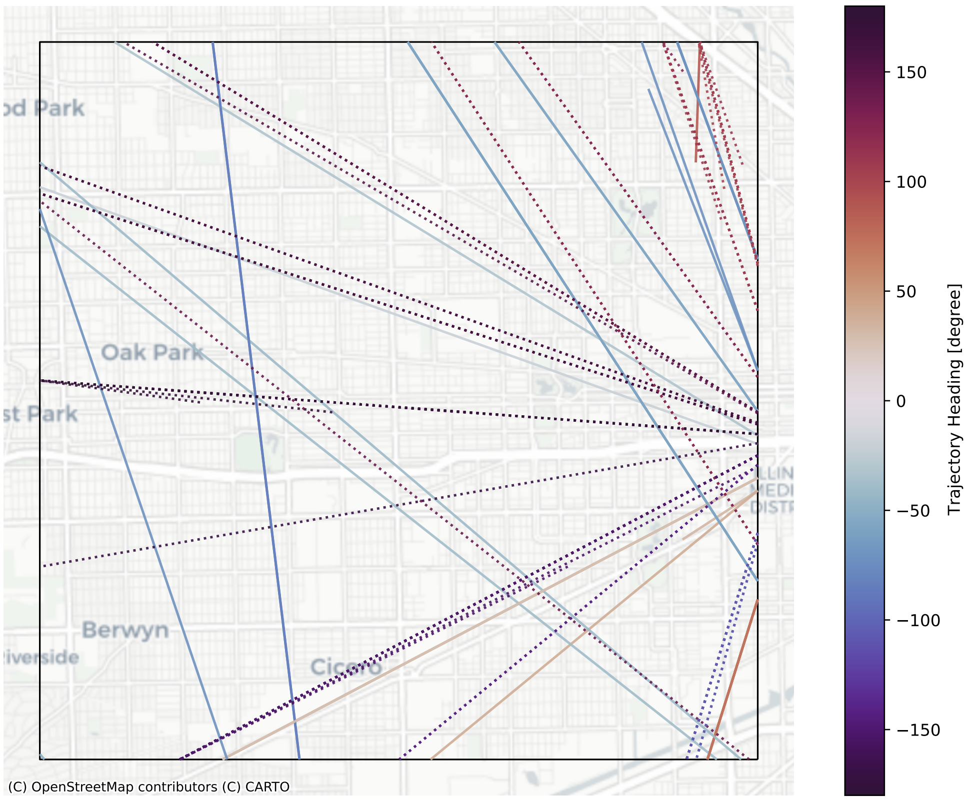

Figure 4.32. Vehicle trajectories in the Chicago downtown area with the Baseline Separation Distance and Mid Traffic Scenario (Vehicle Trajectories are colored based on the heading angles. The west-to-east trajectories are in solid lines, while the east-to-west trajectories are in dotted lines.)

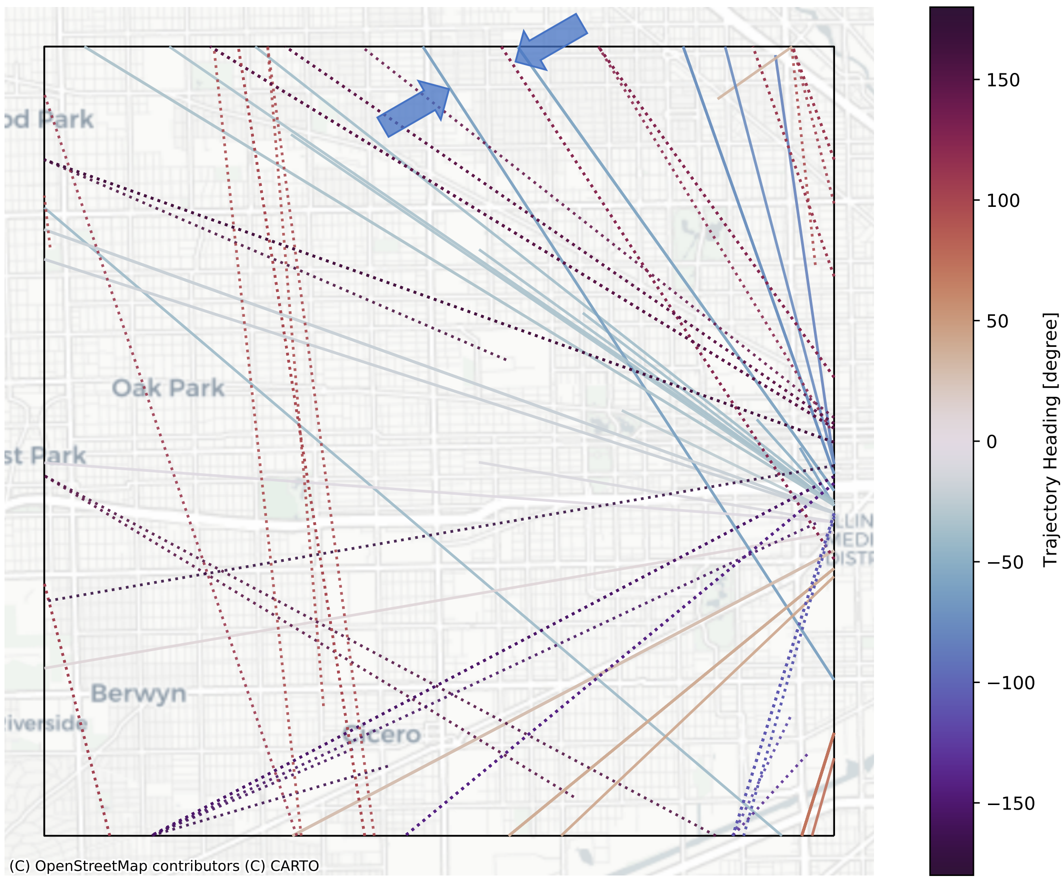

Figure 4.33. Vehicle trajectories in the Chicago downtown area with Loose Structure Scenario (Vehicle Trajectories are colored based on the heading angles. The west-to-east trajectories are in solid lines, while the east-to-west trajectories are in dotted lines.)

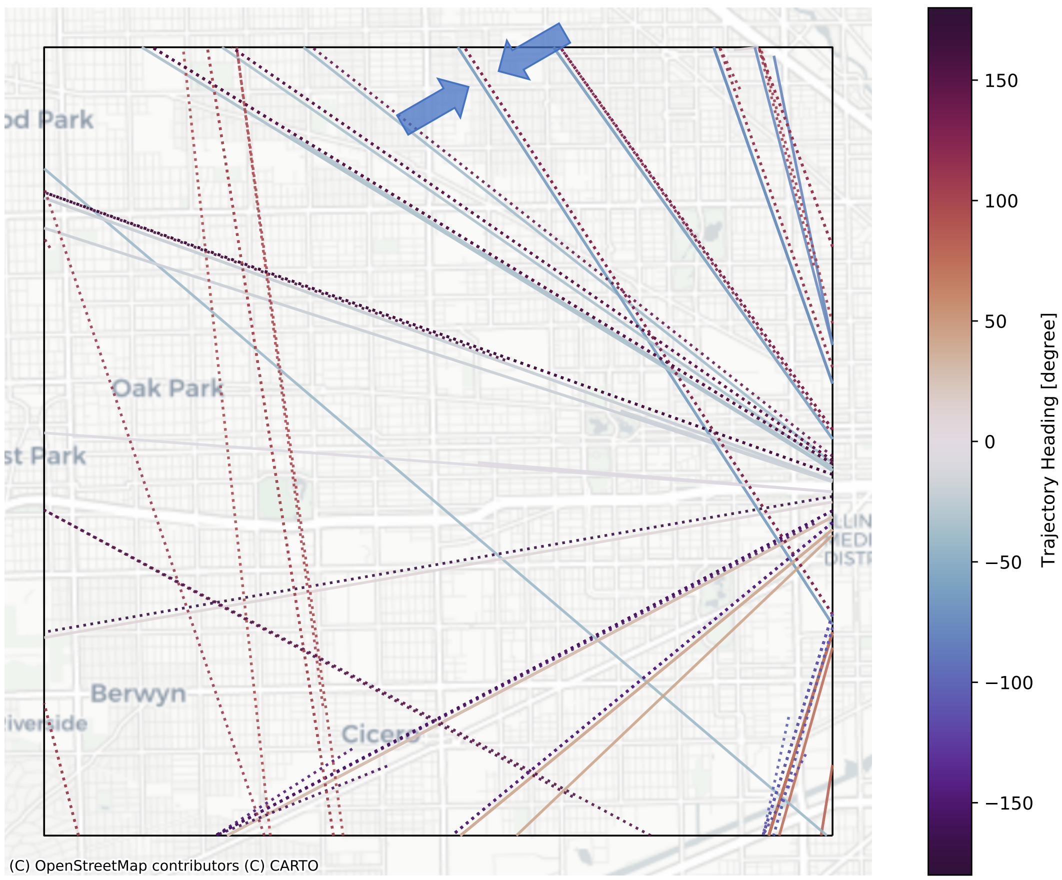

Figure 4.34. Vehicle trajectories in the Chicago downtown area with Tight Structure Scenario (Vehicle Trajectories are colored based on the heading angles. The west-to-east trajectories are in solid lines, while the east-to-west trajectories are in dotted lines.)

Table 4.10. Summary of Simulation Scenarios

Scenario	**Control Factors**	**Fixed Factors**
Traffic Throughput Scenario	Traffic Throughput, Uncertainty Level	Inactive ATA Mechanism, Baseline Traffic Separation Distance
ATA Mechanisms	Traffic Throughput, Uncertainty Level, ATA Mechanisms	Baseline Traffic Separation Distance
Airspace Structure	Traffic Separation Distance, Uncertainty Level	High Traffic Throughput, Inactive ATA Mechanism

temperature value should reveal the confidence level of how severe the airspace is. The temperature should only depend on the minimum distance between vehicles or number of near-miss event.

2. **ATA Mechanisms**: Since the goal of the ATA mechanisms should regulate the air traffic, the temperature metric should reveal the effectiveness of the mechanism. Additionally, it should reveal how different mechanism influences the air traffic patterns.

3. **Airspace Structure**: Different traffic separation distances can result in different types of safety threats. A tight traffic structure may cause the head-to-head near-miss event, while the loos traffic structure may increase the path conflict between the trajectories of the air vehicles. The temperature metric should reveal the strength and weakness of different airspace structure designs.

4.4.2 Temperature Responds to Traffic Throughput

With different traffic throughput, the temperature metric should be independent from the number of air vehicles and reveal the confidence level of how severe the airspace is. This section includes the simulation results with different air traffic settings and environmental uncertainty level.

Airspace-Level Analysis — Real-Time Airspace Monitoring

The traffic temperature metric should help the ATA identify the status of air traffic in airspace. Figure 4.35 shows the traffic status of the Chicago downtown area with the traffic temperature and other metrics of scenarios with Nominal uncertainty. The first row shows the traffic temperature evolution based on the real-time vehicle state estimations under different traffic conditions. And the blue, orange, and green lines show the Low traffic, Mid traffic, and High traffic conditions, respectively. The second row in Fig. 4.35 the minimum distance between all vehicles in the airspace. The red dashed line indicates the near-miss threshold. A near-miss event happens if any two vehicles have a relative distance shorter than the threshold. Then, the third row shows how many near-miss events are identified every second. Unfortunately, there is no near-miss event from these simulation results. Finally, the last row in Fig. 4.35 shows the number of vehicles in the airspace for each second.

It is hard to use one metric to summarize the safety level of airspace. The minimum distance between vehicles metric (the second row in Fig. 4.35) shows the pair of vehicles with the most unsafe condition. It cannot show if other air vehicles were in unsafe conditions or not. The number of the near-miss events (the third row in Fig. 4.35) is not ideal neither because it shows values after the near-miss event happened. Additionally, if there is no near-miss event, it cannot present the airspace condition or compare airspace safety level. Finally, the number of vehicle counts (the last row in Fig. 4.35) can show the vehicle density. However, high-density airspace may not be dangerous if there are an effective airspace structure and operational regulations. For example, the last plot in Fig. 4.35 shows that the high traffic scenario is always more dangerous than the other scenarios because it has the highest vehicle counts.

The temperature metric can summarize airspace safety level and is independent of the number of UAM vehicles in the airspace, so it is helpful to compare the airspace conditions with fluctuating traffic flows. Although the different traffic patterns result in various numbers of UAM vehicles in the airspace, the traffic temperature values are similar between these traffic thresholds. Additionally, the first row and the second row of Fig. 4.35 show that the

Figure 4.35. Nominal Environmental Uncertainty with Traffic Temperature, Minimum Distance Between Vehicles, Number of Near Miss, and Vehicle Count Evolution (There is no near-miss event in these simulations.)

temperature tends to be higher if the minimum distance between vehicles is lower because the temperature indicates the level of confidence of how severe the air traffic condition is.

Two factors can also influence temperature evolution. The state estimation error is the first factor and can reduce the temperature peaks. If the state estimation errors are not on the principal axes of the traffic safety severity function, the state estimation errors reduce the temperature peak value. If the state estimation errors are on the principal axes, it is more likely that vehicles are closer than the distance based on the estimated locations. Hence, the temperature increases. The second factor is the number of vehicles pairs that are too close to each other. Since the minimum vehicle distance metric can only show the worst case, it cannot identify how many other vehicle pairs might have a slightly longer distance than the minimum vehicle distance. If the relative distances between other vehicle pairs are also short, the temperature peaks are much higher. For example, the temperature from the high-traffic scenario hovers around 13 from 230 to 320 seconds. During the same period, the minimum vehicle distance stays below 500 meters. During this period, many vehicles are close to each other. Whenever a pair of air vehicles start to separate, the other vehicle pairs can keep converging. Hence, the minimum vehicle distance keeps below 500 meters during this period. And the temperature responds to this scenario and keeps the value above 13.

The first and third rows in Fig. 4.35 demonstrate that the temperature metric can summarize air traffic condition even if there is no near-miss event. The ATA can easily set an upper bound to identify if the airspace is unsafe for new vehicles to join in. For example, the temperature of 11 can be a satisfying threshold. Then, the airspace with the low traffic throughput is under unsafe state from 440 to 460 seconds. And, from the minimum distance graph, some vehicles are too close to each other and activate the collision avoidance algorithm. Similarly, the airspace with the high traffic throughput is unsafe from 120 to 380 seconds. During the same period, the minimum distance between vehicles is lower than 700 meters.

Figure 4.36 shows the same plots with the higher environmental uncertainty condition. The relationships between the temperature, the minimum vehicle distance, the number of near-miss events, and the vehicle count are the same. However, the traffic temperature under the high uncertainty scenario (Fig. 4.36) is slightly lower than the temperature in the Nominal uncertainty scenario (Fig. 4.35).

This phenomenon happens because the uncertainty increases on all dimensions of the state vector. For example, the temperature is stable with the low traffic throughput scenario from 80 to 320 seconds. During this period, the air vehicles are far away. Then, only the uncertainty on the velocity dimensions can influence the temperature and traffic safety severity function. Since the true vehicle states are stochastic variables, vehicles can have the same velocity values and at different locations. The temperature metric considers that these cases dilute the level of confidence of the traffic safety severity assessment and produce a lower temperature value. However, when the near-miss event is about happening, the uncertainty on the location dimensions can also influence the temperature and traffic safety severity function. Hence, the temperature peaks are similar between the nominal and high uncertainty scenarios.

If an authority needs to monitor the traffic conditions of several traffic sectors, the traffic temperature metric can identify the traffic condition and help the authority make decisions. A traffic sector is too unsafe if the temperature is too hot, Instead of checking the vehicle states from each airspace sector, the temperature metric should help the authority quickly compare the traffic conditions between different sectors in real-time.

Vehicle-Level Analysis — Airspace Structure Design Assessment

The traffic temperature can assess the level of confidence of how severe the **traffic condition** is. It can also evaluate the confidence level of how severe the **vehicle condition** is. Hence, a heat map based on the locations and temperature of UAM vehicles in the airspace can visualize the geographical distribution of the vehicle temperature. The heat map generation procedure is as follows.

1. Discretize the airspace

2. Calculate the vehicle temperature and record the location of the vehicle

3. Use the vehicle locations and temperature to calculate the temperature of each cell

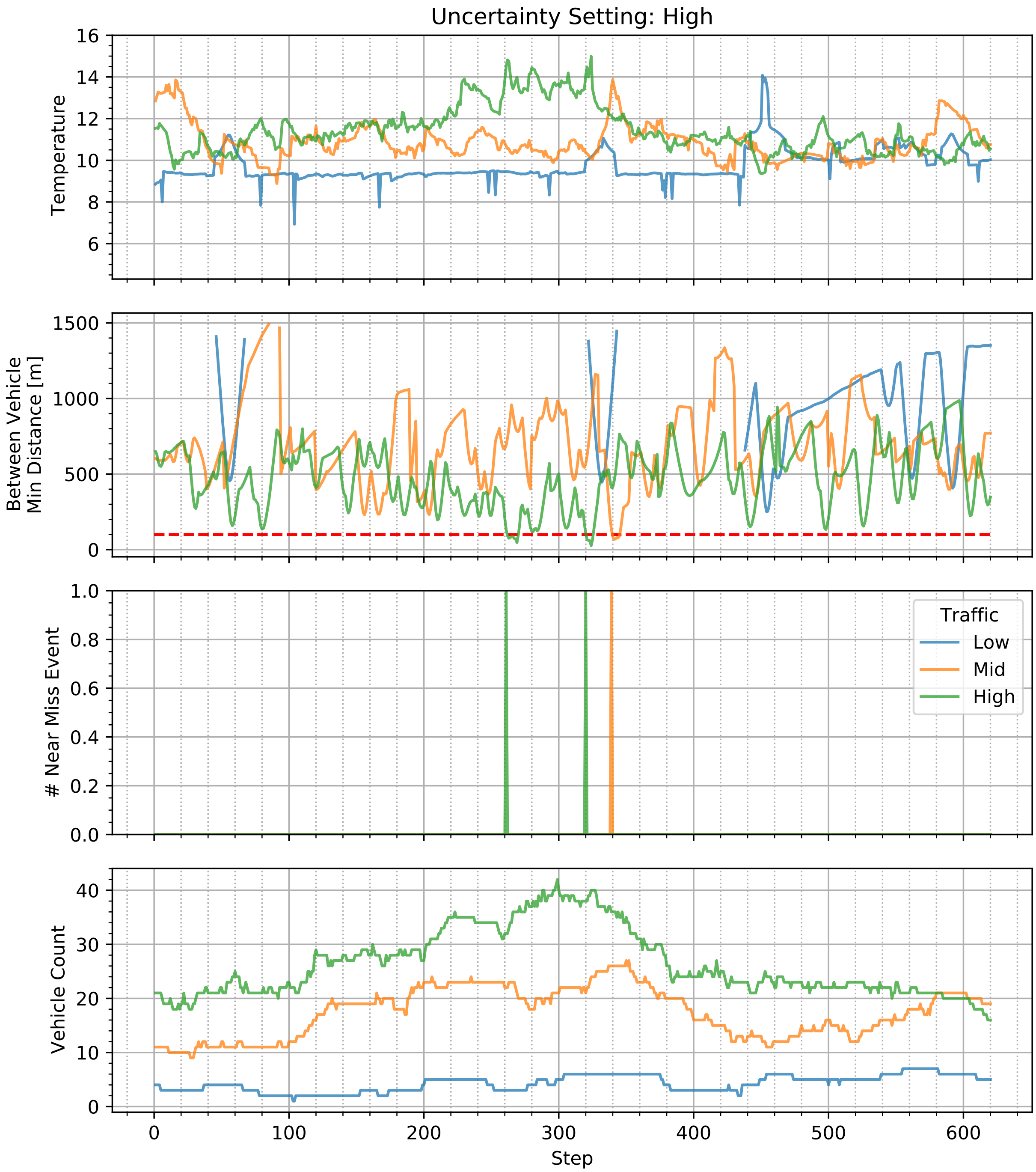

Figure 4.36. High Environmental Uncertainty with Traffic Temperature, Minimum Distance Between Vehicles, Number of Near Miss, and Vehicle Count evolution

4. Go through each time step through the simulation to identify the average temperature of each airspace

Figure 4.37 shows the heat maps of the Chicago Downtown. The first column and the second column show the nominal and high environmental uncertainty conditions, respectively. The rows from top to down show the scenarios with the Low, the Mid, and the High traffic throughput. The areas surrounded by the dashed line show the higher temperature regions. The lines in Fig. 4.37 represent the flight trajectories of the air vehicles by comparing the figure with Figs. 4.30, 4.31, and 4.32. The hotter routes indicate that the ATA has higher confidence that the vehicles on the hotter routes are under unsafe condition. In other words, these routes are the unsafe areas in the Chicago downtown airspace. Additionally, the airspace around the vertiport on the right-hand side of the study region in Fig. 4.27 has hotter temperatures during the High traffic conditions. Without a proper take-off or landing procedure of the vertiport, high throughput traffic makes airspace around the vertiport unsafe.

The areas surrounded by the dashed lines represent the higher temperature and unsafe areas. For the Mid traffic throughput scenarios, the upper right and left bottom regions are the high-temperature regions. These regions are due to the high amount of traffic flying in both directions. Air Vehicles in these regions may be in dangerous situations if the onboard flight controllers cannot maintain the required navigational accuracy. Or, a strategic deconflict mechanism can reduce the temperature in this area.

For the High traffic throughput scenarios under the Nominal uncertainty setting, the area on the middle right of the map shows a high temperature region. The high traffic throughput and the complicated airspace structure result in a higher chance of the near-miss event. Furthermore, the upper left and bottom left regions also have a higher temperature due to the crossing traffic. Although no near-miss event happened in the Nominal environmental uncertainty scenario, the temperature metric can still identify the dangerous areas and helps the airspace designer improve airspace safety.

For the scenarios with a High Uncertainty setting, the heat maps are similar to the High Uncertainty setting results. The hot spots from the Nominal uncertainty region are still hot

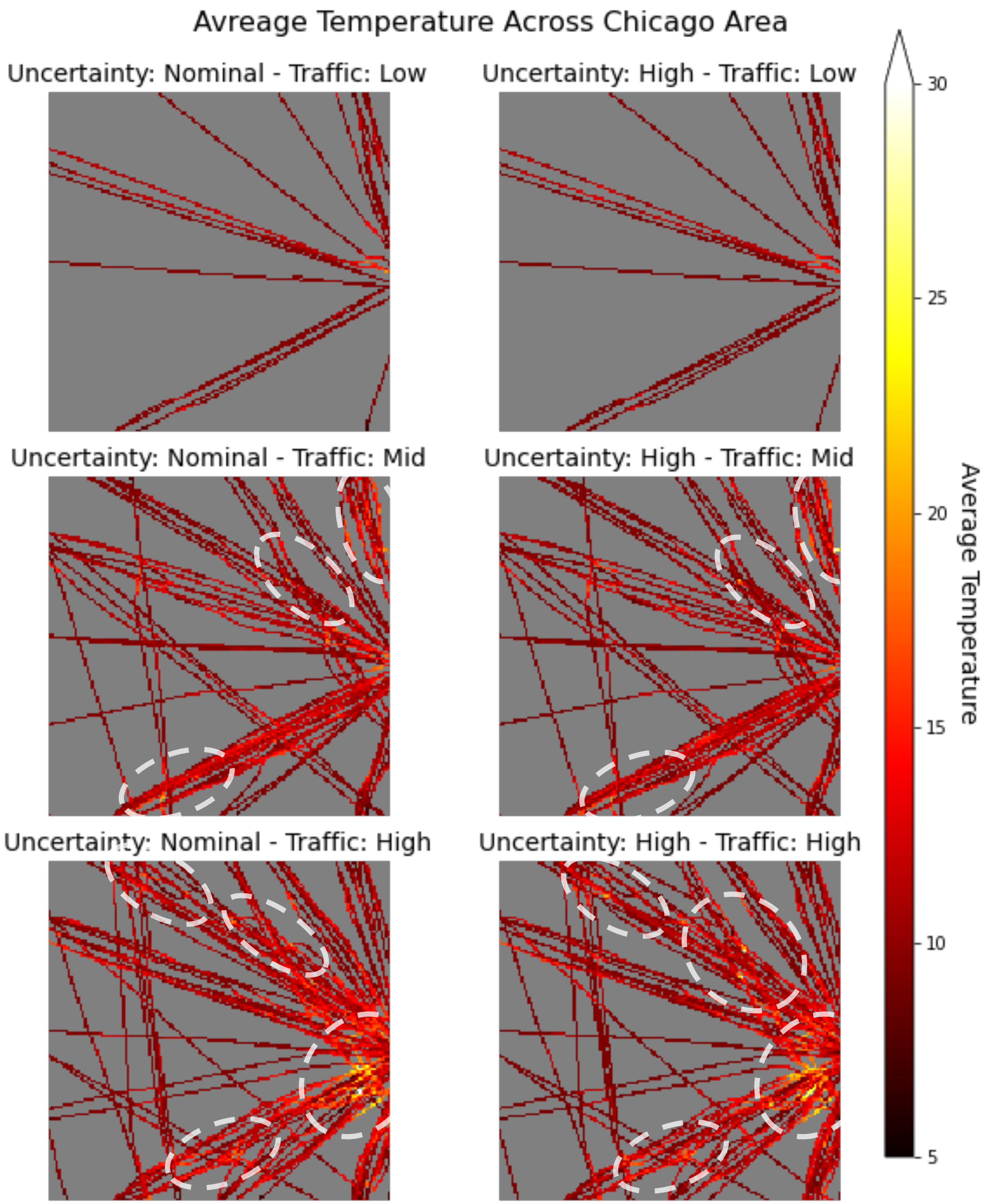

Figure 4.37. Heat Map of Chicago Downtown (The dashed areas indicate high temperature region. The dotted areas show the higher uncertainty region with low temperature.)

spots in the High Uncertainty region. This phenomenon shows that the traffic patterns induce these hot spots. However, the High uncertainty conditions can affect the peak temperature values. Since the heat map depends on the vehicle statuses at each location, the high uncertainty condition induces an instance that might be more dangerous or safe than the Nominal uncertainty condition. Although this study shows one instance of the simulation results, researchers can conduct the Monte Carlo simulation to smooth out the statistical fluctuation and identify the hot spots in the airspace.

4.4.3 Temperature Responds to ATA Traffic Management Mechanism

This study focuses on how the temperature metric responds to the different ATA traffic management mechanisms. The ATA traffic management mechanisms are the VTBF adjustment mechanism and the Minimum Separation adjustment mechanism. The results show how the two mechanisms affect the temperature evolution, the number of near-miss events, and the minimum distance between vehicles. The results also reveal how effective the two mechanisms are.

Airspace-Level Analysis — Real-Time Airspace Monitoring

Figure 4.38 shows the results with the high environmental uncertainty and the active VTBF adjustment mechanism. Figure 4.38 has minor differences from Fig. 4.36, which is the baseline. The main difference is from 280 seconds to 340 seconds of the high traffic throughput scenario. The temperature peak values from the scenario with the active VTBF adjustment mechanism are slightly lower than the scenario without the VTBF adjustment mechanism. The decrements of the temperature peak values are due to the increments of the minimum vehicle distance. And, there is one less near-miss event. In summary, the VTBF adjustment mechanism has a minor impact on temperature evolution. But, the mechanism can improve airspace safety by resolving a few potential near-miss events.

Figure 4.39 shows the metric evolutions from the scenario with the Nominal environmental uncertainty and the active Minimum Separation adjustment mechanism. The temperature values from Fig. 4.39 are lower than the baseline case in Fig. 4.35. The low temperature

Figure 4.38. High Environmental Uncertainty and Active VTBF Adjustment Mechanism with Traffic Temperature, Minimum Distance Between Vehicles, Number of Near Miss, and Vehicle Count evolution

is due to the increasing minimum vehicle distance and slower vehicle speeds. The minimum vehicle distance plots show that the case with the active Minimum Separation adjustment mechanism can effectively increase the minimum vehicle distance. Additionally, the temperature of the high traffic throughput scenario from 200 to 380 seconds is much lower from the scenario with the active mechanism than the inactive mechanism. This phenomenon shows that the Minimum Separation adjustment mechanism can also increase the relative distance of other vehicles.

The temperature evolution from the mid and high traffic throughput scenarios can be lower than the low traffic throughput scenario. For example, the temperature from 400 to 440 seconds from the Mid and High traffic scenario is lower. During the same period, the minimum vehicle distances of the two cases increase from 200 to 800 meters. The minimum vehicle distance plots show that some vehicles during this period execute collision avoidance maneuvers. The collision avoidance maneuvers can increase the vehicle state estimation uncertainty and slow down the air vehicles. Section 4.2.2 shows that the impacts of the state estimation uncertainty on the temperature are minor. The temperature decrements are due to the slow vehicle speed. Because the traffic safety severity function includes the kinetic energy, the slow vehicle speed reduces the safety severity level and the temperature.

Figure 4.39 also shows that the peak of the vehicle count from the high traffic throughput scenario is higher than the baseline scenario from Fig. 4.35. Due to the aggressive collision avoidance maneuvers, the vehicles have to detour from their original courses, slows down, and increase the traveling time. Hence, the Minimum Separation mechanism can increase a higher density of air vehicles than the scenario without the traffic management mechanism.

Vehicle-Level Analysis — Airspace Structure Design Assessment

The vehicle-level analysis can show the effectiveness of the traffic management mechanisms in the different areas in the airspace. Figure 4.40 compares the results with and without the VTBF adjustment mechanism. The traffic throughput increases from the top row to the bottom row. The left column shows the simulation without the VTBF adjustment mechanism, while the right column presents the results with the active mechanism.

Figure 4.39. Nominal Environmental Uncertainty and Active Minimum Separation Adjustment Mechanism with Traffic Temperature, Minimum Distance Between Vehicles, Number of Near Miss, and Vehicle Count evolution

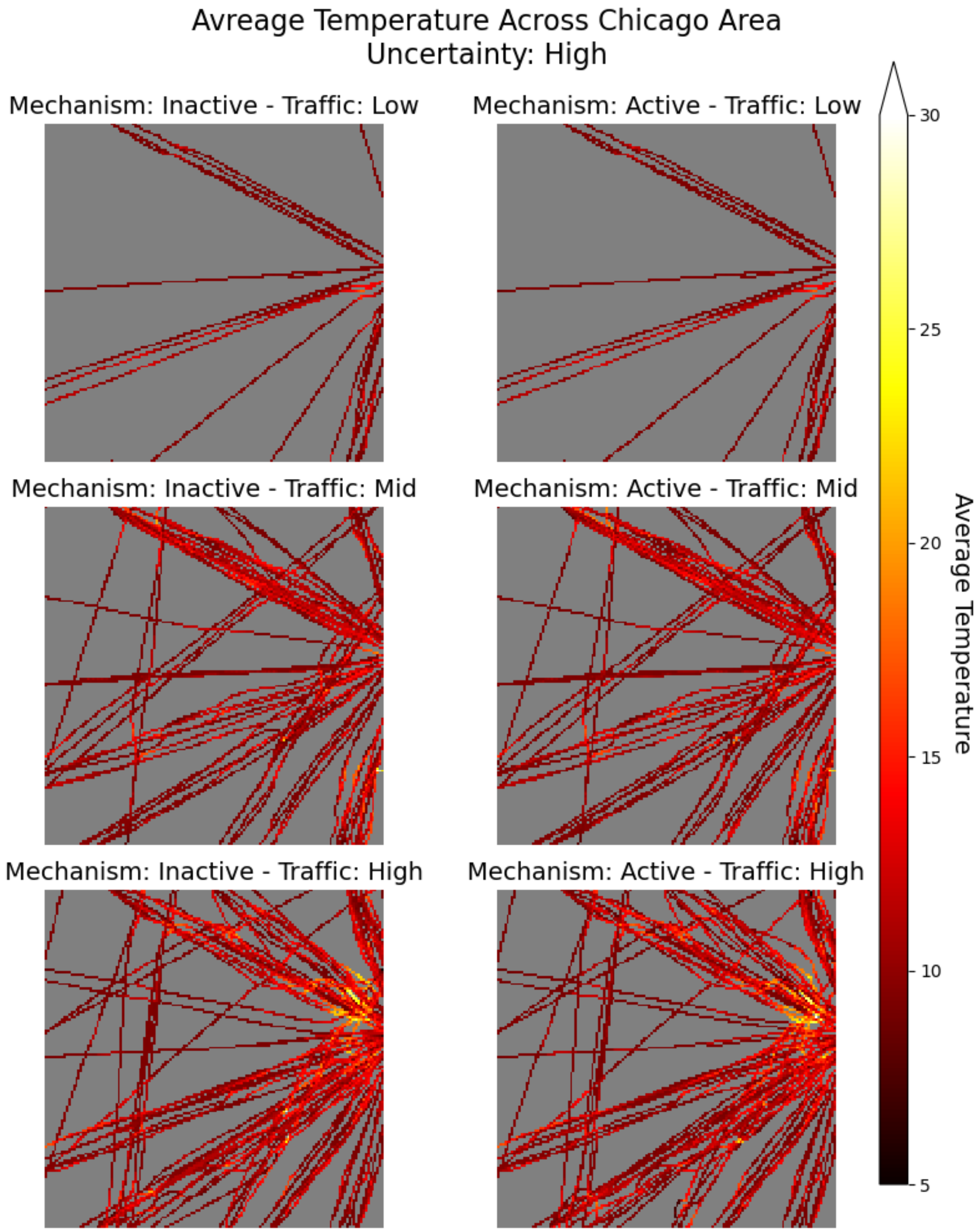

Figure 4.40. Heat Map of Chicago Downtown with High Environmental Uncertainty Setting (The right column shows the results with the active VTBF adjustment mechanism, while the left column shows the results with no mechanism.)

The results show that the difference between the heap maps with and without the VTBF adjustment mechanism is insignificant. The VTBF adjustment mechanism supposes to help the vehicle state estimation. However, the heat map shows that the temperature distributions through the airspace are almost identical with and without the VTBF adjustment mechanism. The results are consistent with the previous studies that the effectiveness of the VTBF adjustment is insignificant.

Figure 4.41 shows the results with and without the Minimum Separation adjustment mechanism. The left column shows the results without the mechanism, while the right column presents the results with the active Minimum Separation adjustment mechanism.

The heat maps show that the Minimum Separation adjustment mechanism can result in more chaotic collision avoidance trajectories. The heat maps with the minimum separation adjustment mechanism reveal that the trajectories spread out in the airspace due to vehicles' collision avoidance maneuvers. Additionally, the vehicle temperature is lower when the trajectories curve away from their original courses. Since the safety severity includes the kinetic energy, the collision avoidance maneuvers slow down the vehicles and reduce the temperature on the collision avoidance trajectories.

Even though the minimum separation adjustment mechanism can reduce the temperature, the heap maps still show a few hot spots from the High traffic throughput scenario. The hot spots happen around the center-right edge of the study region. Because there is an aerodrome outside of the center-right edge (Fig. 4.27), the high-density traffic increases the chance of the near-miss with the new air vehicles even with the active Minimum Separation adjustment mechanism. The results echo with previous studies that a good landing and take-off procedure is necessary around the aerodrome.

4.4.4 Temperature Responds to Airspace Structure

This study investigates how the temperature metric responds to the different airspace structures. The temperature metric can help airspace structure designers identifies hot spots and cold regions from an airspace structure. This study uses heat maps to visualize the safety level of the airspace structure under different environmental uncertainty scenarios.

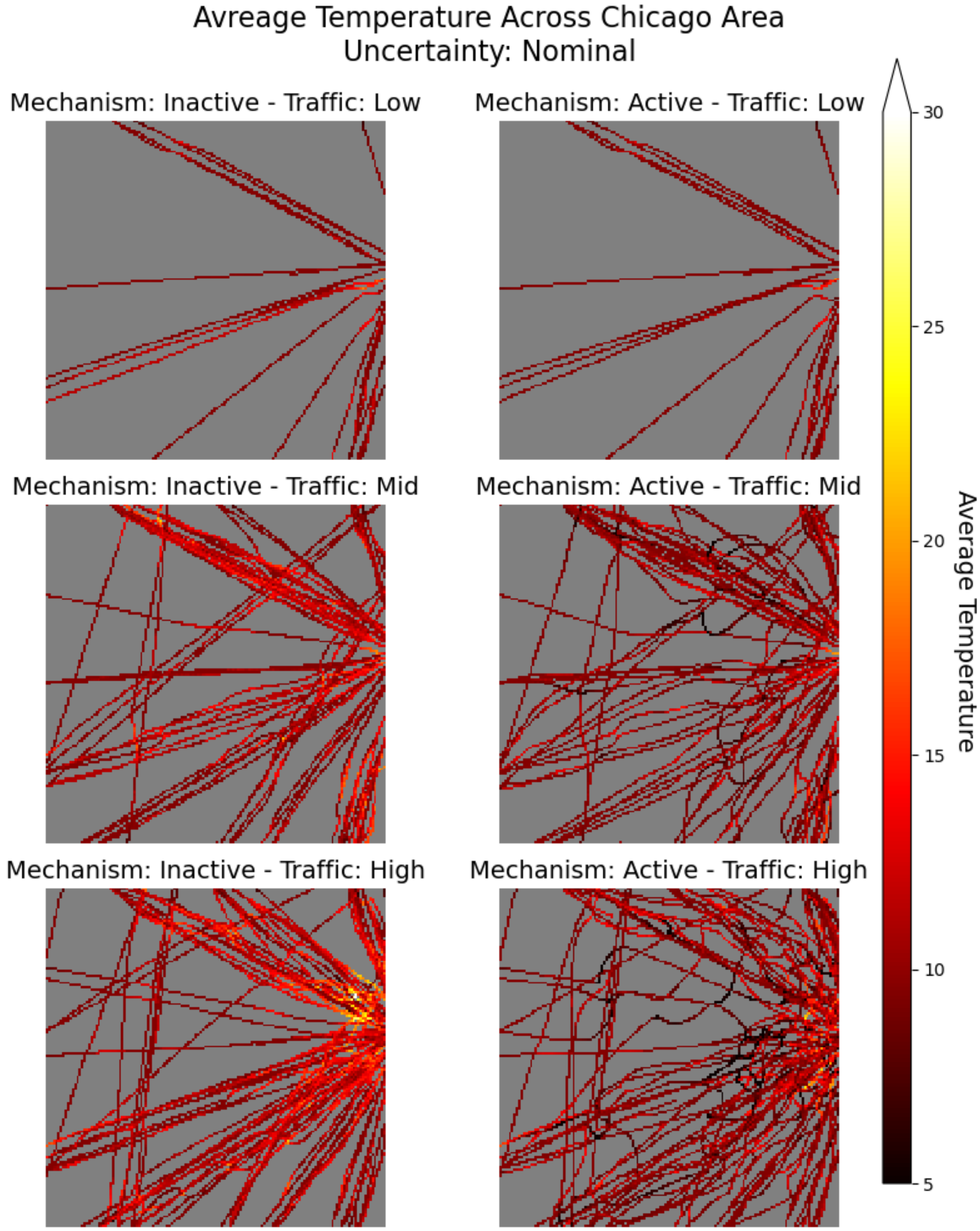

Figure 4.41. Heat Map of Chicago Downtown with Nominal Uncertainty Setting. (The right column shows the results with the active Minimum Separation adjustment mechanism, while the left column shows the results with no mechanism.)

This study aims to demonstrate how to use the temperature metric to identify unsafe conditions of an airspace structure. The goal is not to distinguish which airspace structures are the safest for the Chicago Downtown airspace. If an airspace structure designer proposes an optimal airspace structure for Chicago airspace, the airspace structure designer can use the temperature metric to assess the airspace safety levels under different air traffic throughput and environmental uncertainty scenarios. Furthermore, if researchers can well model the vehicle collision avoidance maneuvers, the temperature metric can also reveal how the collision avoidance maneuvers influence the ATA's vehicle state estimation accuracy and how likely the collision avoidance maneuvers induce other unsafe conditions.

Vehicle-Level Analysis — Airspace Structure Design Assessment

Figure 4.42 shows the heat maps of the simulation results with different airspace structure settings and environmental uncertainty settings. The left column shows the results with the nominal uncertainty setting, while the right column shows the results with the high uncertainty scenario. The top row presents the baseline airspace structure with the baseline separation between the traffic, while the bottom row shows the loos airspace structure with the 800 meters separation distance between the traffic. Last, the areas circled by dashed lines represent the high-temperature regions.

In the scenarios with the baseline separation distances, there are several hot spots on each stream of the traffic. The hot spots indicate where the air vehicles are too close due to either the head-on or crossing traffic. Additionally, the area around the center-right edge of the map has a broad high-temperature region. The high temperature is due to the converging traffic to the aerodrome, which is just outside of the study area. When vehicles approach the aerodrome, the relative distances between the traffic streams are shorter and shorter. Additionally, an inbound traffic stream may need to cross several outbound traffic streams for leaving the aerodrome. These two phenomena increase the likelihood of the near-miss event and endanger airspace safety.

The number of hot spots from the scenarios with the loos airspace structure reduces. For example, there is a hot spot due to the crossing traffic in the top-left corner of the baseline

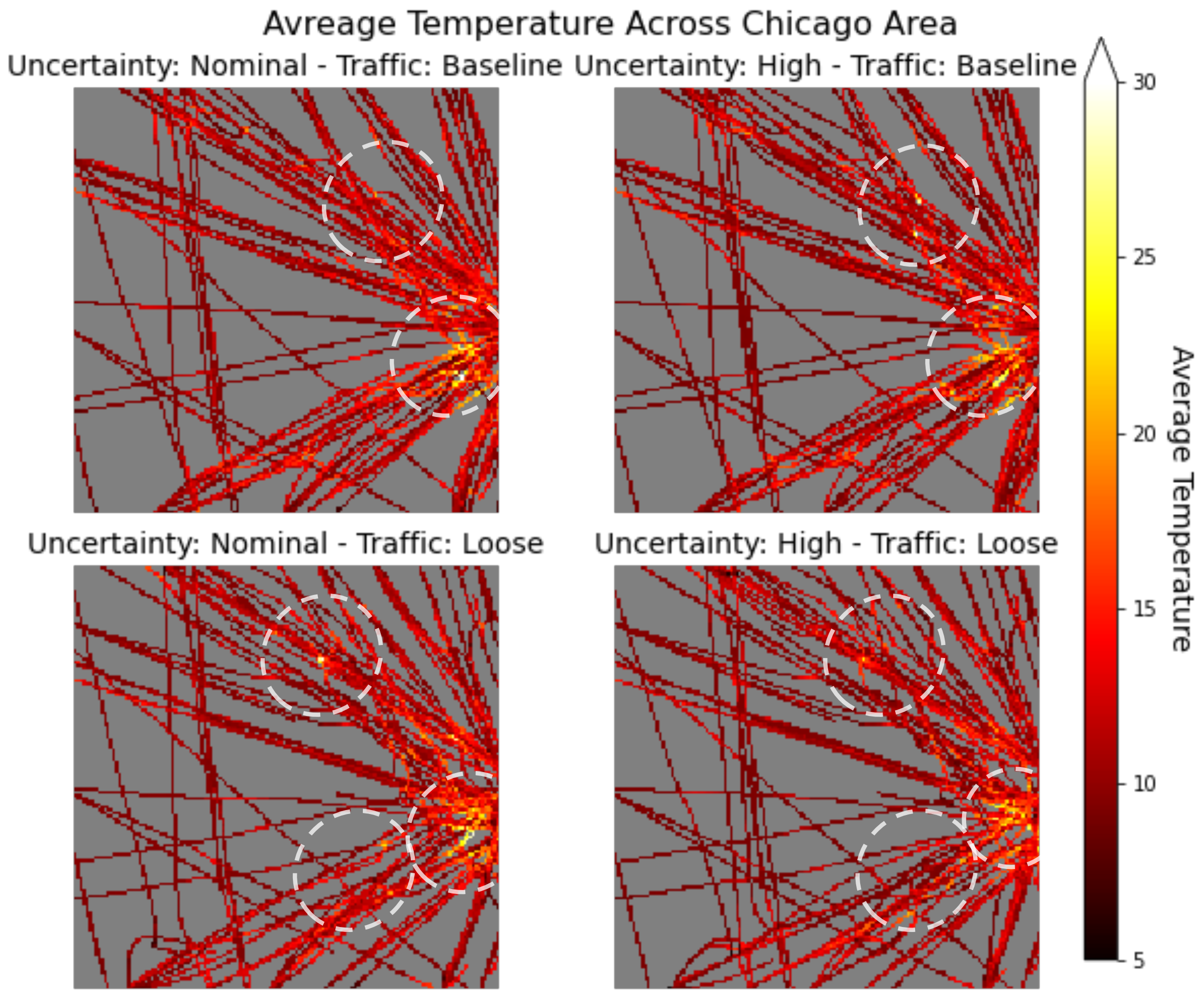

Figure 4.42. Heat Map of Chicago Downtown with different Airspace Structures (The right column shows the results with the Nominal Uncertainty Setting, while the left column shows the results with the High Uncertainty Setting.)

airspace structure scenario. The same area has a lower temperature in the loose airspace structure scenario. The widely spread traffic from the loose airspace structure increases the relative distance between vehicles and airspace safety. However, there is still a few very hot spots from the loose traffic structure scenario. A strategical separation mechanism is necessary for completely removing these hot spots.

The area around the center-right edge is still a high-temperature region from both scenarios. Although the exact locations of the hot spots are different from both cases, the loose traffic structure still cannot effectively mitigated the traffic safety severity. The converging traffic to the aerodrome requires better take-off or landing procedures to regulate the traffic and increase airspace safety.

The impact of the environmental uncertainty on the heat maps is not significant. Figure 4.42shows that the hot spots from the Nominal uncertainty scenario are at similar locations as the ones from the High uncertainty scenario. But, the temperature at the hot spots might be higher or lower. Since the vehicle temperature depends on the locations of other vehicles at the same time step, the environmental perturbations can shift vehicle locations, influence the accuracy of vehicle state estimations, and affect the temperature values. The traffic pattern determines approximately where two vehicles can get too close to each other, while the environmental perturbation influences the exact relative distance between two vehicles, the vehicle state estimation accuracy, and the temperature value. Running multiple simulations with the same settings can mitigate this type of statistical fluctuation.

Figure 4.43 shows the heat maps of the scenarios with the baseline airspace structure and the tight airspace structure. The top row shows the results from the baseline airspace structure, while the bottom row shows the results from the tight airspace structure with 100 meters traffic separation distance.

The tight airspace structure should make vehicles have a higher chance to fly by from each other in a shorter relative distance. Figure 4.43 reveals that more hot spots are from the tight airspace structure than the baseline airspace structure scenarios with the same environmental uncertainty setting. The higher number of hot spots indicates that vehicles are too close to each other at different locations on the map. Additionally, most of the hot spots from the tight airspace structure have higher temperature values than the same hot spots from the baseline airspace structure scenario. This phenomenon confirms that the tight airspace structure is more dangerous than the baseline airspace structure because the tight airspace structure induces hotter and more hot posts in the airspace.

Some hot spots from the tight structure are at the crossing of air traffic streams (Fig. 4.43). The tight airspace structure increases the traffic safety severity on the traffic streams with lots of bi-directional traffic. Also, the tight airspace structure can increase the temperature at the crossing of the traffic streams. One possible explanation is that the vehicles do not

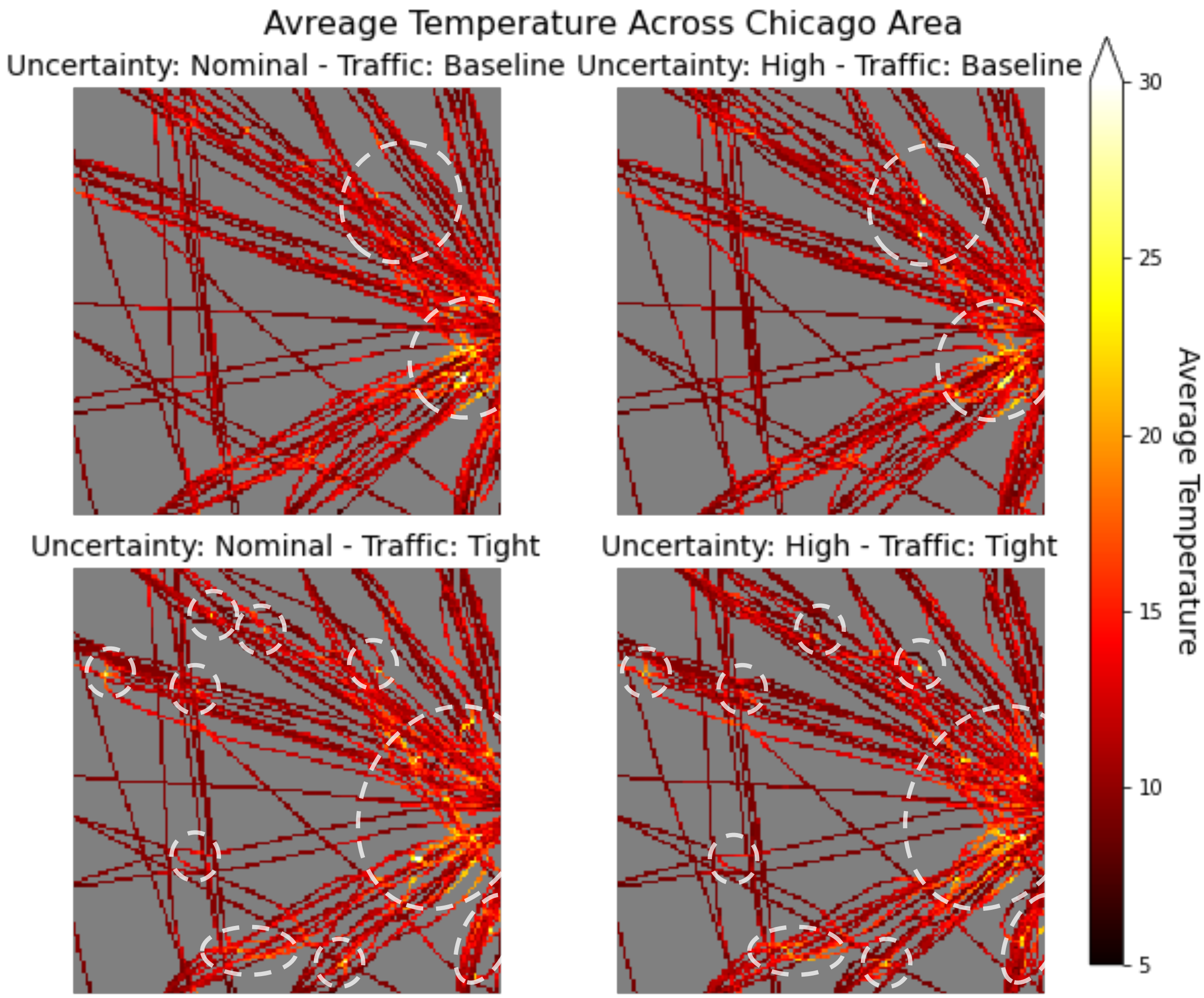

Figure 4.43. Heat Map of Chicago Downtown with different Airspace Structures (The right column shows the results with the Nominal Uncertainty Setting, while the left column shows the results with the High Uncertainty Setting.)

have enough room to clear airspace for the crossing traffic. Whenever one vehicle executes any collision avoidance maneuvers, it interferes with the nearby vehicles due to the tight traffic separation distance. Hence, the temperature at hot spots around the crossings of traffic streams can be higher than the baseline structure scenario.

The impacts from the environmental uncertainty are the same on the tight airspace structure. The hot spots from the Nominal uncertainty scenario are very likely to happen from the High uncertainty scenario. And, the temperature of the hot spots might be different from one scenario to the other. Since the heat maps from Fig. 4.43 just shows one simulation results from one combination of the setting, it is hard to distinguish the hot spots are a special case or are the properties of the airspace structure. Hence, using the Monte Carlo Simulation can smooth the statistical fluctuation and reveal the real properties of the structure.

This study reveals that the loose airspace can induce fewer hot spots in the airspace than other airspace structures. But, air vehicles need to cross more traffic streams to reach their destinations. The crossings of the traffic streams result in hot spots in the airspace and reduce airspace safety. Hence, a strategical deconfliction mechanism can help the loose airspace structure reduce the vehicle temperature from the crossing traffic conditions and improve airspace safety. Finally, the heat map shows that the tight airspace structure increases the number of hot spots and the hot spot temperature. A sufficient separation distance between the traffic is still necessary.

5. CONCLUSION

This dissertation developed, demonstrated, and evaluated the traffic temperature and the traffic entropy as means for quantifying the air traffic safety levels. The metrics leverage the information from the state probability density functions, which consider the state uncertainty level, rather than estimate of the exact vehicle state. This approach is applicable to either piloted or autonomous vehicles if the vehicle state prediction/estimation algorithms can be applied to both types of vehicles. This study uses the Kalman filter to illustrate how an Air Traffic Authority (ATA) can track the evolution of the state probability density function. Three increasingly complex simulation scenarios are established for investigating the properties of the proposed metrics and demonstrating the potential use-cases. The latter of the scenarios uses data and constraints from a downtown Chicago simulation for UAM operations.

5.1 Properties of Traffic Temperature & Traffic Entropy

The traffic entropy quantifies the uncertainty level of the vehicle state probability function. In the two-vehicle simulation setup, the results show that the traffic entropy can reveal when air vehicles enter a region with high wind perturbations, degraded GPS signals, and a lower message receiving probability. However, the traffic entropy is not suitable for quantifying the traffic conditions with different numbers of air vehicles in the airspace because the traffic entropy increases with traffic throughputs. The traffic entropy equals the summation of the information entropy of the state probability function and a constant. Because the traffic entropy is directly related to information entropy, an ATA can use the traffic entropy to develop mechanisms for the regulation of airspace traffic. The Vehicle Telemetry Broadcast Frequency (VTBF) adjustment mechanism uses information entropy to assess communication capacity for lowering traffic estimation uncertainty. Although the VTBF adjustment mechanism only reduces 1% of the near-miss rate, it demonstrates the possibilities of developing algorithms based on statistical entropy or information entropy.

The traffic temperature quantifies the level of confidence of how severely air vehicles violate given airspace regulations. Additionally, the traffic temperature is independent of the number of air vehicles in the airspace. Hence, the traffic temperature can represent the level of confidence of the airspace safety severity. The two-vehicle simulation setup demonstrates that the temperature-based near-miss event trigger is as effective as the CPA-based near-miss event trigger. The multi-vehicle simulation setup shows that the traffic temperature represents the safety severity levels of the structure traffic pattern and the random traffic pattern. The interesting results show that the traffic temperature from the scenarios with the structure traffic pattern is higher than the scenarios with the random traffic pattern. As the number of air vehicles in the same corridor increases, the relative distance between the air vehicles decreases and results in unsafe conditions. Finally, the multi-vehicle simulation also reveals that the minimum vehicle distance and the traffic temperature have a negative correlation. The negative correlation indicates that the temperature increases as the safety level, based on the minimum vehicle distance, decreases.

The Chicago Downtown airspace simulation setup demonstrates the potential applications of the traffic temperature. Even if the number of air vehicles in the airspace keeps changing, the traffic temperature can represent the relative airspace safety severity level through the simulations and between the scenarios with different air traffic throughput. The simulation results show that the traffic temperature is associated with the minimum distance between air vehicles and with the number of near-miss events. The traffic temperature at the vehicle level can show the safety level of the airspace structure. The demonstrated results reveal the hot spots of the Chicago downtown airspace based on the scenarios with different amounts of air traffic. The airspace decision-makers can leverage this information to identify the strategies of managing the air traffic around the hot spots for enhancing airspace safety.

5.2 Potential Application of Metrics

There are two use cases for the traffic temperature metric. The “Real-time airspace monitoring for multiple airspace sectors” can help the ATA monitor the airspace safety level and the air traffic state estimation accuracy in real-time. If the traffic temperature is out of a reasonable range, the ATA should respond to resolve any contingent event. Secondly, the “Airspace Structure Assessment” shows how to assess different designs of routes or infrastructure even if the contingent events rarely happen. The decision-makers can use the traffic temperature to identify the dangerous points in the airspace system. The following sections include detailed discussions about the two potential applications based on the traffic temperature.

5.2.1 Real-Time Airspace Monitoring for Multiple Airspace Sectors

This dissertation reveals that the temperature metric can represent the level of confidence of how severe the traffic condition is. Ch. 4.2 shows that, with measurement noise, the temperature metric is associated with the near-miss event between two vehicles based on the given traffic safety severity function. By using the probability function of the predicted vehicle state, the temperature metric can even reach a similar near-miss prediction accuracy as the CPA. Furthermore, Ch. 4.3 discusses that the traffic temperature relates to the near-miss event and the minimum vehicle distance under different airspace structures. The results show that the traffic temperature can be a good metric for summarizing the air traffic states.

Chapter 4.4 constructs scenarios similar to real-world conditions with different environmental uncertainty settings. The results show that the airspace traffic temperature can summarize air traffic safety levels based on given airspace regulations. The traffic temperature rises when vehicles are too close to each other. And the traffic temperature lowers down when the traffic safety level increases. Hence, the results demonstrate that the ATA should confine the temperature within a reasonable range. A high-temperature condition indicates that the airspace is likely to encounter contingent events, while the low temperature means that the airspace many operate with high effectiveness.

A higher-level airspace control authority might need to monitor the conditions of multiple airspace sectors. Then, real-time traffic temperature monitoring can help the authority identify and compare the traffic conditions between airspace sectors. For example, if the temperature in an airspace sector increases, the authority can limit entries of new vehicles to the airspace sector by deferring take-off of vehicles in the airspace sector and diverting air traffic to low-temperature sectors. The authority can also develop mechanisms based on the traffic temperature for (1) triggering warning signals to the authority, (2) resolving any unsafe events, and (3) adjusting the airspace operational regulations for ensuring airspace safety.

5.2.2 Airspace Structure Assessment

An airspace structure designer needs some metrics for assessing the safety level of the airspace structure design, which includes the corridor structure designs, the airspace operational regulations, the ATA traffic management mechanisms, etc. The metric should summarize the overall air traffic safety level. The minimum vehicle distance is not an optimal metric because it only focuses on the worst-case and ignores the number of vehicle pairs under dangerous conditions. Additionally, the number of near-miss events is not ideal because it is hard to assess different airspace structure design when the near-miss event rarely occurs. Finally, for the urban air vehicle operations, the airspace designer has to consider the impacts of environmental perturbations on the vehicle navigation accuracy. In conclusion, the traffic temperature can be a good candidate for airspace structure designers to assess the safety levels of their designs.

Chapter 4.4 introduces the heat map based on the vehicle-level traffic temperature. The traffic temperature is a metric that converts a probability distribution of a state of an aerial vehicle to a positive number. Hence, calculating the traffic temperature of a single air vehicle is also doable. Discretizing airspace into cells is the first step to generating a heat map. Then, the next step is calculating the average temperature of each cell according to the vehicle locations and the vehicle temperature. The geographical temperature distribution can reveal the safety severity level in the airspace and the regions with higher environmental uncertainty.

Chapter 4.4 also demonstrates how the heat map can reveal the critical spots with a given airspace structure, a pre-set environmental uncertainty setting, and given ATA traffic management mechanisms. Although the simulation result may not have any contingent event, the heat map can still highlight the unsafe areas. The hot spots highlight regions where an airspace designer should focus. For example, Ch. 4.4 demonstrates that the area around the aerodrome is the hot region regardless of the airspace structure and ATA traffic management mechanism. Hence, the airspace designer should develop mechanisms and regulations for managing air traffic. The simulation results also reveal that the loose airspace structure can increase the relative distance between vehicles in the same traffic stream. However, it cannot resolve the locations with many crossing traffic streams. The strategical deconfliction mechanism is still necessary for resolving the situation.

The vehicle-level traffic temperature can continuously identify the level of confidence of how severe the vehicle state is. Even if the unsafe event rarely occurs in the simulation, the airspace structure designer can still assess the safety severity levels of the airspace structure with the temperature metric. The heat map can visualize the geographical distribution of the temperature and help the airspace structure designer identify the hot spots and enhance airspace safety.

5.3 Future Work

The proposed metrics quantify the safety level of a traffic state distribution function. They can also evaluate the heterogeneous traffic containing vehicles with various autonomous levels and flying capabilities, as long as the vehicle state estimation/prediction algorithms can handle the heterogeneity. It is worth further exploring the properties of the metrics in the following two future research directions.

5.3.1 Predicting Airspace Condition

Predicting airspace conditions is essential for managing air traffic. There are two possible approaches for estimating the future airspace states with the developed metrics. Since the developed metrics can quantify the traffic safety level according to a given traffic state distribution, the metrics can analyze the predicted traffic state distributions. For example, Kalman filter algorithms and deep learning techniques can predict the traffic state distributions. Then, the proposed metrics can summarize the information from the distribution functions and help ATA assess airspace conditions.

The second approach is analyzing the dynamics of the proposed metrics based on real-time traffic state estimations. Some machine learning (ML) techniques can learn complex dynamics from historical data. Hence, the ML techniques can learn from the dynamics of the past temperature evolution. Then, the ATA can predict the future temperature with the trained ML model.

Both approaches can assess the future values of the proposed metrics. These values can predict airspace safety levels and help ATA manage air traffic. However, it is unclear about the strength and weaknesses of both approaches. The first approach relies on a good traffic state prediction algorithm, which is a challenging research problem. The second approach depends on the ML model for learning the complex dynamics of the temperature evolution. Since the proposed metrics map complex airspace operations to a few values, it is unknown if any ML model can perform well for predicting the metrics.

5.3.2 Scaling for Very High Density Vehicle Operations

This dissertation applied the proposed metrics to various traffic density conditions. However, it had not pushed the metrics to extreme conditions, like a very high-density traffic scenario. Because traffic entropy and traffic safety severity depend on the number of vehicles, their values can be large and hard to understand. However, the traffic temperature is independent of the number of air vehicles. The traffic temperature can still present the traffic safety level for extremely high-density traffic scenarios. However, its properties may change based on the number of air vehicles. The traffic temperature should increase with the fraction of vehicle pairs under dangerous conditions. If there is a pair of air vehicles under unsafe situations in high-density traffic, the change of the traffic temperature may be smaller than low-density traffic. The small temperature change may decrease the sensitivity of identifying dangerous traffic conditions. However, further research is necessary for quantifying the impacts of traffic density on traffic temperature evolution.

REFERENCES

[1] *Advancing Aerial Mobility: A National Blueprint (2020)*. Washington D.C.: The National Academies Press, 2020, ISBN: 9780309670265. DOI: 10.17226/25646.

[2] *FAA Aerospace Forecasts*, 2019. [Online]. Available: https://www.faa.gov/data_research/aviation/aerospace_forecasts/.

[3] Booz Allen Hamilton, "Final Report Urban Air Mobility (UAM) Market Study," Booz Allen Hamilton, Tech. Rep., 2018, p. 160. [Online]. Available: https://ntrs.nasa.gov/api/citations/20190001472/downloads/20190001472.pdf.

[4] Amazon, *Amazon Prime Air*, 2015. [Online]. Available: https://www.amazon.com/Amazon-Prime-Air/b?ie=UTF8&node=8037720011%20http://www.amazon.com/b?node=8037720011.

[5] "Fast-Forwarding to a Future of On-Demand Urban Air Transportation," UBER Elevate, Tech. Rep., Oct. 2016. [Online]. Available: https://www.uber.com/elevate.pdf.

[6] P. Kopardekar, J. Rios, T. Prevot, M. Johnson, J. Jung, and J. E. R. Iii, "Unmanned Aircraft System Traffic Management (UTM) Concept of Operations," in *16th AIAA Aviation Technology, Integration, and Operations Conference*, Washington, D.C.: AIAA, 2016, pp. 1–16. DOI: 10.2514/6.2016-3292. [Online]. Available: http://arc.aiaa.org.

[7] Steve Bradford, "Concept of Operations v1.0 Foundational Principles Roles and Responsibilities Use Cases and Operational Threads Unmanned Aircraft System (UAS) Traffic Management (UTM)," U.S. Department of Transportation Federal Aviation Administration, Washington, DC, USA, Tech. Rep., 2018. [Online]. Available: https://utm.arc.nasa.gov/docs/2018-UTM-ConOps-v1.0.pdf.

[8] U. D. o. T. F. A. Administration, "Unmanned Aircraft System (UAS) Traffic Management (UTM) Concept of Operations V2.0," U.S. Deperatment of Transportation Federal Avaition Administration, Washington D.C., Tech. Rep., 2020. [Online]. Available: https://www.faa.gov/uas/research_development/traffic_management/media/UTM_ConOps_v2.pdf.

[9] S. Bradford, "Urban Air Mobility (UAM) Concept of Operations v1.0," U.S. Department of Transportation, Federal Aviation Administration, Washington D.C., USA, Tech. Rep., Jun. 2020, pp. 1–42. [Online]. Available: https://nari.arc.nasa.gov/sites/default/files/attachments/UAM_ConOps_v1.0.pdf.

[10] "UAM Vision Concept of Operations (ConOps) UAM Maturity Level (UML) 4," Deloitte, Tech. Rep., 2020. [Online]. Available: https://ntrs.nasa.gov/api/citations/20205011091/downloads/UAM%20Concept%20of%20Operations%2018DEC2020.pdf.

[11] A. Boukerche, H. A. Oliveira, E. F. Nakamura, and A. A. Loureiro, "Vehicular Ad Hoc Networks: A New Challenge for Localization-Based Systems," *Computer Communications*, vol. 31, no. 12, pp. 2838–2849, Jul. 2008, ISSN: 01403664. DOI: 10.1016/j.comcom.2007.12.004.

[12] C. A. Wargo, J. Glaneuski, G. Hunter, J. DIfelici, T. Blumer, D. Hasson, P. Carros, and R. J. Kerczewski, "Ubiquitous surveillance notional architecture for system-wide DAA capabilities in the NAS," in *IEEE Aerospace Conference Proceedings*, vol. 2018-March, IEEE Computer Society, Jun. 2018, pp. 1–14, ISBN: 9781538620144. DOI: 10.1109/AERO.2018.8396420.

[13] C. Liu and W.-H. Chen, "Disturbance Rejection Flight Control for Small Fixed-Wing Unmanned Aerial Vehicles," *Journal of Guidance, Control, and Dynamics*, vol. 39, no. 12, pp. 2810–2819, Dec. 2016, ISSN: 0731-5090. DOI: 10.2514/1.G001958. [Online]. Available: https://arc.aiaa.org/doi/10.2514/1.G001958.

[14] R. Leila, G. Stephen, K. Rafe, T. Tejal, and M. Mary, "Challenges and opportunities to integrate UAS in the National Airspace System," in *ICNS 2017 - ICNS: CNS/ATM Challenges for UAS Integration*, Institute of Electrical and Electronics Engineers Inc., Aug. 2017, ISBN: 9781509053759. DOI: 10.1109/ICNSURV.2017.8011942.

[15] T. Nguyen, "Dynamic Delegated Corridors and 4D Required Navigation Performance for Urban Air Mobility (UAM) Airspace Integration," *Journal of Aviation/Aerospace Education & Research*, vol. 29, no. 2, pp. 57–72, Jan. 2020, ISSN: 2329-258X. DOI: https://doi.org/10.15394/jaaer.2020.1828. [Online]. Available: https://commons.erau.edu/jaaer/vol29/iss2/4.

[16] M. Xue and M. Kowalski, "Parametric Study of Federated Conflict Resolution for UAM Operations," Aug. 2021. DOI: 10.2514/6.2021-2348. [Online]. Available: https://arc.aiaa.org/doi/abs/10.2514/6.2021-2348.

[17] M. Kotwicz Herniczek, E. Yilmaz, O. Sanni, and B. German, "Drawing the Highways in the Sky for Urban Air Mobility Operations," Aug. 2021. DOI: 10.2514/6.2021-2376. [Online]. Available: https://arc.aiaa.org/doi/abs/10.2514/6.2021-2376.

[18] D. A. DeLaurentis, "Understanding Transportation as System-of-Systems Design Problem," in *43rd AIAA Aerospace Sciences Meeting and Exhibit*, 2005, ISBN: 978-1-62410-064-2. DOI: 10.2514/6.2005-123. [Online]. Available: http://arc.aiaa.org.

[19] M. W. Maier, "Architecting Principles for Systems-of-Systems," *Systems Engineering*, vol. 1, no. 4, pp. 267–284, 1998, ISSN: 10981241. DOI: 10.1002/(SICI)1520-6858(1998)1:4<267::AID-SYS3>3.0.CO;2-D.

[20] D. A. DeLaurentis and R. K. Callaway, "A system-of-systems perspective for public policy decisions," *Review of Policy Research*, 2004, ISSN: 1541132X. DOI: 10.1111/j.1541-1338.2004.00111.x.

[21] P. Belobaba, A. Odoni, and C. Barnhart, *The Global Airline Industry*. John Wiley and Sons, 2009, pp. 1–494.

[22] A. Majumdar, W. Y. Ochieng, J. Bentham, and M. Richards, "En-route sector capacity estimation methodologies: An international survey," *Journal of Air Transport Management*, vol. 11, no. 6, pp. 375–387, Nov. 2005, ISSN: 0969-6997. DOI: 10.1016/J.JAIRTRAMAN.2005.05.002. [Online]. Available: https://www.sciencedirect.com/science/article/pii/S0969699705000396#bib8.

[23] H. Chao, A. Maheshwari, D. DeLaurentis, and W. Crossley, "Weather Impact Assessment for Urban Aerial Trips in Metropolitan Areas," 2021. DOI: 10.2514/6.2021-3176.

[24] C. Reiche, A. P. Cohen, and C. Fernando, "An Initial Assessment of the Potential Weather Barriers of Urban Air Mobility," *IEEE Transactions on Intelligent Transportation Systems*, vol. 22, no. 9, 2021, ISSN: 15580016. DOI: 10.1109/TITS.2020.3048364.

[25] O. K. Isik, J. Hong, I. Petrunin, and A. Tsourdos, "Integrity analysis for GPS-based navigation of UAVs in urban environment," *Robotics*, vol. 9, no. 3, 2020, ISSN: 22186581. DOI: 10.3390/ROBOTICS9030066.

[26] "Integration of Civil Unmanned Aircraft Systems (UAS) in the National Airspace System (NAS) Roadmap Federal Aviation Administration Second Edition," Federal Aviation Administration, Tech. Rep., 2018. [Online]. Available: https://www.faa.gov/uas/resources/policy_library/media/Second_Edition_Integration_of_Civil_UAS_NAS_Roadmap_July%202018.pdf.

[27] *14 CFR PART 107 - SMALL UNMANNED AIRCRAFT SYSTEMS*, 2021.

[28] A. F3411-19, *Standard Specification for Remote ID and Tracking*. DOI: 10.1520/F3411-19. [Online]. Available: http://www.astm.org/cgi-bin/resolver.cgi?F3411-19.

[29] A. M. Stoll, J. B. Bevirt, P. P. Pei, and E. V. Stilson, "Conceptual design of the joby S2 electric VTOL PAV," in *AIAA AVIATION 2014 -14th AIAA Aviation Technology, Integration, and Operations Conference*, 2014. DOI: 10.2514/6.2014-2407.

[30] J. C. Chin, E. D. Aretskin-Hariton, D. J. Ingraham, D. L. Hall, S. L. Schnulo, J. S. Gray, and E. S. Hendricks, "Battery evaluation profiles for x-57 and future urban electric aircraft," in *AIAA Propulsion and Energy 2020 Forum*, 2020. DOI: 10.2514/6.2020-3567.

[31] B. L. Litherland, N. K. Borer, and N. S. Zawodny, "X-57 Maxwell High-Lift Propeller Testing and Model Development," 2021. DOI: 10.2514/6.2021-3193.

[32] N. K. Borer, D. E. Cox, and R. D. Wallace, "Flight performance maneuver planning for nasa's x-57 "maxwell" flight demonstrator – part 1: Power-off glides," in *AIAA Aviation 2019 Forum*, 2019. DOI: 10.2514/6.2019-2855.

[33] M. Feary, "A decomposition framework for describing advanced air mobility mission functions," in *AIAA AVIATION 2020 FORUM*, vol. 1 PartF, 2020. DOI: 10.2514/6.2020-3249.

[34] C. Adam and S. Susan, "Urban Air Mobility: Opportunities and Obstacles," in *International Encyclopedia of Transportation*, 2021. DOI: 10.1016/b978-0-08-102671-7.10764-x.

[35] D. Federal Aviation Administration (FAA), *Airspace 101 – Rules of the Sky*, 2021. [Online]. Available: https://www.faa.gov/uas/recreational_fliers/where_can_i_fly/airspace_101/.

[36] D. Federal Aviation Administration (FAA), *Airspace*, 2020.

[37] D. Federal Aviation Administration (FAA), *See FAA UAS Data on a Map*, 2021. [Online]. Available: https://faa.maps.arcgis.com/apps/webappviewer/index.html?id=9c2e4406710048e19806ebf6a06754ad.

[38] A. Majumdar and J. Polak, "Estimating Capacity of Europe's Airspace Using a Simulation Model of Air Traffic Controller Workload," *Transportation Research Record: Journal of the Transportation Research Board*, pp. 30–43, 2001. DOI: 10.3141/1744-05.

[39] A. Miura, A. Tomoeda, and K. Nishinari, "Formularization of entropy and anticipation of metastable states using mutual information in one-dimensional traffic flow," *Physica A: Statistical Mechanics and its Applications*, vol. 560, p. 125 152, Dec. 2020, ISSN: 03784371. DOI: 10.1016/j.physa.2020.125152.

[40] B. S. Kerner and P. Konhäuser, "Cluster effect in initially homogeneous traffic flow," *Physical Review E*, vol. 48, no. 4, R2335–R2338, Oct. 1993, ISSN: 1063-651X. DOI: 10.1103/PhysRevE.48.R2335. [Online]. Available: https://link.aps.org/doi/10.1103/PhysRevE.48.R2335.

[41] H. Reiss, A. D. Hammerich, and E. W. Montroll, "Thermodynamic treatment of nonphysical systems: Formalism and an example (Single-lane traffic)," *Journal of Statistical Physics*, vol. 42, no. 3-4, pp. 647–687, Feb. 1986, ISSN: 00224715. DOI: 10.1007/BF01127733. [Online]. Available: https://link.springer.com/article/10.1007/BF01127733.

[42] M. Lowry, "Entropy-based Design of Air Traffic Management," *16th AIAA Aviation Technology, Integration, and Operations Conference*, no. June, pp. 1–12, 2016. DOI: doi:10.2514/6.2016-4377. [Online]. Available: http://dx.doi.org/10.2514/6.2016-4377.

[43] D. Delahaye and S. Puechmorel, "Air traffic complexity based on dynamical systems," in *Proceedings of the IEEE Conference on Decision and Control*, Budapest, Hungary: HAL, Jun. 2010, pp. 2069–2074, ISBN: 9781424477456. DOI: 10.1109/CDC.2010.5718004. [Online]. Available: https://hal-enac.archives-ouvertes.fr/hal-00938403.

[44] M. A. Ishutkina, E. Feront, and K. D. Bilimoria, "Describing air traffic complexity using mathematical programming," in *Collection of Technical Papers - AIAA 5th ATIO and the AIAA 16th Lighter-than-Air Systems Technology Conference and Balloon Systems Conference*, vol. 3, Arlington, Virginia: American Inst. Aeronautics and Astronautics Inc., Sep. 2005, pp. 1500–1508, ISBN: 1563477408. DOI: 10.2514/6.2005-7453. [Online]. Available: https://arc.aiaa.org/doi/abs/10.2514/6.2005-7453.

[45] H. Hamidi and A. Kamankesh, "An Approach to Intelligent Traffic Management System Using a Multi-agent System," *International Journal of Intelligent Transportation Systems Research*, vol. 16, no. 2, 2018, ISSN: 18688659. DOI: 10.1007/s13177-017-0142-6.

[46] J. C. Hill, J. K. Archibald, W. C. Stirling, and R. L. Frost, "A multi-agent system architecture for distributed air traffic control," in *Collection of Technical Papers - AIAA Guidance, Navigation, and Control Conference*, vol. 3, 2005. DOI: 10.2514/6.2005-6049.

[47] M. Brittain and P. Wei, "Autonomous Air Traffic Controller: A Deep Multi-Agent Reinforcement Learning Approach," May 2019. [Online]. Available: http://arxiv.org/abs/1905.01303.

[48] H. L. WEIDEMANN, "Entropy Analysis of Feedback Control Systems1 1The research for this paper was supported in part by funds from the United States Air Force Office of Scientific Research under AFOSR Grant 699-67.," in *Advances in Control Systems*, vol. 7, Elsevier, Jan. 1969, pp. 225–255. DOI: 10.1016/b978-1-4831-6713-8.50011-7.

[49] H. Touchette and S. Lloyd, "Information-theoretic approach to the study of control systems," *Physica A: Statistical Mechanics and its Applications*, vol. 331, no. 1-2, pp. 140–172, Jan. 2004, ISSN: 03784371. DOI: 10.1016/j.physa.2003.09.007.

[50] X. Li and E. Mupondwa, "Life cycle assessment of camelina oil derived biodiesel and jet fuel in the Canadian Prairies," *Science of the Total Environment*, vol. 481, no. 1, pp. 17–26, 2014, ISSN: 00489697. DOI: 10.1016/j.scitotenv.2014.02.003.

[51] H. Li, "Entropy Analysis of CPS With Application in Smart Grids: From Discrete Network to Continuum Limit," *2015 IEEE International Conference on Smart Grid Communications 9SmartGRidComm): Communications and Networks to Enable the Smart Grid*, pp. 707–712, 2015. [Online]. Available: http://web.eecs.utk.edu/courses/fall2011/ece505/CPS/SmartGridComm2015_3%20/Entropy.pdf.

[52] H. Li, “Entropy reduction via communications in cyber physical systems: How to feed maxwell’s demon?” *IEEE International Symposium on Information Theory - Proceedings*, vol. 2015-June, pp. 2206–2210, 2015, ISSN: 21578095. DOI: 10.1109/ISIT.2015.7282847.

[53] H. Li and J. B. Song, “Communications for distributed state estimation in CPSs with application in smart grids,” in *2015 IEEE International Conference on Smart Grid Communications, SmartGridComm 2015*, Miami, FL: IEEE, 2015, pp. 701–706, ISBN: 9781467382892. DOI: 10.1109/SmartGridComm.2015.7436383.

[54] H. Li, “Interdependency analysis of communications and control in networked cyber physical systems: An entropy framework,” *2016 50th Annual Conference on Information Systems and Sciences, CISS 2016*, pp. 151–156, 2016. DOI: 10.1109/CISS.2016.7460493.

[55] H. Li, “Information efficiency of communications for networked control in cyber physical systems: When carnot meets shannon,” in *2016 IEEE 55th Conference on Decision and Control, CDC 2016*, IEEE, 2016, pp. 1865–1870, ISBN: 9781509018376. DOI: 10.1109/CDC.2016.7798536.

[56] H. Li, “Does Feedback Control Always Reduce Entropy/Communication Requirement in Smart Grid?” In *2017 IEEE Global Communications Conference, GLOBECOM 2017*, Singapore, Singapore: IEEE, 2017, pp. 1–6, ISBN: 9781509050192. DOI: 10.1109/GLOCOM.2017.8254459.

[57] H. Li, “Analysis on the Nonlinear Dynamics of Deep Neural Networks: Topological Entropy and Chaos,” 2018. [Online]. Available: https://arxiv.org/pdf/1804.03987.pdf%20http://arxiv.org/abs/1804.03987.

[58] F. Colonius and C. Kawan, “Invariance entropy for control systems,” *SIAM Journal on Control and Optimization*, vol. 48, no. 3, pp. 1701–1721, May 2009, ISSN: 03630129. DOI: 10.1137/080713902. [Online]. Available: https://epubs.siam.org/page/terms.

[59] C. Kawan, *Invariance Entropy for Deterministic Control Systems - An Introduction*, 1st ed., ser. Lecture Notes in Mathematics. Cham: Springer International Publishing, 2013, vol. 2089, ISBN: 978-3-319-01287-2. DOI: 10.1007/978-3-319-01288-9. [Online]. Available: http://link.springer.com/10.1007/978-3-319-01288-9.

[60] T. Tanaka, P. M. Esfahani, and S. K. Mitter, “LQG control with minimum directed information: Semidefinite programming approach,” *IEEE Transactions on Automatic Control*, vol. 63, no. 1, pp. 37–52, Jan. 2018, ISSN: 00189286. DOI: 10.1109/TAC.2017.2709618.

[61] S. Tatikonda, A. Sahai, and S. Mitter, “Stochastic Linear Control Over a Communication Channel,” *IEEE TRANSACTIONS ON AUTOMATIC CONTROL*, vol. 49, no. 9, pp. 1549–1561, Sep. 2004. DOI: 10.1109/TAC.2004.834430. [Online]. Available: http://people.eecs.berkeley.edu/~sahai/Papers/Stochastic_Control.pdf.

[62] V. Kostina and B. Hassibi, “Rate-Cost Tradeoffs in Control,” *IEEE Transactions on Automatic Control*, vol. 64, no. 11, pp. 4525–4540, Nov. 2019, ISSN: 15582523. DOI: 10.1109/TAC.2019.2912256.

[63] R. Clausius, “Ueber eine veränderte Form des zweiten Hauptsatzes der mechanischen Wärmetheorie,” *Annalen der Physik*, 1854, ISSN: 15213889. DOI: 10.1002/andp.18541691202.

[64] L. Boltzmann, “Über die Mechanische Bedeutung des Zweiten Hauptsatzes der Wärmetheorie,” in *Wiener Berichte*, 1866, pp. 195–220. DOI: 10.1017/cbo9781139381420.003.

[65] D. V. Schroeder, *An introduction to thermal physics*, [Nachdr.]. San Francisco Calif.: Addison Wesley, 2000, p. 422, ISBN: 9780321277794. [Online]. Available: https://www.worldcat.org/title/introduction-to-thermal-physics/oclc/634677190.

[66] C. E. Shannon, “A Mathematical Theory of Communication,” *The Bell System Technical Journal*, vol. 27, pp. 623–656, 1948. [Online]. Available: http://math.harvard.edu/~ctm/home/text/others/shannon/entropy/entropy.pdf.

[67] L. Brillouin, *Science and information theory.* 2d ed. New York: Academic Press, 1962.

[68] E. T. Jaynes, “Information theory and statistical mechanics,” *Physical Review*, vol. 106, no. 4, pp. 620–630, May 1957, ISSN: 0031899X. DOI: 10.1103/PhysRev.106.620. [Online]. Available: https://journals.aps.org/pr/abstract/10.1103/PhysRev.106.620.

[69] Edwin Thompson Jaynes, “Information Theory and Statistical Mechanics,” W. A. Benjamin, Inc., New York, Tech. Rep., 1963, pp. 181–218. [Online]. Available: https://bayes.wustl.edu/etj/articles/brandeis.pdf.

[70] E. T. Jaynes, “Prior Probabilities,” *Ieee Transactions on Systems and Cybernetics*, vol. 0, no. 3, 1968. [Online]. Available: https://philpapers.org/rec/JAYPP.

[71] R. T. Dean and W. T. M. Dunsmuir, “Dangers and uses of cross-correlation in analyzing time series in perception, performance, movement, and neuroscience: The importance of constructing transfer function autoregressive models,” *Behavior Research Methods 2015 48:2*, vol. 48, no. 2, pp. 783–802, Jun. 2015, ISSN: 1554-3528. DOI: 10.3758/S13428-015-0611-2. [Online]. Available: https://link.springer.com/article/10.3758/s13428-015-0611-2.

[72] M. Bayazit and B. Önöz, “To prewhiten or not to prewhiten in trend analysis?” *https://-doi.org/10.1623/hysj.52.4.611*, vol. 52, no. 4, pp. 611–624, Aug. 2009. DOI: 10.1623/HYSJ.52.4.611. [Online]. Available: https://www.tandfonline.com/doi/abs/10.1623/hysj.52.4.611.

[73] S. Roy, A. Maheshwari, W. A. Crossley, and D. A. Delaurentis, "A study on the impact of aircraft technology on the future of regional transportation using small aircraft," in *2018 Aviation Technology, Integration, and Operations Conference*, 2018. DOI: 10.2514/6.2018-3056.

[74] A. Maheshwari, D. A. DeLaurentis, and W. A. Crossley, "Analyzing Impact of Unusual Changes in Travel Pattern on UAM Attractiveness," in *Operational Aspects of On-demand Mobility and Transformational Flight II*, 2021 AIAA Aviation, 2021.

[75] S. Roy, A. Maheshwari, W. A. Crossley, and D. A. DeLaurentis, "Future Regional Air Mobility Analysis Using Conventional, Electric, and Autonomous Vehicles," *Journal of Air Transportation*, vol. 29, no. 3, 2021, ISSN: 23809450. DOI: 10.2514/1.d0235.